CANADIAN THESES

THÈSES CANADIENNES

NOTICE

The quality of this microfiche is heavily dependent upon the quality of the original thesis submitted for microfilming. Every effort has been made to ensure the highest quality of reproduction possible.

If pages are missing, contact the university which granted the degree.

Some pages may have indistinct print especially if the original pages were typed with a poor typewriter ribbon or if the university sent us an inferior photocopy.

Previously copyrighted materials (journal articles, published tests, etc.) are not filmed.

Reproduction in full or in part of this film is governed by the Canadian Copyright Act, R.S.C. 1970, c. C-30.

AVIS

La qualité de cette microfiche dépend grandement de la qualité de la thèse soumise au microfilmage. Nous avons tout fait pour assurer une qualité supérieure de reproduction.

S'il manque des pages, veuillez communiquer avec l'université qui a conféré le grade.

La qualité d'impression de certaines pages peut laisser à désirer, surtout si les pages originales ont été dactylographiées à l'aide d'un ruban usé ou si l'université nous a fait parvenir une photocopie de qualité inférieure.

Les documents qui font déjà l'objet d'un droit d'auteur (articles de revue, examens publiés, etc.) ne sont pas microfilmés.

La reproduction, même partielle, de ce microfilm est soumise à la Loi canadienne sur le droit d'auteur, SRC 1970, c. C-30.

THIS DISSERTATION
HAS BEEN MICROFILMED
EXACTLY AS RECEIVED

LA THÈSE A ÉTÉ
MICROFILMÉE TELLE QUE
NOUS L'AVONS REÇUE

NL-339 (r.86/06)

Canada

A DEVELOPMENT OF HYBRID FD-TD/TLM METHOD AND ITS APPLICATION TO PLANAR MILLIMETER-WAVE WAVEGUIDE STRUCTURES

by

Dok-Hee Choi

A thesis
presented to the University of Ottawa
in fulfillment of the
thesis requirement for the degree of
Doctor of Philosophy
in
The Department of Electrical Engineering
Faculty of Science and Engineering

OTTAWA, Ontario, 1986

ISBN 0-315-36485-8

UNIVERSITÉ D'OTTAWA
UNIVERSITY OF OTTAWA

The University of Ottawa requires the signatures of all persons using or photocopying this thesis. Please sign below, and give address and date.

To the memory of

my father Choi, S.M.

and

my wife Joo-Yun

ABSTRACT

Novel computer algorithms for the time domain analysis of electromagnetic field problems have been developed, and their application to a wide variety of eigenvalue problems related to microwave and/or millimeter wave resonators and waveguide structures is presented in this thesis.

Firstly, the scalar Transmission Line Matrix(TLM) method has been developed on the basis of the original TLM method and Hertzian potential concept. However, this method can only handle relatively simple structures where solutions can be decomposed into TE and/or TM modes.

Secondly, the concept of the Finite Difference Time Domain(FD-TD) method have been extended to calculate eigenvalue solutions of inhomogeneous and/or anisotropic resonators. A new feature of this algorithm comprises initial field value assignment and the Fourier transform technique.

Thirdly, the newly developed algorithm has been modified further in order to utilize the irregular mesh technique. The numerical results obtained by this irregular mesh technique are virtually identical to those of the irregular mesh TLM method while computer expenditure is reduced to almost one third.

In order to illustrate the capability of the developed algorithm, several different types of finlines , inhomogeneous resonators, and anisotropic microstrips are analysed. Where ever possible, most results are compared with analytical data and those obtained by other numerical methods, i.e. spectral method and transverse resonant method, and good agreement is noted.

ACKNOWLEDGEMENTS

The author wishes to express his sincere appreciation to to his advisor Prof. Wolfgang J.R. Hoefer for his help, and guidance throughout this work.

Special thanks are also due to Prof. G. Costache and Dr. S.K. Biswas for their helpful suggestions ,and to the members of the microwave group, especially to Mr. Ihn Suk Kim and Mrs. Sara Meszaros for their review and comments.

The author expresses his gratitude to Mr. Robert Branden for his guidance in writing style.

Lastly, but by no means least, the author would like to express his thank to his wife Joo-yun for the typing of all the equations and the proof reading of this manuscript.

The financial assistance of the Natural Science and Engineering Research Council and Ontario Graduate Scholarship during the period of this research is acknowledged.

CONTENTS

Chapter I

INTRODUCTION

Electromagnetic problems involve the solution of Maxwell's equations subject to the appropriate boundary conditions valid for a particular situation. With the assumption of time harmonic variation, Maxwell's equations reduce to the familiar Helmholtz equation which is more generally classified as an elliptic type of partial differential equation. A number of techniques are available to solve these elliptic partial differential equations. However, until three decades ago, only analytic approaches were used. With the development of high speed digital computers, several numerical techniques have evolved to obtain approximate solutions to these equations.

The most commonly used technique is the general finite difference method which discretizes the three-dimensional space into a regular cubic mesh and gives an approximate solution at each mesh point. The accuracy of the model increases as more mesh points are used to represent the region under study, but at the expense of higher computer memory and CPU time.

More recently developed methods are the finite element method and the moment method. The finite element model requires that the solution region is analytically modelled or approximated by replacing it with an ensemble of discrete elements. On the other hand in the moment method, the unknown function is first expressed in terms of basis or expansion functions in the region under study. The coefficients of the expansion functions are determined such that the error between the exact solution and the expansion is minimized.

All the above mentioned methods may be considered, as a class, to be frequency-domain methods, which are based upon the assumption of an $\exp(j\omega t)$ time dependence in Maxwell's equations. In general, methods of this type lead to a large system of linear simultaneous equations, and the solution of these may require considerable computer resources or require some special expertise in the solution of linear equations.

In recent years, two different techniques which are simple yet very powerful for the solution of Maxwell's equations in the time domain, have been developed independently. These are the Transmission Line Matrix (TLM) method [6]-[16], and the Finite Difference Time Domain (FD-TD) method [27]-[35]. Even though they exhibit close similarities in computer simulation and in the requirement for gridded mesh time and space segmentation, major conceptual dif-

ferences exist in the algorithms. The TLM method obtains time domain solutions to Maxwell's equations using a model made up of transmission lines connected in a three-dimensional mesh network, whereas the FD-TD method directly solves time dependent Maxwell's equations by employing a finite difference scheme in time and space coordinates. The frequency domain solution or eigenvalues of the bounded structure may be obtained very simply by taking the Fourier transform of the time domain solution.

These time-domain techniques compare very favorably with the more 'conventional' frequency-domain methods, i.e. moment method, finite difference and finite elements both in computational efficiency and accuracy, except for very special geometries [8],[35].

However, the time domain method is much more general in that it permits the solution to be obtained without any mathematical processing of Maxwell's equations. Maxwell's equations are solved directly in their general three-dimensional vector form and the boundary conditions are supplied to the computer program as input data. The permittivity , permeability and conductivity of the propagation space are allowed to assume arbitrary values in space and time.

The TLM method has been used to solve a wide range of problems involving inhomogeneous or even anisotropic media[17]. At the same time, several improvements to the meth-

od have been proposed and implemented to enhance accuracy and to reduce computer resource requirements. One of the most important improvements has been proposed by Al-Mukhtar, and independently by Saguet [22]-[23], which involves the use of a variable mesh technique leading to drastic reductions in CPU time. However, in order to obtain the solution of highly localized fields within a complex planar transmission line structure with reasonable accuracy, this method still requires considerable memory and CPU time. The reason for this memory demand resides in the basic three-dimensional TLM concept.

The FD-TD method was first formulated by Yee [27], and has been extensively applied to the solution of scattering and coupling problems of complex scatterers with open boundaries [28]-[35]. So far, the application of this technique has been limited only to deterministic problems. With different initial conditions and Fourier transform techniques adapted from the TLM method, the FD-TD method can be utilized in eigenvalue problems.

In this thesis, the computer resource requirements of the TLM method have been considerably reduced. Firstly, the scalar TLM has been developed for application to a special case where modal solutions can be decomposed into TE and TM modes in a simple resonator. By this approach, required memory size is reduced by a factor of four while maintaining

similar numerical accuracy as the TLM method (chapter IV). Secondly, for the general solution of hybrid type modes, a new numerical technique was developed by adapting Yee's algorithm for the finite difference-time domain method to the conventional TLM method. With this procedure, the network variables of the TLM method were replaced by more direct quantities(field variables) while the remaining procedures of the TLM were retained. This method shows a marked improvement in computer resource requirements while maintaining the accuracy of the original TLM method. CPU memory and times were reduced by a factor of three (chapter V).

In order to make the FD-TD algorithm more efficient and flexible for application to complex geometries, an irregular mesh model of this technique was then developed. The requirement for computer CPU memory was further considerably reduced as compared to the uniform mesh FD-TD technique (chapter VI).

The application of the method to general microwave and millimeter wave circuits will be presented in chapter 7.

This thesis is divided into eight chapters which are outlined below :

In chapter II, the current state of the art of millimeter wave E-plane circuits as well as uniform finline analysis is

presented. A qualitative discussion outlines the difficulties in obtaining modal solutions for these structures.

Chapter III describes the historical background and the original concept of the TLM method. Several improvements made since the introduction of the original TLM method are reviewed, and the improvement of a three-dimensional resonator analysis proposed by the author is also introduced.

Chapter IV deals with the scalar TLM technique where Hertzian potential has been employed to simulate wave propagation in three-dimensional structures in order to reduce CPU requirements for a special class of eigenvalue problems.

Chapter V forms the main part of the thesis where the concept of the FD-TD will be presented together with the implementation of the computer algorithm. Some numerical results and a detailed error analysis will be given to demonstrate the accuracy of this method.

In chapter VI, a further evolution of the FD-TD technique, a irregular mesh FD-TD method, is developed. Some numerical results and a comparison study with the irregular mesh TLM method developed by Al-Mukhtar[23] is presented. For similar accuracy, the comparison shows that the FD-TD method compares favorably.

In chapter VII, several examples, mostly millimeter wave planar waveguide circuits where the developed FD-TD method

has been applied, will be presented. In most cases, the numerical results obtained by this method, are compared with values from other numerical methods, (conventional TLM and spectral domain method), for confirmation of validity.

Chapter VIII contains the conclusions reached in this thesis.

Chapter II

REVIEW OF PLANAR MICROWAVE AND MILLIMETER-WAVE CIRCUIT TECHNOLOGY

2.1 INTRODUCTION

Microwave and millimeter wave integrated circuits have been developed in recent years, and are expected to be in high demand in the future for a wide variety of applications in computers, communications, signal processing etc.. Although standard microstrip has been used as a building block in integrated circuits up to 140 GHz, several problems arise in millimeter wave applications. These problems are generally associated with critical tolerances and very narrow conductor strips where radiation loss becomes severe. In order to solve these problems, a general type of transmission line, the so called E-plane circuit or finline has been proposed and widely implemented at millimeter wave frequencies.

Besides finline, several other printed transmission lines are used in millimeter wave applications. Fig.2.1 shows four types of finlines, namely unilateral, bilateral, and antipodal finlines, as well as shielded microstrip, coplanar line, and suspended strip lines. All of these may be mounted in a metal waveguide housing split in the E-plane.

Finlines are planar structures suspended in the E-plane of a rectangular waveguide ,and their conductors can be printed in various patterns on the substrate. There are two ways to connect fins to the waveguide walls, as shown in Fig. 2.2. In the approach of Fig. 2.2.a), the fins are insulated from the housing at DC, but they are grounded at RF by chokes formed within the wall of the housing. By making the walls one quarter of the wavelength in the substrate thick, the fins are effectively grounded at the inner wall of the housing. In the grounded approach of Fig.2.2.b the fins are directly connected to the housing. Finlines exhibit certain advantages over other structures:

a) low losses (typically about one third of microstrip lines)
b) Larger bandwidth than waveguide
c) Possibility of photolithographic production
d) Potential for circuit integration

The first practical finline was proposed by Meier[36] as a new transmission line for millimeter wave integrated circuits to overcome or alleviate the shortcomings of conventional microstrip circuits. Before this, finlines were only proposed for a very special purpose involving orthogonal mode launching in circular waveguides[37]. Since this basic form of finline did not provide isolation from the waveguide

mount, items such as dc bias, IF, or modulation connection could not be accomplished.

During the last decade, the finline has been combined with other planar waveguide structures like microstrip and coplanar line to form versatile hybrid integrated circuits mounted in the E-plane of a metal waveguide housing. Since printed E-plane waveguide are basically planar slot and strip media, it is clear that from the begining the idea behind the new technology was to implement semiconductors in beam lead or chip form. Consequently, the first integrated E-plane circuits were PIN diode attenuators and switches.

Meier also pointed out that hybrid devices could be shunt- mounted across the fins, or mounted in series over a gap interupting one fin. Since then, several authors have presented PIN diode attenuators using two to four diodes in a parallel or series type circuit[38]-[40]. Both basic types of PIN diode attenuators have been realized up to 110 GHz with commercially available diodes.

Over the years, the operating frequency and bandwidth of SPST switches and attenuators has steadily increased. The progress includes operation in the bands 26 to 40 GHz, 50 to 70 GHz and 75 to 100 GHZ. More recently, the entire W band has been covered [41], and SPDT, or SP3T switches and attenuators have been realized for 80 - 90 GHz[42].

Mixers, on the other hand, were first realized for the Ka band by Meier[43], as a single-ended configuration, and by Gysel[44] in a balanced form. Following this early work, the operating frequency and bandwidth obtainable steadily increased. The progress includes operation in the bands 50 to 70 GHz and 60 to 90 GHz [45]. Several modified and scaled designs for frequencies up to 140 GHz have been reported since then [46]. Conversion loss measurements range from 5.5 dB at 70 GHz to 7.5 dB at 140 GHz.

Common circuit elements found in finline components include transitions, tapers, transformers, inductive or capacitive stubs. In the realization of these fundamental elements, discontinuities are introduced and parasitic elements must be included in the design model. The first finline discontinuities which were investigated, were finline inductive strips, and their use as an element of finline filters was suggested. Meier has taken a completely empirical approach to characterize inductive strips printed on a dielectric substrate. This investigation has led to a design chart for the equivalent circuit elements of the strip discontinuities. Using this result, band pass filters have been realized demonstrating the feasibility of the employed equivalent-circuit approach. Recently a theoretical approach has been presented by Arndt and Valdieck[47], which takes into account both the finite metalization thickness and the interaction between the inductive strips. Three resonator bandpass filters have been realized on quartz substrate.

Other integrated circuits based on finline technology include detectors, oscillators, directional couplers, nonreciprocal devices, and most other devices utilized in microwave engineering.

Furthermore, considerable reduction in size and weight of millimeter wave subsystems has been realized by integrating separate circuits on one substrate in a single package. Examples of such so-called hybrid microwave integrated circuits(HMIC's) are a medium distance pulse radar front end for 35 GHz on a single substrate and a dual-polarization 94 GHz radar module [48] which includes an E-plane circulator, a waveguide turnstile junction, metalic E-plane bandpass filters and a finline subassembly.

In the future, higher level integration of finline subsystems is expected with operating frequencies up to 140 GHz, as well as higher power generating capabilities.

2.2 CHARACTERIZATION OF THE UNIFORM FINLINE

Finline technology and trends have been briefly discussed in the previous section. With increasing interest in finline integrated circuits, there has been a need for accurate and economical numerical analysis of this medium. In this section, the principal characteristics of a uniform finline such as equivalent dielectric constant, guided wavelength and characteristic impedance will be discussed.

Finlines exhibit a combination of the characteristics of dielectric loaded and finned waveguide. They can be described either as dielectric loaded ridged waveguides or as slot lines shielded by a rectangular waveguide.

In a practical finline, the dielectric substrate serves mainly as a mechanical support for the delicate metal fins and the devices connected to them, while the fin geometry dominates the electrical properties of the line. It is desirable that the dielectric be as thin as mechanical considerations permit, and that its permittivity as well as its loss tangent be as small as possible.

If the dielectric is completely removed in a unilateral or bilateral finline circuit, the resultant waveguide is the well known ridged waveguide. Both waveguides exhibit very similar characteristics.

Firstly, research has been carried out towards the determination of the propagation constant, and the characteristic impedance. The first approximate calculation of the effective dielectric constant and characteristic impedance was made by Meier[38], based on the premise that the guided wavelength is nearly the same as in a ridged waveguide of identical cross-section, filled uniformly with a fictitious "equivalent" dielectric of permittivity k_e The guided wavelength and effective dielectric constant in such an equivalent homogeneous model are:

$$\lambda_g = \lambda[k_e - (\lambda/\lambda_c)^2]^{-1/2}$$

$$\varepsilon_{eff} = k_e - (\lambda/\lambda_c)^2$$

$$Z_o = Z / \varepsilon_{eff}$$

where λ_c is the cutoff wavelength of the commensurate air filled ridged waveguide and Z is the characteristic impedance at infinite frequency. In order to obtain k_e, Meier made a test measurement in a finline cavity. However, the realization of a test cavity is expensive and time consuming for engineering purposes. For this reason, Sharma and Hoefer[49] developed an empirical formula for determining k_e analytically. Results obtained with these expressions for the guided wavelength and the effective dielectric constant agree within 2% with numerical values obtained by the more accurate full wave analysis.

Simple but reasonably accurate results for finline parameters were obtained by Saad and Schunemann[50] who employed only transverse components and made some approximations in eigenvalue calculations.

Although the above methods are simple and useful for engineering purposes, they lack rigor and therefore they have been replaced by analytical methods which do not involve initial simplifying assumptions.

The first rigorous approach to finline parameter determination was carried out by Hofmann[51]. He used the moment method formulation with Galerkin's solution in the spectral domain to calculate the fields of an idealized model with zero metalization thickness using sinusoidal basis functions. Different types of basis functions, namely rectangular and triangular pulses, were used by Chang, and Itoh[52].

The spectral domain method was first described under this name by Mittra and Itoh who applied it to compute the dispersion characteristics of microstrip lines[53] and slot line. The method employs a Fourier transform of the coupled integral equations in the space domain. A reduction of the number of equations may be achieved by an appropriate choice of expansion functions. A particularly successful formulation of the problem in terms of the equivalent transmission line concept in the spectral domain is attributed to Schmidt and Itoh[54]. They extended this concept further to calcu-

late the characteristic impedance of higher order modes of a finline. The application of the method to finlines has been described by other authors[55]-[57] as well.

The first application of the TLM method to a finline structure was carried out by Ros and Hoefer[19] who presented the resonant frequencies of a finline resonator for dominant and higher modes. Later, finline cutoff frequencies were calculated by Shih and Hoefer[21]. Even though the TLM method requires more computer memory than the spectral domain technique, it is much more flexible in its application to complicated geometries and is much easier to formulate, because the spectral domain technique requires considerable mathematical preparation before formulating the algorithm, and is limited to the geometries with rectangular boundaries.

Due to the nature of a finline which contains a very thin dielectric slab in the middle of the housing, the employment of the conventional TLM method with a uniform mesh is too expensive. This may be the main reason why many engineers shied away from the method. However, variable mesh TLM techniques which were developed independently by Al-Mukhtar[23] and Saguet[22] reduce these requirements to such an extent that the method becomes competitive with other techniques. Consequently, a generalized TLM computer program based on the graded mesh TLM concept has been developed in this the-

sis and applied to various finline structures. Subsequently, most numerical results were compared with the data obtained by the spectral domain method or the Finite Difference-Time Domain method which is described later in this thesis[60]. Good agreement between numerical results from different methods was obtained.

2.3 DIFFICULTIES IN FINLINE FIELD ANALYSIS

Accurate analysis of finlines is difficult for two reasons, namely the inhomogeneous dielectric filling of the cross-section, and the presence of sharp edges.

Like microstrip, a finline is a printed circuit transmission line in which propagation occurs in an inhomogeneous medium as shown in Fig.2.2. The phase velocity of a transverse electromagnetic wave in the dielectric is different from that in air or free space. The finline structure then cannot support true TE or TM waves but can only support a hybrid mode. This can be seen rather easily from the following considerations.

Consider the cross section of a unilateral finline shown in Fig.2.2. If the fins are removed from the waveguide, it reduces to a partially filled dielectric slab waveguide that can generally support LSE or LSM types of modes[58]. One exceptional case is the TE_{no} mode. Suppose we attach two fins to the upper and lower waveguide walls. Their insertion

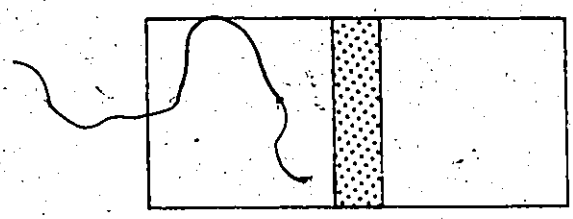

a) Dielectric loaded waveguide

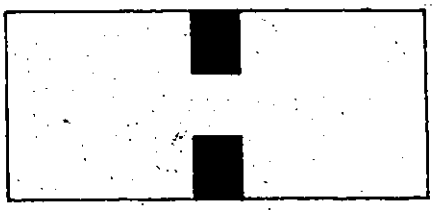

e) Ridged waveguide

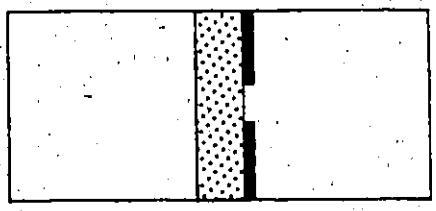

b) Unilateral finline

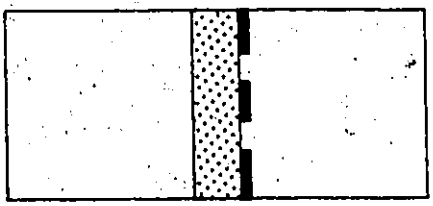

f) Coplanar line

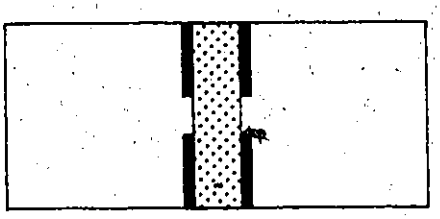

c) Bilateral finline

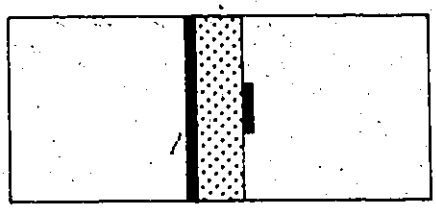

g) Shielded microstrip

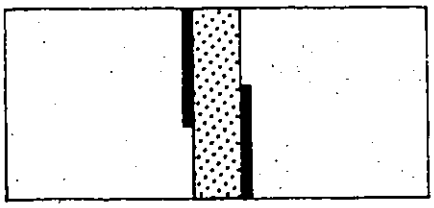

d) Antipodal finline

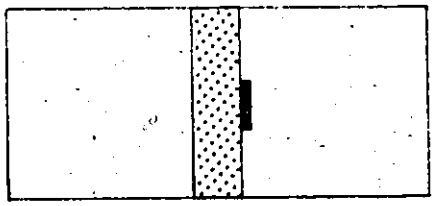

h) Suspended stripline

Fig. 2.1 Cross-section of several E-plane transmission lines

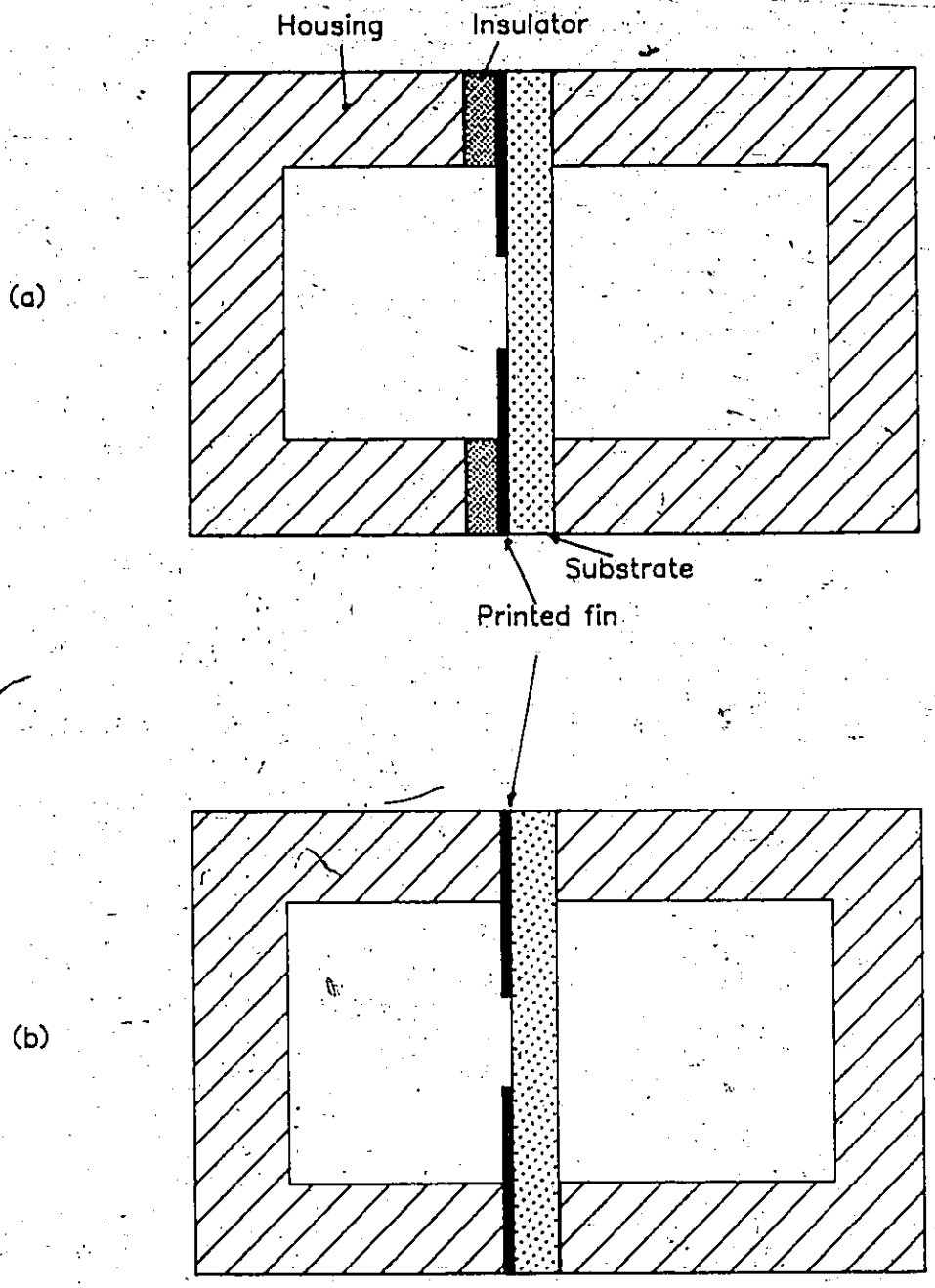

Fig. 2.2 Insulated (a) and grounded (b) finlines

causes currents to flow in both the y and z directions on the fins. These, in turn, serve to couple the LSE and LSM modes so that the final mode configuration in the finline is hybrid in nature.

As an additional difficulty, the presence of sharp edges causes the field values to exhibit singularities, leading to convergence problems in the numerical computation of the finline characteristics.

Chapter III

REVIEW OF THE TLM METHOD

3.1 HISTORICAL BACKGROUND

The application of equivalent networks to the solution of electromagnetic problems gained the interest of many scientists and electrical engineers long before the computer age. Impedance networks were already developed in the 1930's for the simulation of power distribution problems in large electrical networks. Their first application to a true field problem appears to have been made by Beuken who, in 1937, described an electrical model for transient heat-flow problems. For the network analogy, the points of the discretized system are connected by lumped circuit elements, resistances or reactances, or both.

It was Kron who developed the most general impedance networks for a variety of field equations[1]-[3]. He derived complicated equivalent circuits for the simulation of the general form of the Maxwell's equations for any system of orthogonal curvilinear coordinates. However, only circuits applicable to certain special cases were implemented. These cases involve problems[4] in two-dimensional systems for which half of the six components of the electromagnetic

field vectors vanish. It is worthwhile to note Kron's observation: "It is only possible that in two dimensions one of the networks representing a simple TE or TM mode happens to assume the form of a two-dimensional transmission line"[2]. This principle has been confirmed by Whinnery and Ramo[4].

Almost thirty years later, this realizable two-dimensional transmission line circuit was utilized as a basic unit of the so called "Transmission Line Matrix (TLM) method" pioneered by P.B.Johns[6].

The second basis of the TLM method has been established by adopting the wave propagating concept as postulated by Huygens who considered a wavefront to consist of a number of secondary radiators which give rise to spherical wavelets. Johns has shown that rectilinear propagation occurs in a two-dimensional TLM network when the wave is considered as an impulsive disturbance[9].

However, this is not obvious in the three-dimensional TLM case because a three-dimensional TLM unit cell consists of six two-dimensional hybrid nodes, and it is very difficult even to visualize the scattering process. This difficulty may be understood with the reasoning that the Huygens's wave is basically a scalar model, while electromagnetic waves must be described by a vector wave equation. In order to overcome this diffculty, Johns has heuristically simulated a plane wave propagation in a three-dimensional TLM network in

such a way that the ~~exitation~~ of E_y and H_x pulses cancels E_z and H_z components automatically, resulting in rectilinear propagation in the z-direction.

He has thus established the TLM concept in which a group of traveling pulses may simulate EM wave propagation in real space in discretized fashion.

3.2 THE MODEL OF THE TLM METHOD

3.2.1 TLM Method in General

The TLM technique utilizes an equivalent network of ideal two wire transmission lines connected in a three-dimensional mesh in such a way that shunt and series nodes are formed where the lines cross. Attached to the nodes are a number of stubs whose electrical properties are used to represent the electrical characteristics of the propagation space.

Analysis of the transmission line matrix leads to a system of line equations which can be identified with Maxwell's equations by drawing equivalences between voltages, currents, line constants, and stub parameters in the TLM model, and field quantities in the propagation medium. The numerical procedure then entails determining the impulse response of this equivalent network and taking the Fourier transform of the output response function to obtain the spectral domain solution.

The validity of the TLM technique has been demonstrated by its application to a wide range of wave propagation and scattering problems[6]-[25]. To illustrate the type of problems that have been solved using the TLM technique a few examples are stated here.

Johns and Beurle[6] applied the TLM technique to analyze the scattering caused by a waveguide bifurcation. In [7], the cutoff wave numbers of several modes in a homogeneously filled waveguide of arbitrary cross section have been obtained using this technique. Other applications involving waveguide wall losses, magnetic materials and discontinuities have been reported in the literature[10]-[16].

In the TLM model, three shunt and three series stubs are used to represent the dielectric and magnetic properties of the propagation medium. Therefore it seems natural to extend the TLM concept to anisotropic media where the values of permittivity and permeability depend on the propagation direction. This has been carried out by Mariki[17] who has analyzed inhomogeneous and anisotropic substrates for the special case where the permittivity tensor is diagonalized with respect to the chosen coordinate system.

As shown above, the attractive features of the TLM method reside in versatility of its application. However, the discretization of the medium and subsquent modelling by the TLM network lead to some errors in the numerical solution. These

errors are due to the nature of the periodic TLM structure. The characteristics of the periodic structure arise from two basic properties, namely,

1) pass band - stop band characteristics, and
2) support of waves with phase and group velocities much less than the velocity of light.

Thus the TLM model is characterized by a high frequency cutoff for the low frequency passband which limits the highest frequency at which the model can be used to represent a physical propagation medium.

3.2.2 The Two-dimensional TLM Model

Transmission line modeling of Maxwell's equations has led to a Transmission Line Matrix (TLM) algorithm for the solution of the coupled equations.

$$\nabla \times \overline{H} = \varepsilon \, \partial\overline{E}/\partial t$$

$$\nabla \times \overline{E} = -\mu \, \partial\overline{H}/\partial t \qquad (3.1)$$

where $\overline{E}$ and $\overline{H}$ are vectors in three-dimensional space and time, and ε and μ are constants. The TLM method provides for the numerical solution of (3. 1) in the time domain. In the two-dimensional model to which this discussion is restricted, a pair of orthogonal loss-free two-wire transmission lines intersect at the center of the element as shown in

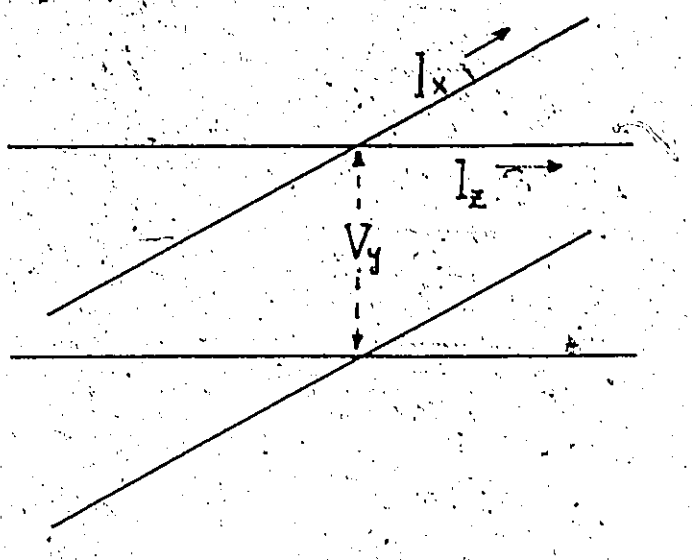

a) Junction between transmission lines

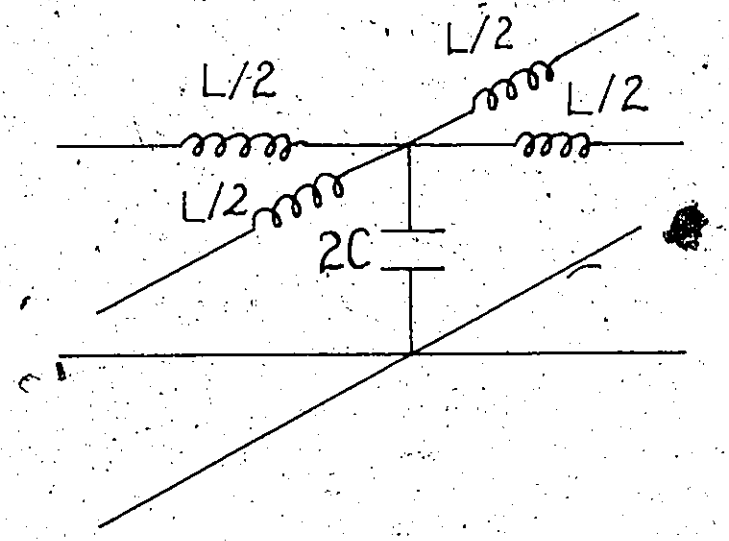

b) Equivalent network

Fig. 3.1 A unit cell of two-dimensional TLM network

Fig.3.1. The differential equations modelled by the network are

$$\begin{aligned} \partial V_y/\partial x &= -L\, \partial I_x/\partial t \\ \partial V_y/\partial z &= -L\, \partial I_z/\partial t \\ \partial I_x/\partial x - \partial I_z/\partial z &= 2C\, \partial V_y/\partial t \end{aligned} \qquad (3.2)$$

The two sets($(E_y\ H_z\ H_x)$ and $(H_y\ E_x\ E_z)$) of the two-dimensional Maxwell's equations can be easily obtained from each scalar equation of (3.1) by setting $\partial/\partial y = 0$. Comparing these sets with (3.2), equivalence between network parameters and field parameters can be seen[6], and the numerical simulation based on this equivalence can be justified. Therefore if the voltage and current for any time and space point are known, the solution of (3.1) can be determined. The matrix response to the initial excitation and the behavior of voltages and currents on the network are calculated using the procedure given by Johns. Let the vectors

$$V_m^i = [\ V1\ V2\ V3\ V4\ V5\ ]_m^i|_k$$

$$V_m^r = [\ V1\ V2\ V3\ V4\ V5\ ]_m^r|_k$$

represent the magnitudes of the incident and reflected voltage pulses on terminals 1 to 5 of node m at the k-th iteration. For a complete system of M nodes, the incident and reflected voltage impulses may be represented by the partitioned matrices.

$$V^i|_k = [\ V1\ |\ V2\ |\ V3\ |\ \text{-----}\ |\ VM\ ]|_k^i$$

$$V^r|_k = [\ V1 \mid V2 \mid V3 \mid \text{-----} \mid VM\ ]|^r_k$$

At each node the incident pulses are scattered into reflected pulses which may be expressed in terms of the incident pulses through the scattering matrix S.

$$V^r|_k = S \times V^i|_k \qquad (3.3)$$

It is convenient to decompose S into p and q as

$$S = p \times q + r$$

where p and q and r are partitioned matrices with sub-matrices p_{mm} q_{mm} and r_{mm} (m =1 to M) on the diagonals and zeros elsewhere. For the m-th node:

$$V^r_m|_k = [\ p_{mm} \times q_{mm} + r_{mm}\ ] \times V^i_m|_k$$

where $p_{mm} = [\ p_1\ p_2\ p_3\ p_4\ p_5\ ]$

$p_i = 2/(2 + Y_o)$ $\quad i = 1$ to 5

$Y_o =$ admittance of a stub

and $q_{mm} = [\ q_1\ q_2\ q_3\ q_4\ q_5\ ]$

with $q_i = 1 \quad : i = 1$ to 4

$Y_o \quad : i = 5$

$$r_{mm} = \begin{bmatrix} -1 & 0 & 0 & 0 & 0 \\ 0 & -1 & 0 & 0 & 0 \\ 0 & 0 & -1 & 0 & 0 \\ 0 & 0 & 0 & -1 & 0 \\ 0 & 0 & 0 & 0 & -1 \end{bmatrix}$$

After an iteration time interval dt, pulses reflected from one node become incident pulses on neighbouring nodes, thus $V^i|_{k+1}$ may be related to $V^r|_k$ through a connection matrix C which describes how two nodes are connected together, and includes boundary conditions, i.e.

$$V^i|_{k+1} = C \times V^r|_k \qquad (3.4)$$

For the Cartesian connected mesh of Fig.3.1, C may be expressed also as a partitioned matrix of M x M submatrices of 5 x 5 elements. Most of the elements within C are zero. The off diagonal element $(C_{ij})_{l,n}$ is unity if a connection in the mesh allows a pulse to travel from terminal j of node m to terminal i of node 1. The diagonal submatrices, i.e. $(C_{ij})_{11}$ $(C_{ij})_{22}$ ------ are responsible for the reflections on the boundaries and stubs. Note that the fifth elements $(C_{55})_{11}$ $(C_{55})_{22}$ ------ are all unity.

Once the connecting matrix of (3.4) is obtained, the iteration process for the general TLM method may be summarized by

$$V^i|_{k+1} = C \times S \times V^i|_k = C \times [p \times q + r] \times V^i|_k \qquad (3.5)$$

From (3.5), the final value of V can be calculated by an iterative process. If the initial vector V is given as V_o the output after N iteration will be:

$$V^i|_N = \Pi \, [\, C \times \{p \times q + r\}]_k \times V_o$$
$$= [\, S_t \,] \times V_o \qquad (3.6)$$

If the output point is the m-th node, then

$$V_m^i|_N = (s_t \times V_{om})|_N$$

represents the impulse function of time.

3.2.3 The Three-dimensional TLM Model

The three-dimensional TLM network capable of representing three-dimensional space, and satisfying Maxwell's equation is shown in Fig.3.2. The network is an interconnection of three shunt nodes and three series nodes in such a manner that there are three nodes (two shunt and one series node or vice versa) on each plane. The elementary block from which the entire space is built, is a cube volume of space dl/2 long in each direction. The relationship between network parameters and field variables is well established and is well illustrated in the literature[10]-[16]. These lengthy expressions are omitted here.

To accomodate discontinuities such as a slab of dielectric or magnetic material, open circuited and short circuited stubs of variable characteristic admittances are added to the shunt and series nodes.

Interconnecting many of these three-dimensional nodes makes it possible to describe any complicated inhomogeneous medium. The numerical routine is therefore based upon the

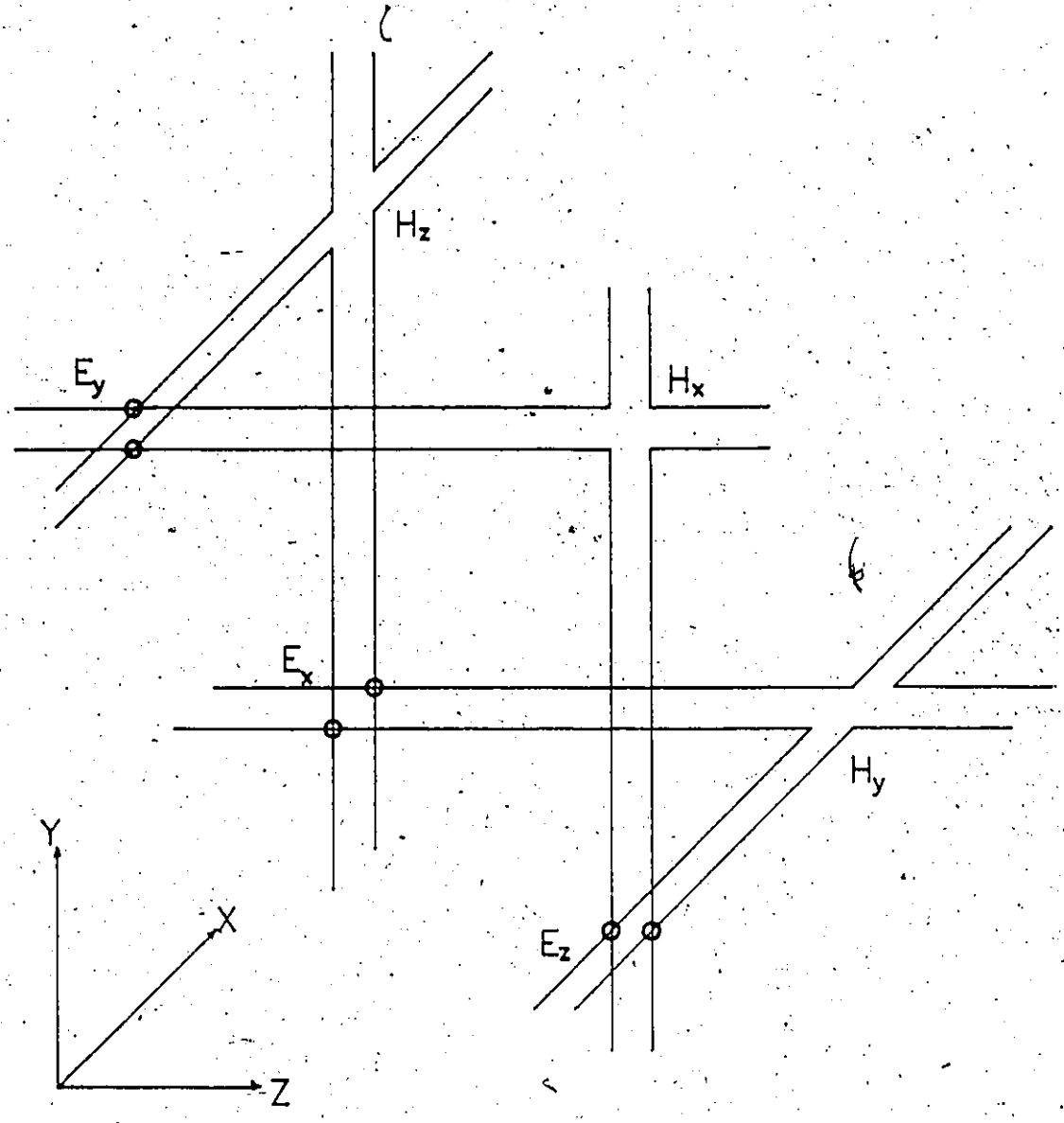

Fig. 3.2 A hybrid 3-D TLM network consisting of three shunt and three series connected nodes.

voltage impulse scattering matrix of the individual two-dimensional shunt and series nodes.

Both the three- and two-dimensional networks are slow wave structures. However, in the three-dimensional case, the low frequency propagation velocity of the wave in the network in any direction is c/2, where c is the velocity of light in free space, while that velocity is $c/\sqrt{2}$ in the two-dimensional case.

3.2.4 Frequency Spectrum and Accuracy of the Results

The output response function consists of a train of impulses of varying magnitude in the time domain, separated by a time interval $\Delta t(=\Delta \ell/c)$. Thus, the theoretical frequency response obtained by taking the Fourier transform of the output response, consists of a series of peaks in the frequency domain corresponding to the modal resonant frequencies of the cavity for which a solution exists.

Since the output is in the form of a discrete series, the integration is replaced by a simple summation. Thus the Fourier transform of the output is :

$$S(f) = \sum^{N} V_n \exp(-j2\pi f n \Delta t) \qquad (3.7)$$

where N is the total number of time steps, and V_n is the output amplitude at time $t = n\Delta t$.

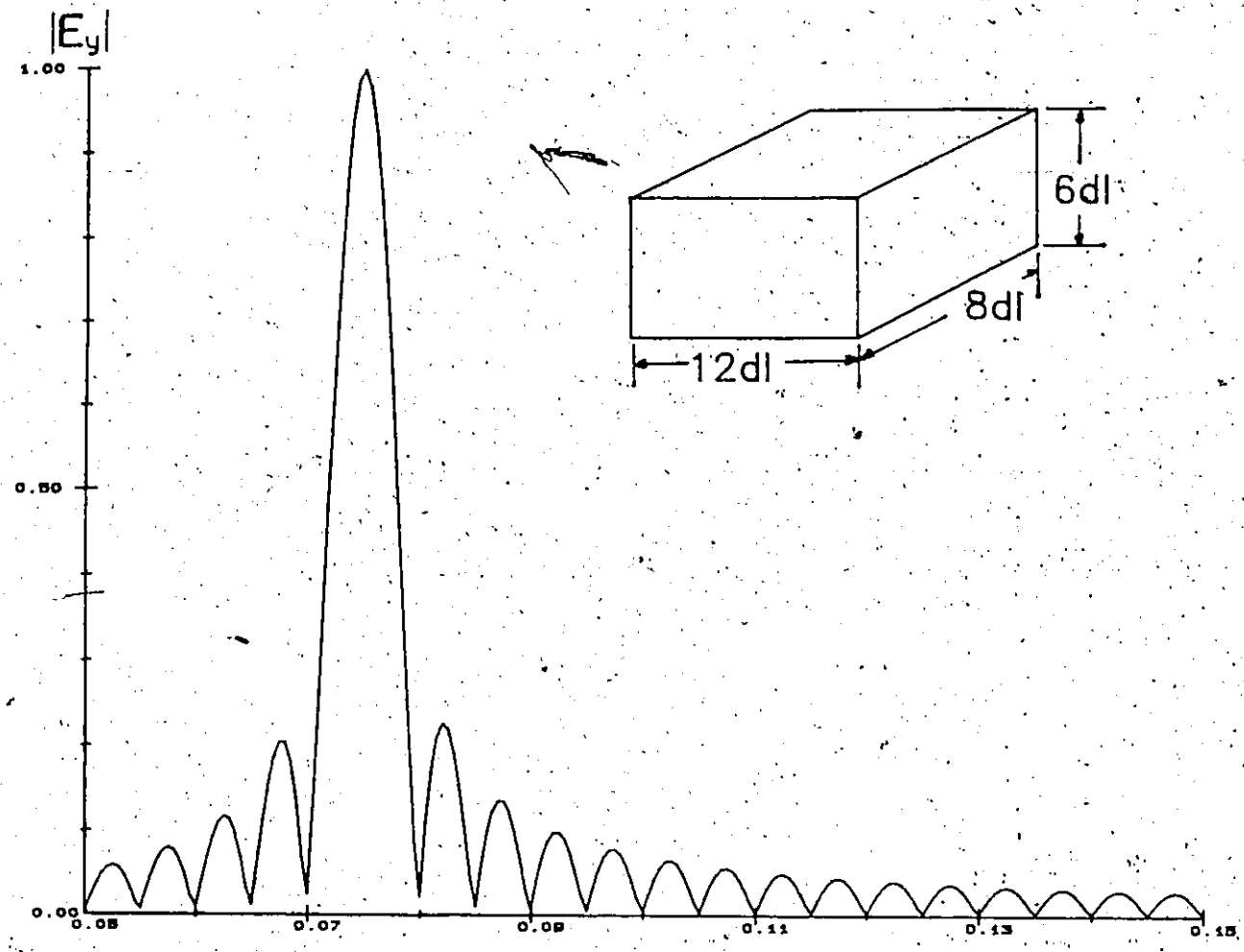

Fig. 3.3 Frequency spectrum of TE_{101} mode of a rectangular cavity

The frequency spectrum obtained from the above summation consists of a series of delta functions in the frequency domain corresponding to the eigenvalues of the given structure under consideration. However, the truncation of the output in the time domain from ∞ to a finite number N causes the spreading out of the solution into sinx/x type curves.

Fig.3.3 shows a typical output curve for the TE_{101} mode in a rectangular cavity. The width of the main lobe in this curve is inversely proportional to the total number of time steps used. For greater resolution in the frequency domain, a sufficient number of time steps must be used to seperate the solution points clearly and reduce the error caused by time truncation of the output.

3.3 ERROR ANALYSIS OF THE TLM METHOD

3.3.1 Truncation Error

The need to truncate the output impulse function leads to the so-called truncation error. Due to the finite duration of the impulse response, its Fourier transform is not a line spectrum but rather a superposition of sinx/x functions which may interfere with each other such that their maxima are slightly shifted. The resulting error in the eigenfrequency, or truncation error, is given[7] by

$$E_t = 3\lambda_c/DN^2\pi^2\Delta\ell \qquad (3.8)$$

where λ_c is the eigenwavelength and $\Delta\ell$ is a step size of the TLM network. N is the number of iterations and D is the distance in the frequency domain between two neighboring spectral peaks.

This expression shows that the truncation error decreases with increasing separation S and increasing number of iteration N. It is thus desirable to suppress all unwanted modes close to the desired mode by choosing appropriate input and output points in the network. Saguet and Pic [20] have proposed a technique to suppress sidelobes by employing various window function in the Fourier transform.

3.3.2 Velocity Error

Due to the periodic structure of the TLM network, the wave propagation in the network experiences filtering effects. These effect usually cause network simulation to deviate from actual space wave propagation, resulting in velocity error.

If the wavelength in the TLM network is large compared with the network parameter $\Delta\ell$ which is distance between the grid points in spase, it can be assumed that the fields propagate with the same velocity in all directions. However when the wavelength decreases, the velocity depends on the direction of propagation[6]. Johns[6] has derived the velocity reduction characteristic for the axial direction.

When the propagation occurs essentially in this direction, i.e. at cutoff frequencies of TE_{no} or TE_{on} modes, this error can be corrected directly using dispersion relation:

$$v_p/c = \theta/2\mathrm{Sin}^{-1}\ (\sqrt{2}\sin\theta/2) \qquad (3.9)$$

$$\text{with } \theta = \omega\Delta\ell/c$$

This concept has been proposed and implemented by Shih and Hoefer [21] to reduce velocity error.

3.3.3 Coarseness Error

The coarseness error occurs when the TLM mesh is too coarse to resolve highly nonuniform fields found at corners and wedges. This error is particularly bothersome when analysing planar structures which contain such regions. A possible but impractical measure would be to choose a very fine mesh. However this leads to large memory requirements particularly for three-dimensional problems. A better response is to introduce a network of variable mesh size to provide higher resolution in the nonuniform field region [22]. this approach, however, requires more complicate programming and is described in the next section.

Shih and Hoefer[21] have proposed an extrapolation technique which employs several different simulations with different mesh sizes and the extrapolation of results. This technique also requires considerable computer resources and

involves engineering approximations. Additionally, utilizing a very high density mesh may increase computer round-off error. Therefore it is important to choose a mesh size between the extremes.

3.3.4 Error From Misalignment of Metalization and Dielectric Interface

Due to the particular way in which boundaries are simulated in a three-dimensional TLM network, dielectric interfaces appear half-way between nodes, while electric and magnetic boundaries appear across such nodes. This can be a problem when simulating planar structures such as microstrip or finline.

The reasoning behind the misalignment of this may be explained in detail as follows.

Referring to Fig.3.4, a conductive boundary in the x-z plane is represented by short circuiting E_{zn}, E_{xn}. However if the dielectric is only below the level ABCD and its relative permittivity is loaded on the open circuit shunt stubs of the nodes $E_{x1}, E_{x2}, E_{z1}, E_{z5}$ etc., the effect of the dielectric will be extended as far as the level $E_{y1}, E_{y2}, E_{y5}, E_{y6}$. This means that a metalic strip laid on a dielectric would have some dielectric overflow over the sides of the strip. The effect of dielectric overflow can only be reduced if a fine mesh is used to represent the dielectric.

3.4 VELOCITY ERROR CORRECTION IN THE 3-D TLM METHOD

Johns has shown that relatively high errors in higher order cutoff frequencies might be attributed to the different angles of propagation [7]. He heuristically explained the similarity between TLM network wave propagation and geometric- optic ray propagation. This concept will be extended here to the three-dimensional case. Once the propagation angle is calculated, it will be used to correct the velocity error in the TE_{101} mode solution.

Let us consider the modal solutions in a rectangular resonator resulting from the interaction of plane TEM waves inclined to each other. A possible path of a pulse wavefront contributing to the TE_{101} mode is shown in Fig.3.5, where a and b dimensions are in x and z directions, respectively. For this mode, the angle of the ray and x direction is

$$\phi = \tan^{-1}(b/a) \qquad (3.10)$$

For one full closed path, the pulse wavefront travels distance l given by

$$l = 2 \times a/ \cos (\phi) \qquad (3.11)$$

During this time the network wave must propagate the distance $l' = 2 \times (a + b)$. If we relate this angle to the dispersion characteristics given in (3.9), we can easily obtain the follwing corrected formula:

$$\sin (r \times \beta_g/2) = 2 \times r \times \sin(\phi/2) \qquad (3.12)$$

where $r = l / l'$

After simplifying (3.12), the corrected value obtained is

$$dl/\lambda|_{cor} = r \times \mathrm{Sin}^{-1}\{2 \times r \times \sin(\pi \times dl/\lambda|_{uncor})\} \quad (3.13)$$

For the general modes TE_{mon} a and b are replaced by an and bm, in equation (3.10).

We have applied the correction formula (3.13) to the resonant frequencies of inhomogeneous structures, shown in Fig. 3. 6. The possible dominant mode is the quasi TE_{101} type. The E_y field was excited with a distribution corresponding to the well-known analytical solution. As expected, an improvement of the results is noted. Henceforth, we employ this correction formula for any solution of a rectangular type resonator.

3.5 TLM ANALYSIS WITH STEPPED IMPEDANCE CONCEPT

To obtain the dispersion characteristics of a waveguiding structure using the TLM, a quarter wavelength section is usually considered, where different values of β and ω are simulated by using different cavity lengths. The disadvantage of this procedure is that for low frequency calculations, very long cavities must be used. Johns and Sitch [59] have proposed a very simple technique, which enables the length of the cavity to be no more than two mesh lengths in

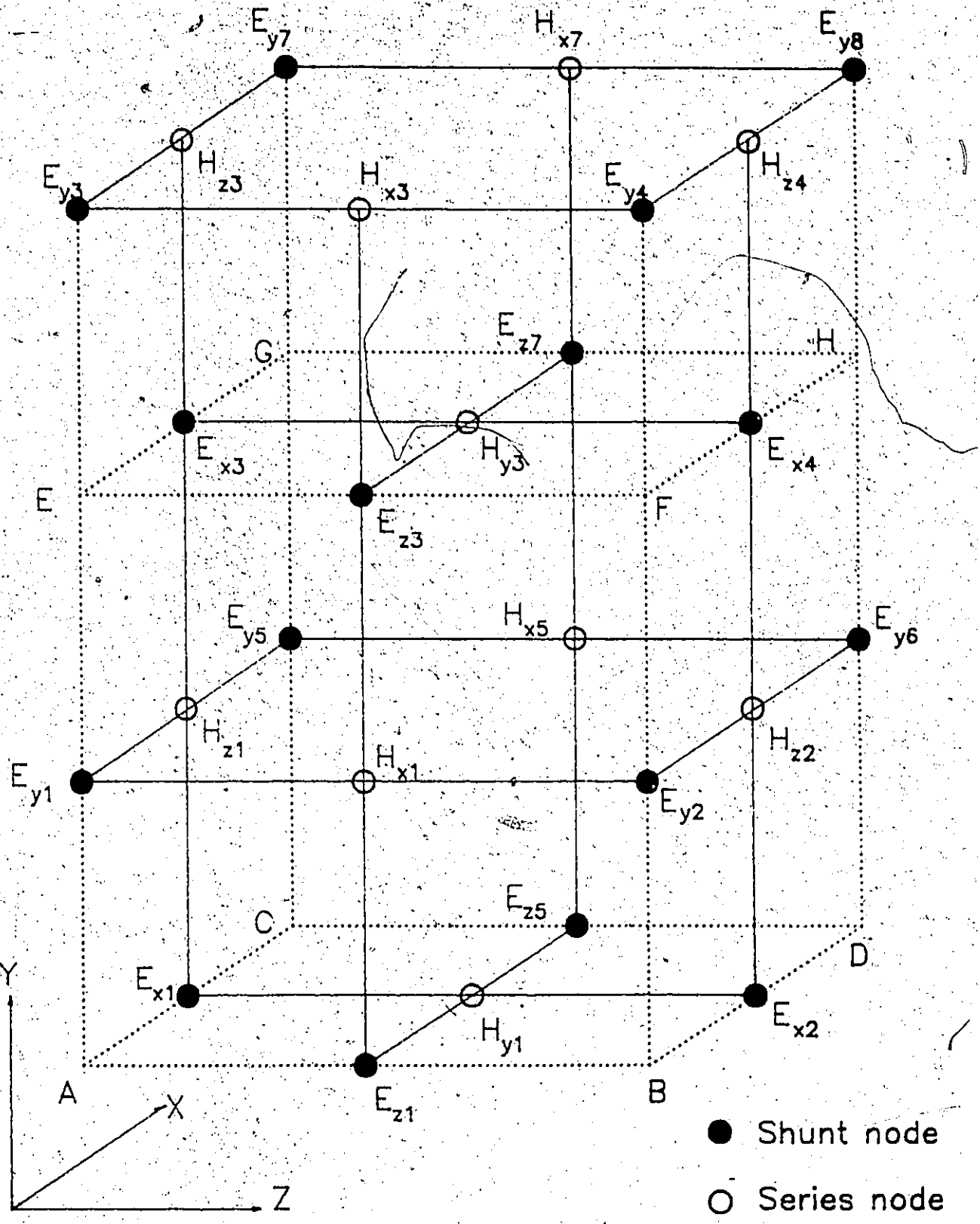

Fig. 3.4 One and a half element section in 3D TLM network model

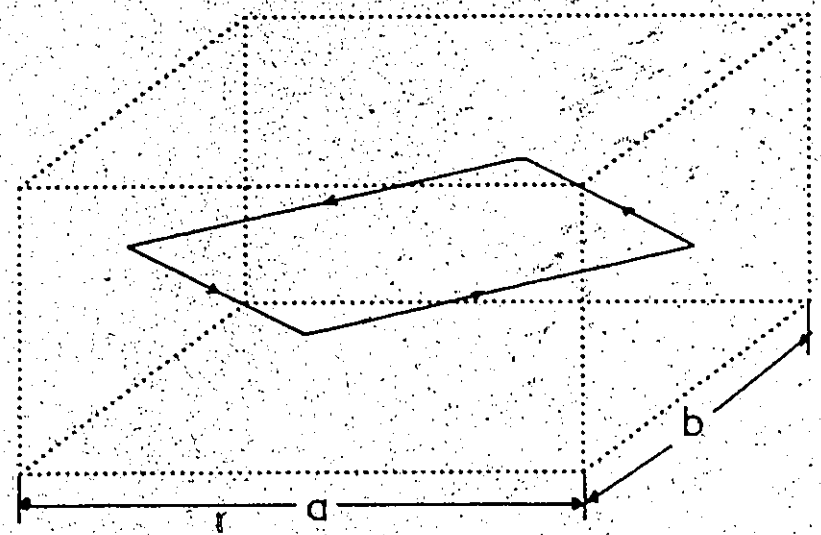

a)

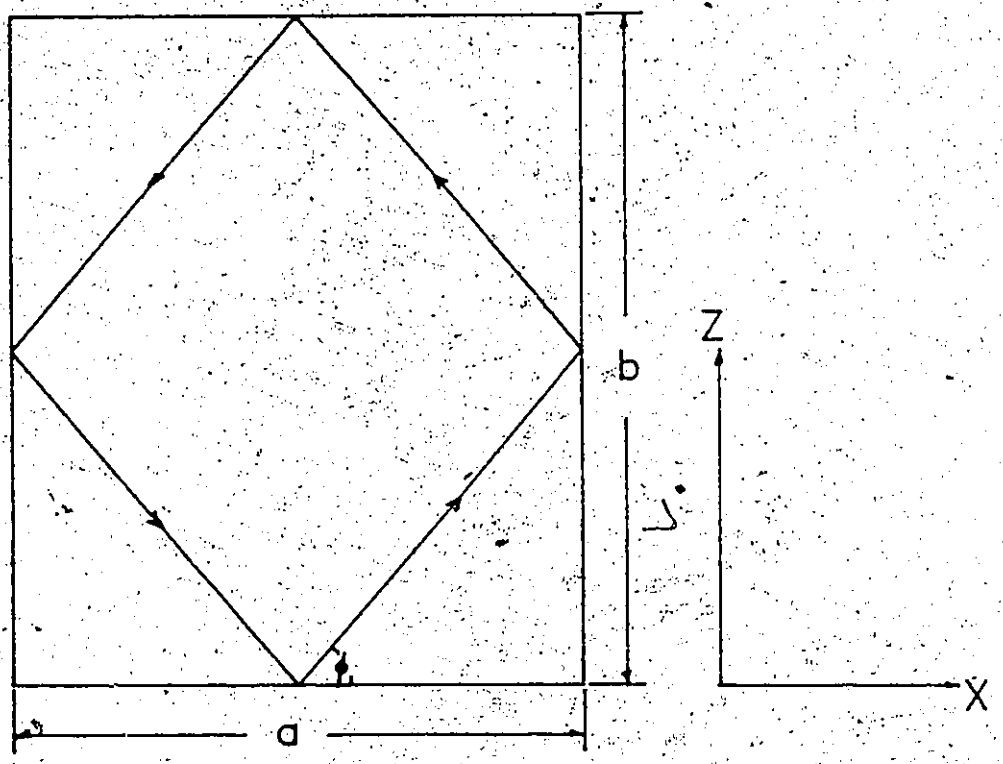

b)

Fig. 3.5 A rectangular cavity and corresponding wave propagation rays

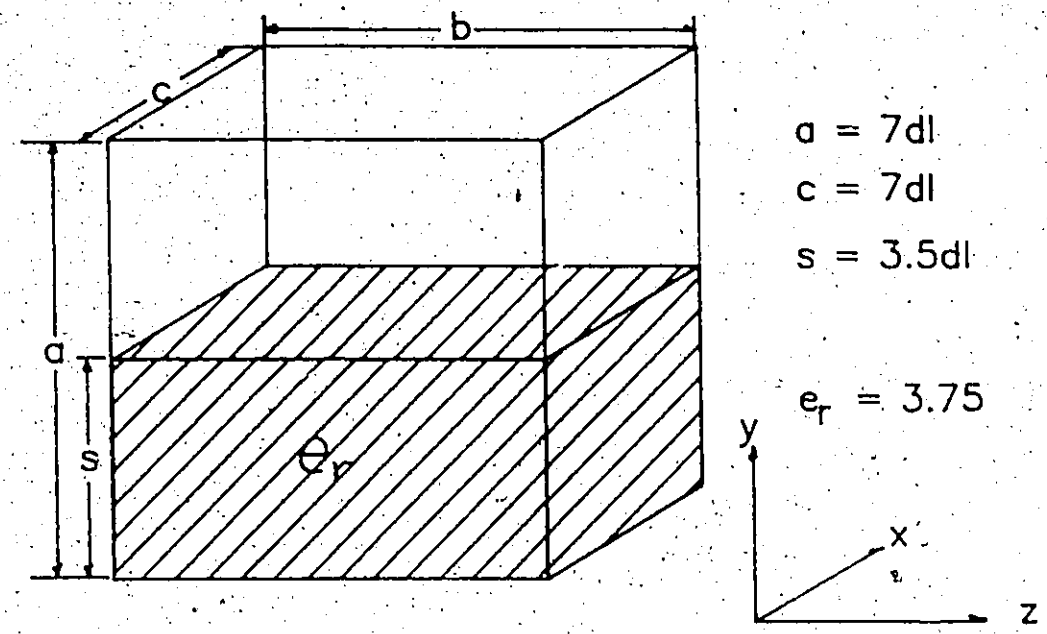

e_r	b/dl	exact value	TLM method	
			original (error%)	corrected (error %)
1.	5	0.12289	0.12180(0.81)	0.12281(0.07)
	6	0.10975	0.10920(0.5)	0.10955(0.18)
	7	0.10102	0.10040(0.6)	0.10093(0.08)
	8	0.09491	0.09440(0.54)	0.09476(0.16)
	9	0.09049	0.09000(0.54)	0.09031(0.2)
e_r	5	0.08701	0.08700(0.1)	0.08644(0.64)
	6	0.07866	0.07940(0.93)	0.07819(0.5)
	7	0.07331	0.07440(1.45)	0.07286(0.6)
	8	0.06954	0.07060(1.49)	0.06878(1.09)
	9	0.06690	0.06780(1.32)	0.06634(0.83)

Fig. 3.6 A partially filled rectangular resonator and its solutions by corrected formular given in (3.13)

two-dimensional analysis and 2.5 mesh lengths for three-dimensional analysis. They reported that the saving in computer time and storage is as great as 100 times. The key point which made this achievement possible is the incorporation of the spatial variation of the fields in the direction of propagation to modify the properties of the transmission line matrix.

Their technique has been tested on microstrip cavities and they obtain very good agreement when comparing the results with conventional TLM and other existing techniques. The only disadvantage is that the technique is only applicable to structures which are uniform in the direction of propagation.

3.6 SIMPLIFIED NODE CONCEPT

Conventional three-dimensional TLM networks require three shunt and three series nodes for the representation of one unit cell as given in Fig.3.2. Should we want all the nodes in one unit cell to be at the same space point, we can gradually move all shunt nodes to series nodes or vice versa. Referring to Fig. 3.4 and A.1, the connecting lines of AE_{x1}, AE_{y1}, $E_{y1}H_{z1}$, $E_{y1}H_{x1}$, $E_{z1}H_{x1}$, $E_{x1}H_{z1}$, $E_{x1}H_{y1}$ and $E_{z1}H_{y1}$ shrink to 0 and the other section of the nodes increases to dl. Therefore the side length of the unit cell is not changed(see Fig. 3.7).

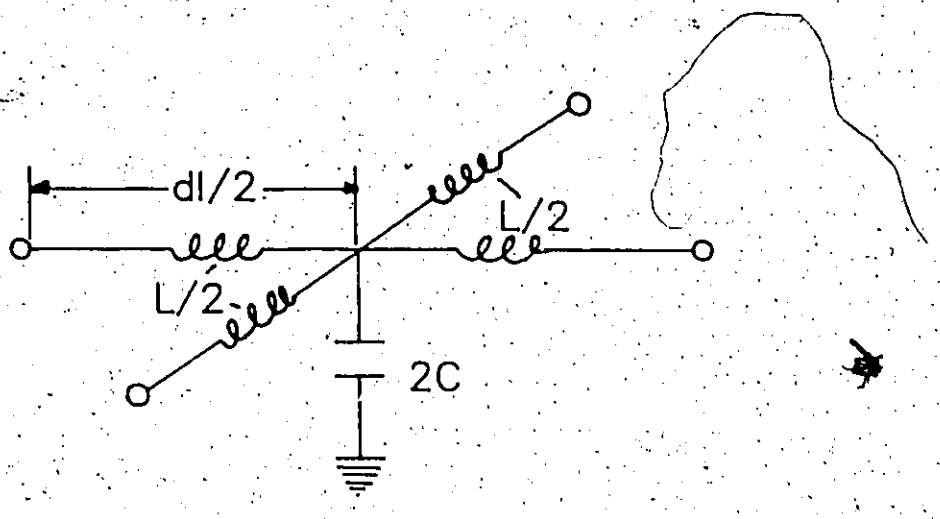

a) A unit cell of the conventional TLM network

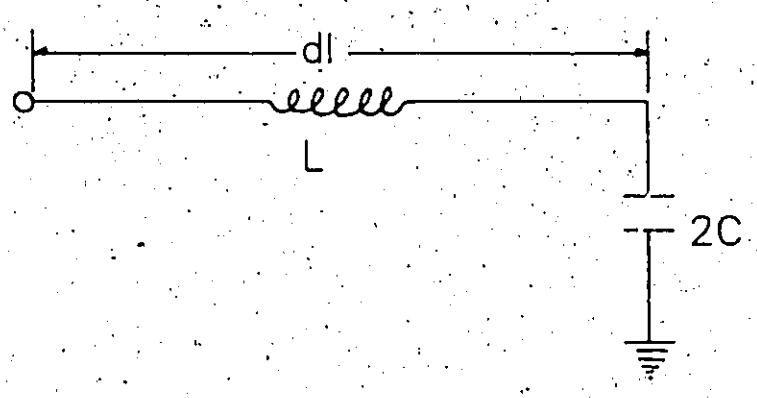

b) A unit cell of the simplified TLM network

Fig. 3.7 A simplified unit cell proposed by Saguet [24].

This concept has been proposed by Saguet and Pic[24] and is equivalent to using short transmission line sections of two rather than three lumped elements. Losses and dielectric or magnetic loading can be simulated with stubs in the same way as discussed previously.

The dispersion characteristics of the network have been derived by a procedure similar to the original TLM. Detailed calculations are given in Appendix A. The final expression is :

$$v_p/c = \theta/[2\sin^{-1}(\sqrt{1+Y_o}\,\sin(\theta/2)\sqrt{1+3\cos^2(\theta/2)/((1+Y_o)\cos\theta)})] \tag{3.14}$$

with $\theta = \omega\Delta\ell/c$

Although some simplification has been made in computer programming, compared to the original TLM, virtually no savings in computer memory and numerical algorithm have been gained. This algorithm still requires 12 real memory spaces and 6 for inhomogeneous stubs.

A computer program based on this simplified node concept has been written to test its capabilities, but the results are slightly less accurate and take more CPU time than the original TLM. The reason for the additional error may be due not only to high velocity error shown in Fig.3.8 but also to an unrealistic wave propagation concept as explained in the following.

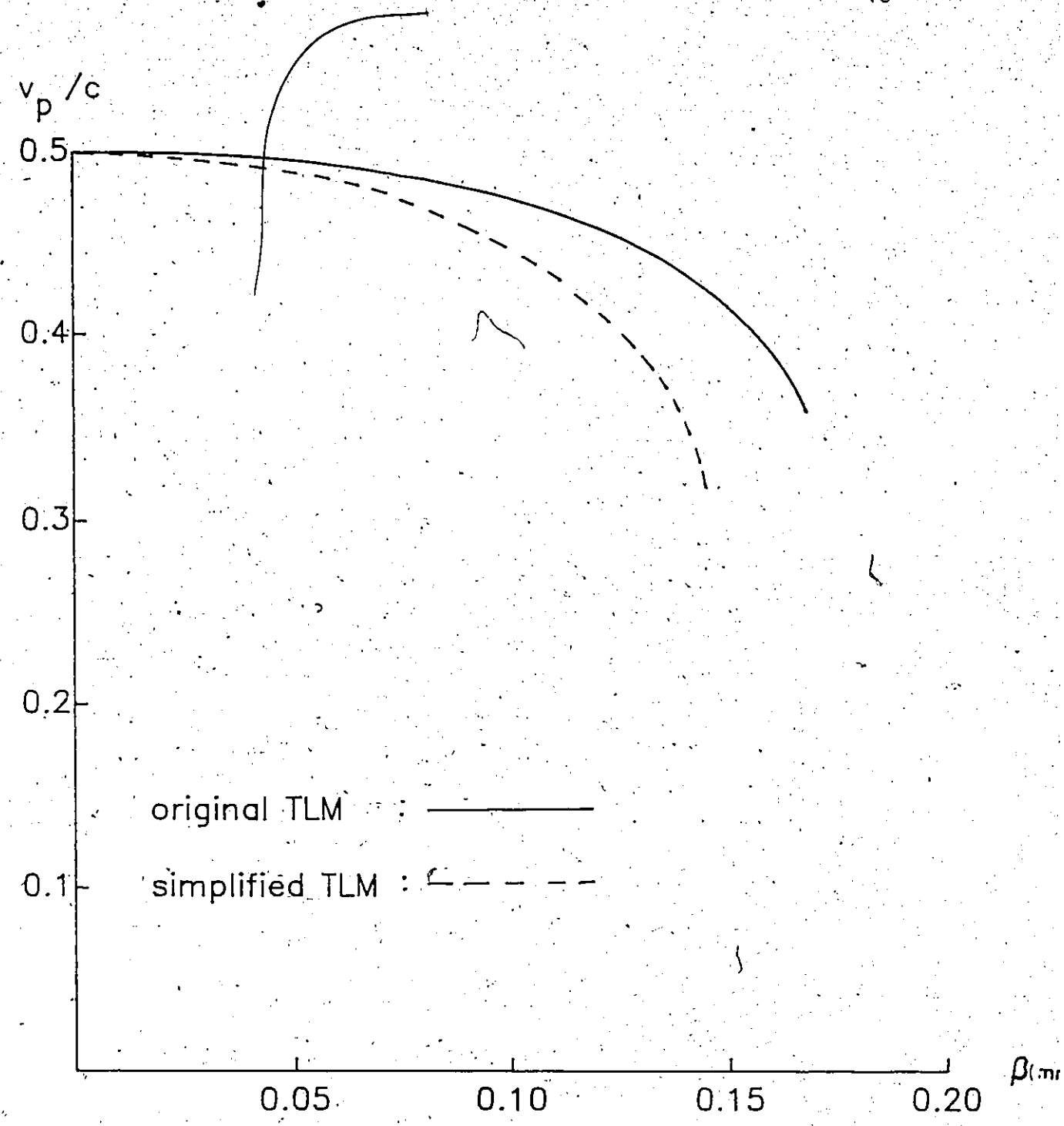

Fig. 3.8 The phase velocity characteristics of the simplified TLM network proposed by Saguet

Akhtarzad and Johns has shown that the propagation of a transverse plane wave can be illustrated very realistically in the three-dimensional TLM network [16] if shunt nodes are situated in the middle between series nodes and vice versa. However, in the simplified node concept, the asymmetrical nature of the nodes does not allow cancellation of the E_z, and H_z components from E_y, and H_x excitation, as is the case in the original TLM. This leads to unrealistic simulation of transverse EM wave propagation. This phenomenon may contribute to a relatively larger error in this simulation.

The field quantities calculated by the TLM method are space-averaged values ,i.e. they are constant in each unit cell. Therefore the hybrid nature of the three-dimensional TLM network may not be as unrealistic as it would at first appear. In this sense , it may be questionable to regard the simplified network to be more realistic than the original TLM.

It has been observed that generaly, the CPU time for simplified node program is 10 % longer than for the original TLM.

3.7 VARIABLE MESH ALGORITHM FOR THE TLM METHOD

In order to ensure synchronism, the conventional TLM network uses a uniform mesh parameter throughout. This can lead to considerable numerical expenditure if the structure contains sharp corners or fins producing highly nonuniform fields and thus demands a high density mesh. Saguet and Pic[22] and Al-Mukhtar and Sitch[23] have independently proposed ways to implement irregularly graded TLM meshs which allow the network to adapt its density to the local nonuniformity of the fields. Both methods are briefly discussed and reviewed in the following.

The unit element of the variable mesh TLM by Saguet and Pic[22] is shown in Fig.3.9 a). This modified TLM with variable mesh size requires different characteristic impedances in the different node branches, while the phase velocity must be the same in all cells regardless of the mesh size. To keep the velocity of travelling impulses the same in all branches, the inductivity per unit length of the longer mesh lines is increased by a factor N, while their capacitance per unit lenth is reduced by 1/N. This , in turn , increases their characteristic impedance by a factor N. Then the equivalent network equation becomes:

$$\begin{aligned} \partial V_y/\partial z &= -L_1 \partial NI_z/\partial t \\ \partial V_y/\partial x &= -L_1 \partial I_x/\partial t \\ \partial NI_z/\partial z + \partial I_x/\partial x &= -2C_1 \partial V_y/\partial t \end{aligned} \qquad (3.15)$$

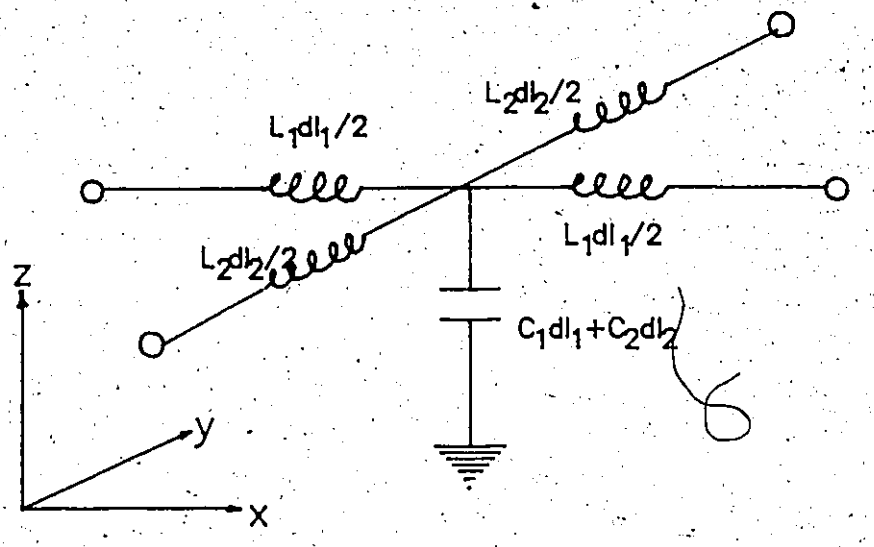

$dl_2 = N dl_1$

$L_2 = NL_1$

$C_2 = C_1/N$

N : grading ratio

a) a unit cell of the variable mesh network by Saguet

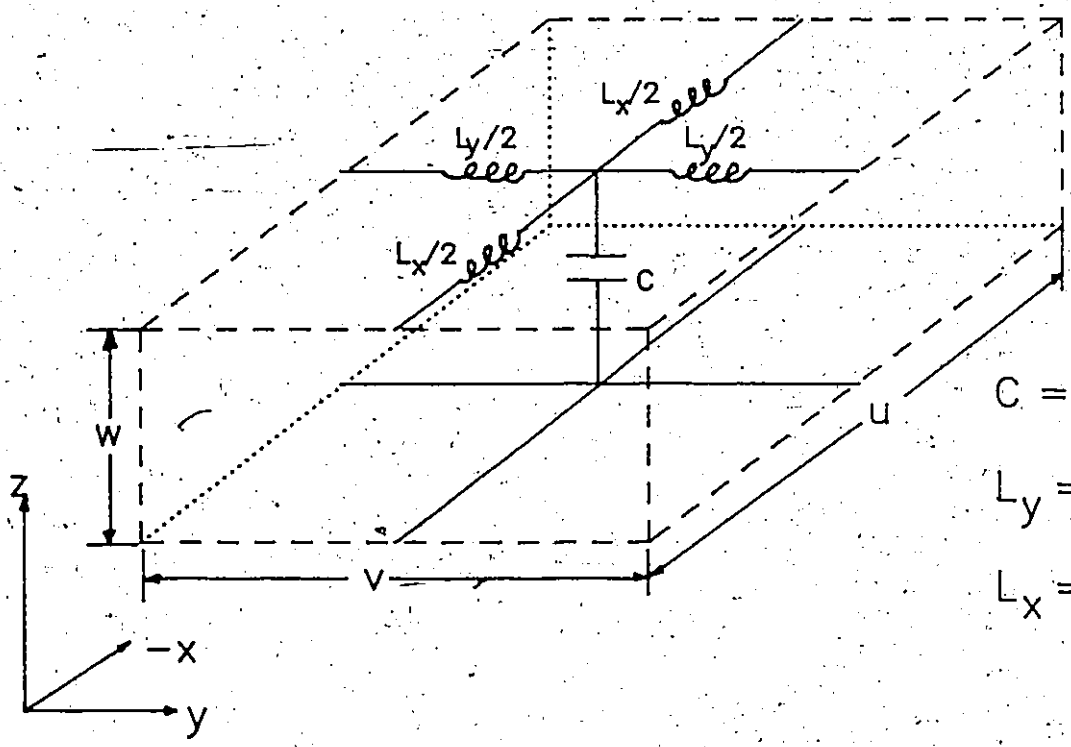

$C = uv/w$

$L_y = wv/u$

$L_x = wu/v$

b) a unit cell of the graded mesh network by Al-Mukhtar

Fig. 3.9 The unit cells of two modified TLM networks

In this network, the reflected and incident waves are related by

$$V_n = 2 \bar{x} \Sigma_m Y_m V_m / \Sigma Y_m - V_m \quad , \quad (3.16)$$

where Y_m is the characteristic admittance of the m-th branch. Therefore , the TLM simulation in a mesh of variable size is very similar to the original TLM concept in that it employs different characteristic impedances as in (3.16). To preserve synchronism, impulses travelling on longer branches are kept in store for N iterations before being reinjected at the next node. For synchronism purposes, the length of each side of the longer line must be an odd integer multiple N of the smallest cell length in the network.

Saguet and Pic have applied this technique to a unilateral finline to calculate the resonant frequencies of a finline resonator[25]. Although computation time was reduced considerably, numerical results show that the accuracy is also worse than that of original TLM program. Furthermore, the added complexity of the algorithm makes this technique less attractive.

A different approach, called a graded index TLM, has been proposed by Al-Mukhtar and Sitch[23]. In order to grade the space irregularly, they incorporated the physical dimensions

of the network element in the unit cell network equations describing the currents and voltages of the lines. Then the total capacitances and inductances of the lines become functions of the element dimensions.

Referring to the three-dimensional unit cell given in Fig. 3.9 b), the network parameters are given as;

$$C_x = \varepsilon\ vw/u \qquad L_x = \mu\ vw/u$$

$$C_y = \varepsilon\ uw/v \qquad L_y = \mu\ uw/v \,. \qquad (3.17)$$

$$C_z = \varepsilon\ uv/w \qquad L_z = \mu\ uv/w$$

where C_x is the capacitance at the shunt node to x direction (E_x) and L_x is the inductance seen by current circulation in the yz-plane i.e. perpendicular to the x-direction.

The basic equations (3.17) give the six fundamental parameters, at each mesh element, in terms of its physical dimensions and properties. In order to ensure time synchronization when shunt and series scatterings are performed successively in each iteration, they assumed unit length, called "link line", between any two nodes. Any additional inductances and capacitancies due to mesh grading given in (3.17) must be loaded by shunt stubs at the shunt node or by series stubs at the series node.

These additional stub parameters C, and L can be calculated as :

$$Y_x = 4\,(\varepsilon_r\, wv\sqrt{h}/u - 1), \quad Z_x = 4\,(\mu_r\, vw\sqrt{h}/u - 1)$$

$$Y_y = 4\,(\varepsilon_r\, uw\sqrt{h}/v - 1), \quad Z_y = 4\,(\mu_r\, uw\sqrt{h}/v - 1) \qquad (3.18)$$

$$Y_z = 4\,(\varepsilon_r\, vu\sqrt{h}/w - 1), \quad Z_z = 4\,(\mu_r\, vu\sqrt{h}/w - 1)$$

where h is a correction factor and all impedances are normalized to $\sqrt{\mu_o/\varepsilon_o}$ The significance of h can be seen from equation (3.18), where some times the factor wv/u or wu/v becomes less than 1 because of the degree of grading, in which case the corresponding stub will have an unrealistically negative impedance. Therefore the value of h is chosen to offset the above inequality so that all the matrix stubs have positive or zero impedance.

The three-dimensional graded TLM computer algorithm can be easily obtained by modification of the conventional TLM. Extra calculations are to obtain the admittances and impedances of (3.18). Then three shunt and three series stubs are connected to the appropriate node of the unit cell. For inhomogeneous media, ε_r or μ_r of (3.18) are functions of position.

The properties of the three-dimensional network, i.e. the phase velocity characteristics, are virtually identical to the original TLM mesh with impedance and admittance stubs, even when homogeneous structures are considered. A difference arises when Fourier transformation is carried out due to the grading factor h. The effect of h can be seen on examining the spectrum, representing the output:

$$S(dl/\lambda) = \sum_n F_n \exp j(2\pi n dl/\sqrt{h}\lambda) \qquad (3.19)$$

We can see from (3.19), higher values of h require more iterations for the same frequency resolution than the uniform mesh technique. This is a serious disadvantage of this technique, and it somewhat limits the grading ratio if a reasonable number of iterations is employed.

3.8 DISCUSSION

This chapter has reviewed several important papers which have reported some improvement over the original TLM technique. The main sources of errors have been discussed, and three-dimensional error corection formulae by extension of the two-dimensional concept have been obtained. A simple example showing the capability of these formulae is also presented. In order to reduce computer resources further, variable mesh techniques have been developed independently, and they have been reviewed and discussed briefly.

So far, the graded mesh TLM method by Al-Mukhtar and Sitch might be the most appropriate model for complicated practical structures. It utilizes both admittance and impedance stubs to represent the modification of the unit mesh length (link line). Therefore a longer mesh line is equivalent to higher values of permittivity and permeability. Conceptually, this three-dimensional graded mesh technique

is very simple, and the additional effort to implement it is minor. A general program has been developed, which incorporates all improvements which includes three-dimensional error corection features and is based on their algorithm[23]. It has been applied to various geometrical structures.

However, even with this grading technique, some planar waveguide structures, for example finlines, require extensive computer resources. The CPU time on VAX 750 VMS system, ranges from several minutes to several hours depending on the complexity of the geometry. This is due to the large memory requirements of the graded TLM. The storage requirement per node has been increased to 32 real memory variables from 22 for the conventional TLM. Furthermore the higher grade ratio h necessitates considerable additional number of time steps for the same frequency resolution. These large memory demands and additional iteration requirements led the author to search for alternative techniques which require less computer resources without sacrificing the simplicity and accuracy of the TLM method. As a result, two different techniques have been developed, and tested extensively. They will be treated in the following chapters and form the major part of the thesis.

Chapter IV

DEVELOPMENT OF SCALAR TLM TECHNIQUE

4.1 INTRODUCTION

In the traditional TLM method of numerical analysis, the propagation of all six components of the electromagnetic field is simulated by the propagation of corresponding voltage and current impulses in a complicated hybrid transmission line mesh. This leads to considerable memory and CPU time requirement. The simulation of all six components is redundent in many practical cases where modes of propagation or resonance can be separated into TE and TM modes (or LSE and LSM).

To obtain the eigenvalues and field configurations of such TE or TM modes, only one field component or, alternatively, one Hertzian potential needs to be simulated. Since such a component or potential satisfies the scalar Helmholtz equation, a new scalar TLM network is proposed in this chapter for the efficient solution of this class of problems.

The scalar TLM model has been applied successfully by the author to the analysis of cylindrical structures with homogeneous dielectric and simple inhomogeneous structures such

as dielectric slab loaded rectangular waveguide. In the following, the properties of the scalar TLM network will be described, and the performance of the method will be demonstrated by sample solutions.

4.2 TLM MODEL FOR SCALAR MODE PROPAGATION

Consider a unit cell of the new three-dimensional network which consists of a two-dimensional TLM network to which additional transmission lines are connected orthogonally at each junction as shown in Fig.4. 1. a). In practice, such a circuit may be realized by interconnecting six-port coaxial line junctions. Since the dimensions of a unit cell must be small compared with the wavelength, the voltages at the six ports are effectively equal to the voltage at the node. Under this assumption, the basic transmission line theory yields the following equations:

$$\nabla \cdot \bar{I} = -3C\, \partial V/\partial t \qquad (4.1.a)$$

$$\nabla\ V = -\, L\, \partial \bar{I}/\partial t \qquad (4.1.b)$$

where $\bar{I} = I_x \hat{x} + I_y \hat{y} + I_z \hat{z}$ and

$$I_x = I_{x1} - I_{x2}$$

$$I_y = I_{y3} - I_{y4}$$

$$I_z = I_{z5} - I_{z6}$$

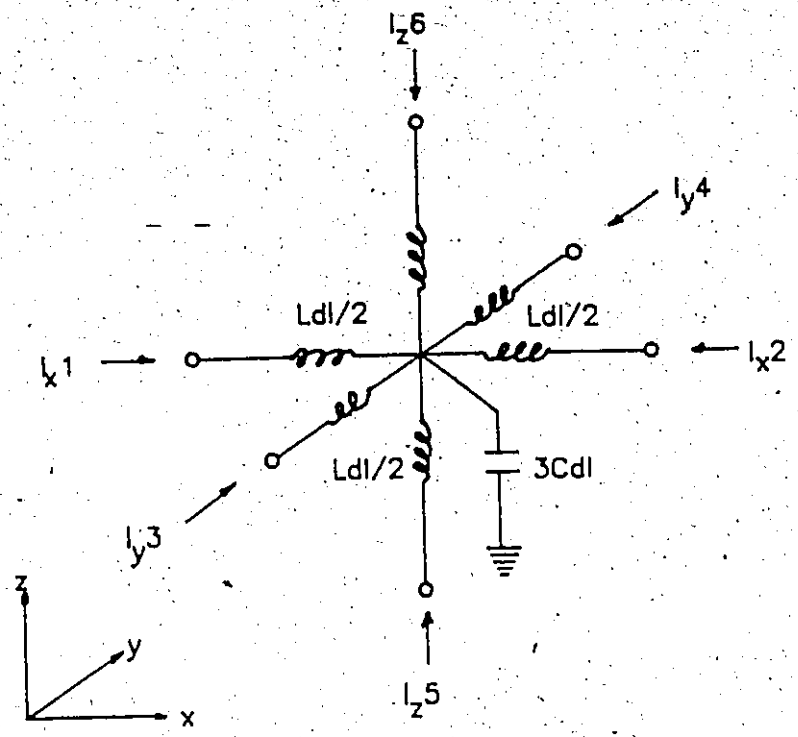

a) Equivalent network of a unit cell

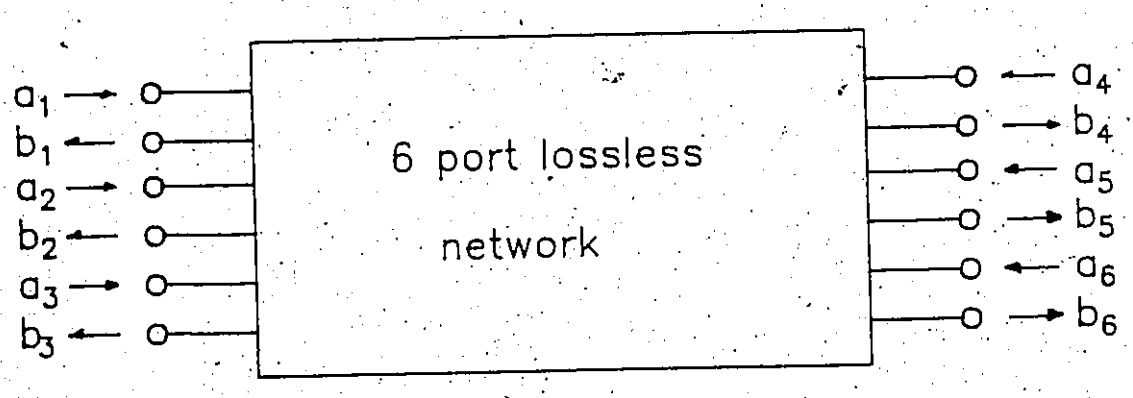

$$a_i = 1/2\ (V + I_i)$$
$$b_i = 1/2\ (V - I_i)$$

b) Six-port network representing a three-dimensional node

Fig. 4.1 A unit cell of three-dimensional scalar TLM network

These coupled equations may be decoupled, yielding the following second order differential equations in V and I:

$$[\nabla^2 - LC\, \partial^2/\partial t^2]\, V = 0 \qquad (4.2.a)$$

$$[\nabla^2 - (\nabla x \nabla x) - 3LC\, \partial^2/\partial t^2]\, \bar{I} = 0 \qquad (4.2.b)$$

Note that although equation (4.2.b) may not look like a wave equation, the second term involving the double curl of $\bar{I}$ is zero as a consequence of (4.1.b).

This suggests that the three-dimensional network given in Fig.4.1.a) can be utilized to simulate the propagation of a voltage wave in three-dimensional space. By using the well known scattering parameter formulation, one can express (4.2.a) in the following way.

Each node can be considered as a lossless six-port (see Fig.4.1.b) which can be used as a basic element of a three-dimensional TLM network and is characterized by the scattering matrix S. The wave quantities propagating in this network satisfy the following scalar wave equation.

$$[\nabla^2 - 3LC\, \partial^2/\partial t^2]\, \left|\begin{matrix} a_q \\ b_q \end{matrix}\right| = 0 \quad q = 1,2, \ldots 6 \qquad (4.3)$$

where a_q and b_q are the incident and reflected waves at the q-th port.

Since in a linear medium each component of an electromagnetic field independently satisfies the scalar wave equation, expression (4. 3) can simulate any of the six components of the three-dimensional field. If we designate one field component by the scalar quantity Ψ it obeys the general wave equation.

$$\{\nabla^2 - \partial^2/(v^2\partial t^2)\}\Psi(x, y, z, t) = 0 \qquad (4.\ 4)$$

where v is the phase velocity of Ψ in this medium. Let us now discretize the space and time by dividing it into unit cells. Then equation (4. 4) becomes:

$$\{\nabla^2 - \partial^2/(v^2\partial t^2)\}\Psi(l, m, n, k) = 0 \qquad (4.\ 5)$$

where l, m, n, k are integers.

If the phase velocity v equals $c/\sqrt{3}$, the wave equations governing $\overline{I}$ and V or a_q b_q are identical. It is convenient to define Ψ as follows:

$$\Psi_{ij}(l,m,n,k) = (1/6) \sum b_q(l,m,n,k) \qquad (4.\ 6)$$

This averaging process is justified because the TLM network is linear. Furthermore, a double index i, j is required to identify the field quantity simulated by Ψ Table 4.1 describes a possible code of identification. One condition for the application of this double index scheme is that the boundaries perpendicular to pthe Hertzian vector must be

index		description of $\Psi_{i,j}$
j	1	Electric field
	2	Magnetic field
	3	Non-electromagnetic field
i	1	x - component
	2	y - component
	3	z - component

Table 4.1 Significance of the indices i, j of $\Psi_{i,j}$

planes. Therefore, in order to obtain the propagation characteristics of an arbitrary cross-sectional waveguide, it may be proper for index i to choose z-component.

The propagation in the discrete space will be described using the following formalism. The wave b_q (q = 1, 2, ---- 6) scattered at the junction (l, m, n) after the k-th iteration will become an incident wave a at the neighbouring junction at time (k+1)T. This process is similar to the "conventional TLM" interaction [7] and can be noted as follows.

$$
\begin{aligned}
a_2(l+1,\ m,\ n) &= b_1(l,\ m,\ n) \\
a_1(l-1,\ m,\ n) &= b_2(l,\ m,\ n) \\
a_4(l,\ m+1,\ n) &= b_3(l,\ m,\ n) \\
a_3(l,\ m-1,\ n) &= b_4(l,\ m,\ n) \\
a_6(l,\ m,\ n+1) &= b_5(l,\ m,\ n) \\
a_5(l,\ m,\ n-1) &= b_6(l,\ m,\ n)
\end{aligned}
\qquad (4.7)
$$

at (k+1)T at kT

Each one of these incident waves is then scattered, giving rise to a new set of reflected waves which can be obtained from the scattering parameters of the node. Hence

$$| B |_{ij} = | S |_{shunt} \times | A |_{ij} \qquad (4.8)$$

where $| A |_{ij}$ and $| B |_{ij}$ are column vectors:

$$| A | = [\ a_1\ a_2\ a_3\ a_4\ a_5\ a_6\ ]^t$$

$$| B | = [\, b_1 \; b_2 \; b_3 \; b_4 \; b_5 \; b_6 \,]^t$$

and

$$| S |_{shunt} = 1/3 \begin{bmatrix} -2 & 1 & 1 & 1 & 1 & 1 \\ 1 & -2 & 1 & 1 & 1 & 1 \\ 1 & 1 & -2 & 1 & 1 & 1 \\ 1 & 1 & 1 & -2 & 1 & 1 \\ 1 & 1 & 1 & 1 & -2 & 1 \\ 1 & 1 & 1 & 1 & 1 & -2 \end{bmatrix}$$

Since each node is a reciprocal and lossless junction, the scattering matrix | S | is symmetrical and unitary. Therefore equations (4. 7) and (4. 8) will completely characterize wave propagation in a three-dimensional structure.

As in the traditional TLM network, the phase velocity in the model is lower than that in a single transmission line, and it depends on the direction as well as on the frequency of the propagating wave. This is due to the periodical and discrete nature of the model. Therefore, in order to determine the limit of its validity, we analyze its propagation characteristic.

One can identify three fundamental directions of wave propagation as shown in Fig.4.2. They are along the main axis, the diagonal of a unit square plane and the diagonal of a unit cube. The detailed characteristic equation of

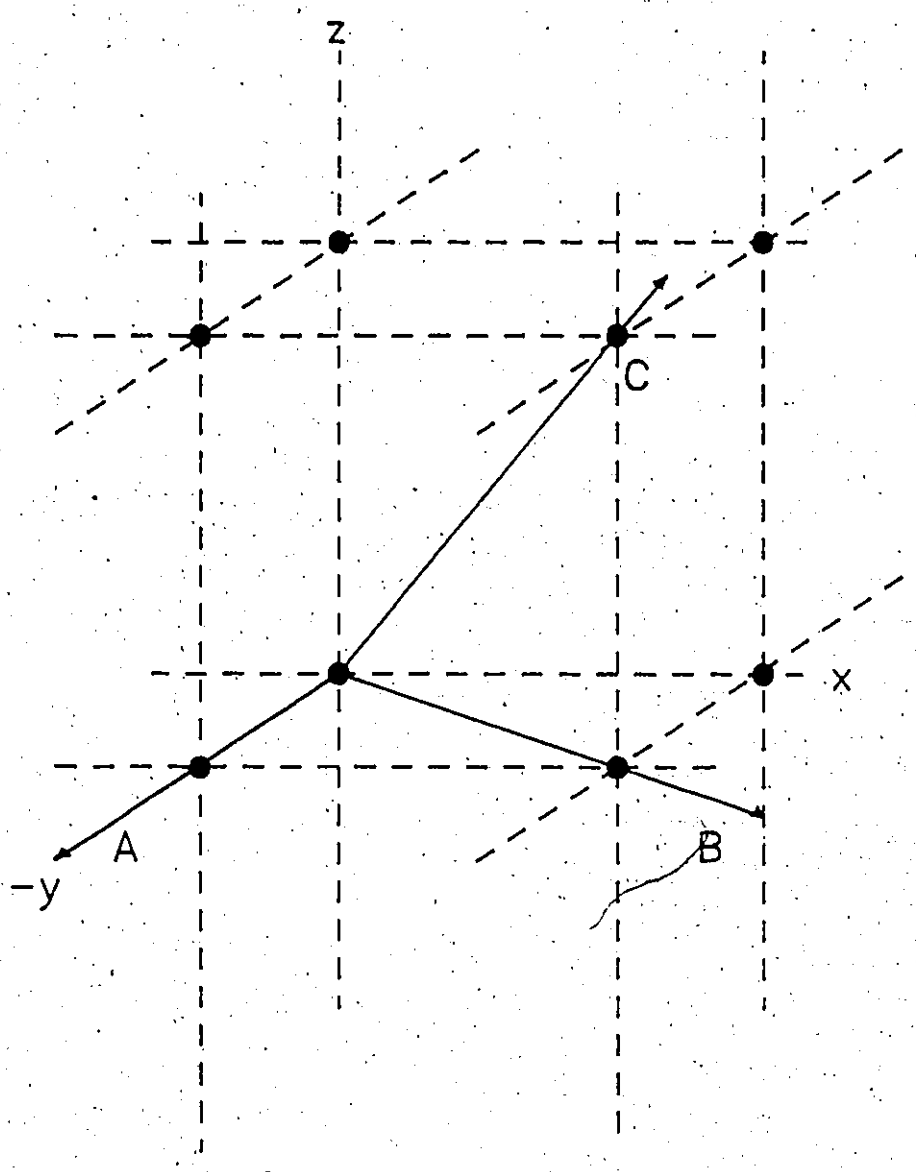

Fig. 4.2 Three fundamental directions of wave propagation in the scalar TLM network.

propagation has been derived in Appendix B from the consideration of equivalent networks of the transmission matrix along the three main directions. The final results are:

$$\sin(\beta dl/2) = \sqrt{3}\sin(\omega dl/2c) \quad \text{in direction A}$$

$$\sin(\beta dl/2\ 2) = \sqrt{3/2}\sin(\omega dl/2c) \quad \text{in direction B} \qquad (4.9)$$

$$\text{and} \qquad \beta/\sqrt{3} = \omega/c \qquad \text{in direction C}$$

The corresponding phase velocities are

$$v_A/c = \theta/\ \mathrm{Sin}^{-1}(\sqrt{3}\sin\theta)$$

$$v_B/c = \theta/\{\sqrt{2}\ \mathrm{Sin}^{-1}(\sqrt{3/2}\sin\theta)\} \qquad (4.10)$$

$$v_C/c = 1/\sqrt{3}$$

where $\theta = \omega\ dl/2c$

For low frequencies, the mesh parameter dl/λ becomes very small, and all three velocities tend toward $c/\sqrt{3}$ which confirms that the approximation made to derive equation (4. 1) is valid as long as $dl/\lambda << 1$. The Brillouin diagram of equation (4. 9) and phase velocity characteristics described by (4.10) are shown in Figs.4.3. and 4.4 respectively. One can see that the dispersion curve shows alternatively capacitive and inductive loading at a period of 2 of the normalized frequency. This is the effect of the periodic loading of the longitudinal transmission line.

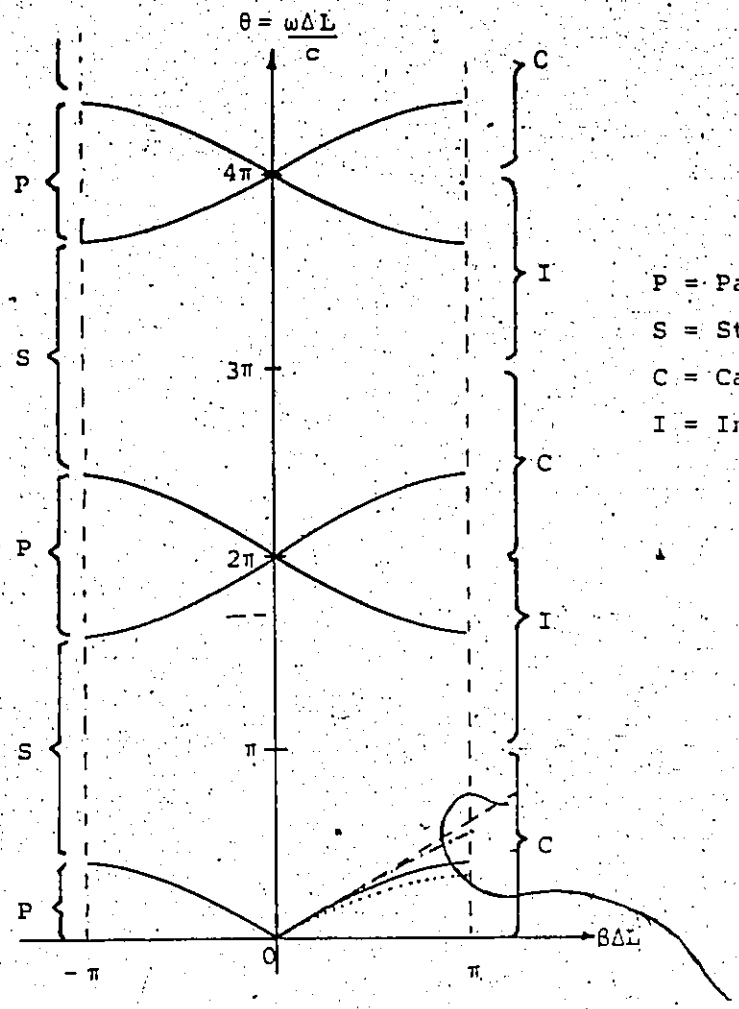

- scalar TLM
  - axial direction (A) ——————
  - diagonal direction (B) —·—·—·—·—
  - diagonal direction (C) – – – – –
- conventional TLM : axial direction .....

Fig. 4.3 The Brillouin diagram for axial wave propagation in the scalar TLM network

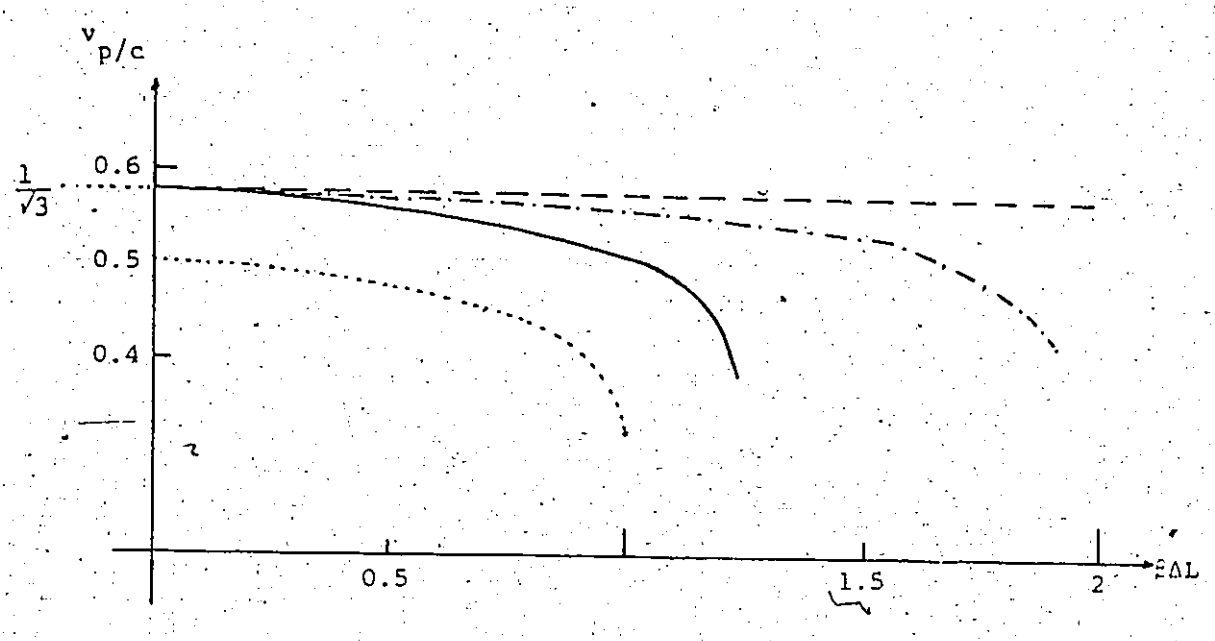

scalar TLM { axial direction (A) ——————
diagonal direction (B) —·—·—·—
diagonal direction (C) - - - - - -

conventional TLM : axial direction .....

Fig. 4.4 Dispersion diagram of the phase velocity in the scalar TLM network

4.3 BOUNDARY-CONDITIONS

The discrete nature of the TLM network requires that boundaries are also discretized in such a way that they are situated half way between two nodes and are perpendicular to the mesh lines.

Since the wave quantity Ψ can represent either transverse or longitudinal field components, it will always be reflected with a coefficient of +1 or -1 by a totally reflecting boundary, depending on the nature of the boundary (electric or magnetic wall) and the interpretation of Ψ (see Table 4.1).

At boundary nodes, the following reflection coefficient matrix $|\rho|$ can be defined:

$$|A(l_o\ m_o\ n_o)|_{i,j} = |\rho|_{i,j} \times |B(l_o\ m_o\ n_o)|_{i,j} \qquad (4.11)$$

Again, the indices i,j identify the nature of the wave function Ψ The $|\rho|_{i,j}$ matrix is a diagonal matrix:

$$|\rho|_{i,j} = \begin{Bmatrix} r1 & 0 & 0 & 0 & 0 & 0 \\ 0 & r2 & 0 & 0 & 0 & 0 \\ 0 & 0 & r3 & 0 & 0 & 0 \\ 0 & 0 & 0 & r4 & 0 & 0 \\ 0 & 0 & 0 & 0 & r5 & 0 \\ 0 & 0 & 0 & 0 & 0 & r6 \end{Bmatrix}_{i,j} \qquad (4.12)$$

The diagonal elements r1, r2,.... r6 are reflection coefficients imposed in the branches 1 to 6 respectively (see Fig.4.1). For those branches which are not terminated by a boundary, the reflection coefficient is zero. Figure 4. 5 shows three typical examples of a boundary nodes where one, two and three branches terminated by a boundary, together with their reflection coefficient matrices. In the extreme case, the number of non-zero diagonal elements would be five. Six non-zero elements would be characteristic of a completely enclosed node.

As mentioned before, the sign of the non-zero reflection coefficients depends on the indices i,j, i.e. the nature of the wave junction Y and the nature of the respective boundary. Even though the determination of the reflection coefficients appears complicated, it is actually straightforward in a practical problem.

Consider a simple rectangular cavity as shown in Fig.4.6.a) which is entirely enclosed by electric walls. For any boundary node, it is easy to determine which branches are not terminated by a boundary. The corresponding diagonal elements are thus equal to zero. The remaining non-zero elements are then obtained from Table 4.2. If any of the electric boundaries is replaced by a magnetic wall the sign of the corresponding reflection coefficients is inverted.

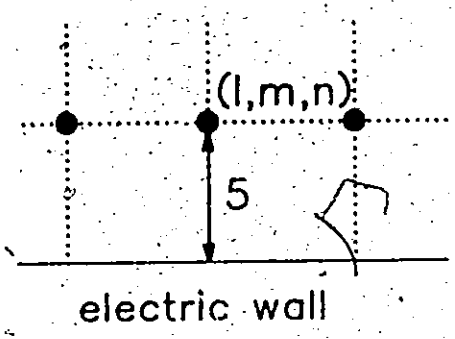

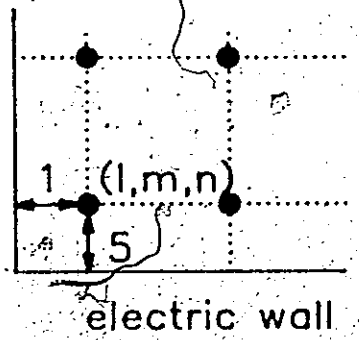

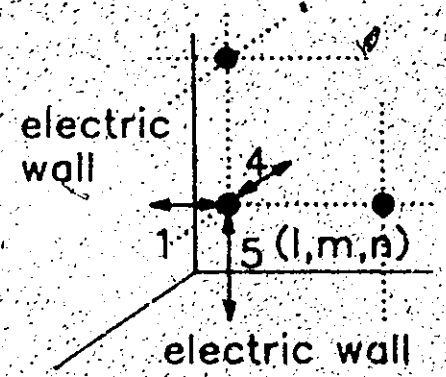

$$\psi_{3,1} = \begin{bmatrix} 0 & 0 & 0 & 0 & 0 & 0 \\ 0 & 0 & 0 & 0 & 0 & 0 \\ 0 & 0 & 0 & 0 & 0 & 0 \\ 0 & 0 & 0 & 0 & 0 & 0 \\ 0 & 0 & 0 & 0+1 & 0 & \\ 0 & 0 & 0 & 0 & 0 & 0 \end{bmatrix} \qquad \psi_{3,1} = \begin{bmatrix} -1 & 0 & 0 & 0 & 0 & 0 \\ 0 & 0 & 0 & 0 & 0 & 0 \\ 0 & 0 & 0 & 0 & 0 & 0 \\ 0 & 0 & 0 & 0 & 0 & 0 \\ 0 & 0 & 0 & 0+1 & 0 & \\ 0 & 0 & 0 & 0 & 0 & 0 \end{bmatrix} \qquad \psi_{3,1} = \begin{bmatrix} -1 & 0 & 0 & 0 & 0 & 0 \\ 0 & 0 & 0 & 0 & 0 & 0 \\ 0 & 0 & 0 & 0 & 0 & 0 \\ 0 & 0 & 0-1 & 0 & 0 & \\ 0 & 0 & 0 & 0+1 & 0 & \\ 0 & 0 & 0 & 0 & 0 & 0 \end{bmatrix}$$

a) b) c)

$\psi_{3,1}$ = Reflection coefficient imposed upon the z-component of the E-field

Fig. 4.5 Reflection coefficient of three different boundary nodes.

a) Node at a plane electric wall

b) Node in a two-dimensional corner.

c) Node in a three-dimensional corner.

index		Coordinate direction					
		x		y		z	
j	i	r1	r2	r3	r4	r5	r6
1	1	+1	+1	−1	−1	−1	−1
	2	−1	−1	+1	+1	−1	−1
	3	−1	−1	−1	−1	+1	+1
2	1	−1	−1	+1	+1	+1	+1
	2	+1	+1	−1	−1	+1	+1
	3	+1	+1	+1	+1	−1	−1
3	1	+1	+1	+1	+1	+1	+1
	2	−1	−1	−1	−1	−1	−1

Table 4.2 Boundary reflection coefficients in a simple rectangular resonator for scalar TLM analysis

4.4 DUAL SCALAR TLM NETWORK

The duality of electric and magnetic fields enables us to also simulate wave quantities by currents in a series-type TLM network. A series node of such a network is shown in Fig.4.7. It is obvious that such a node can be arranged in several ways since it is not symmetrical in three-dimensions, as opposed to the shunt node. Consequently, the scattering matrix of a series node will contain off-diagonal elements having alternatively positive and negative signs. The scattering matrix is thus dependent of the node structure and its orientation with respect to the mesh axis. This fact introduces additional complexities which make the series node less attractive for practical applications. It is therefore mentioned here for completeness only, and a detailed analysis of series networks is not of practical interest at this point.

4.5 PROGRAMMING AND TEST SIMULATION

A scalar TLM solution begins with the selection of the field component to be simulated. If the resonant structure is cylindrical about a given direction, then the logical choice would be the electric or magnetic field in this direction, depending on the modes of interest. Then the boundary conditions are determined and the elements of the $|\rho|$ matrix for the boundary nodes are obtained. The three-

dimensional scalar TLM program is simply an extension of the conventional two dimensional TLM program, and is obtained by adding one more pair of transmission lines per node. The boundary conditions are greatly simplified in comparison with the conventional 3D-TLM method [10], and the number of operations per node are greatly reduced (five additions and one multiplication vs. eighteen additions and six multiplications).

In order to compare the results and the numerical efficiency of the two 3D-TLM methods, we have computed the eigenvalues of a rectangular resonator (Fig.4.6.a) previously treated by Akhtarzad[13]. Table 4.3 compares the results obtained with both methods. This comparison shows that for identical mesh size and number of iterations, the accuracy of the results is very similar. However the time of execution was seven times shorter for the scalar program on an Amdal 470/v78, and the required memory was about one fourth of that for the conventional program.

In the second example, the slab loaded resonator (Fig.4.6.b) was analyzed by simulating the propagation of a magnetic type Hertzian potential normal to the slab-air interfaces. Table 4.4 compares the results with analytical results obtained by solving the transverse resonance condition for the first two LSE modes.

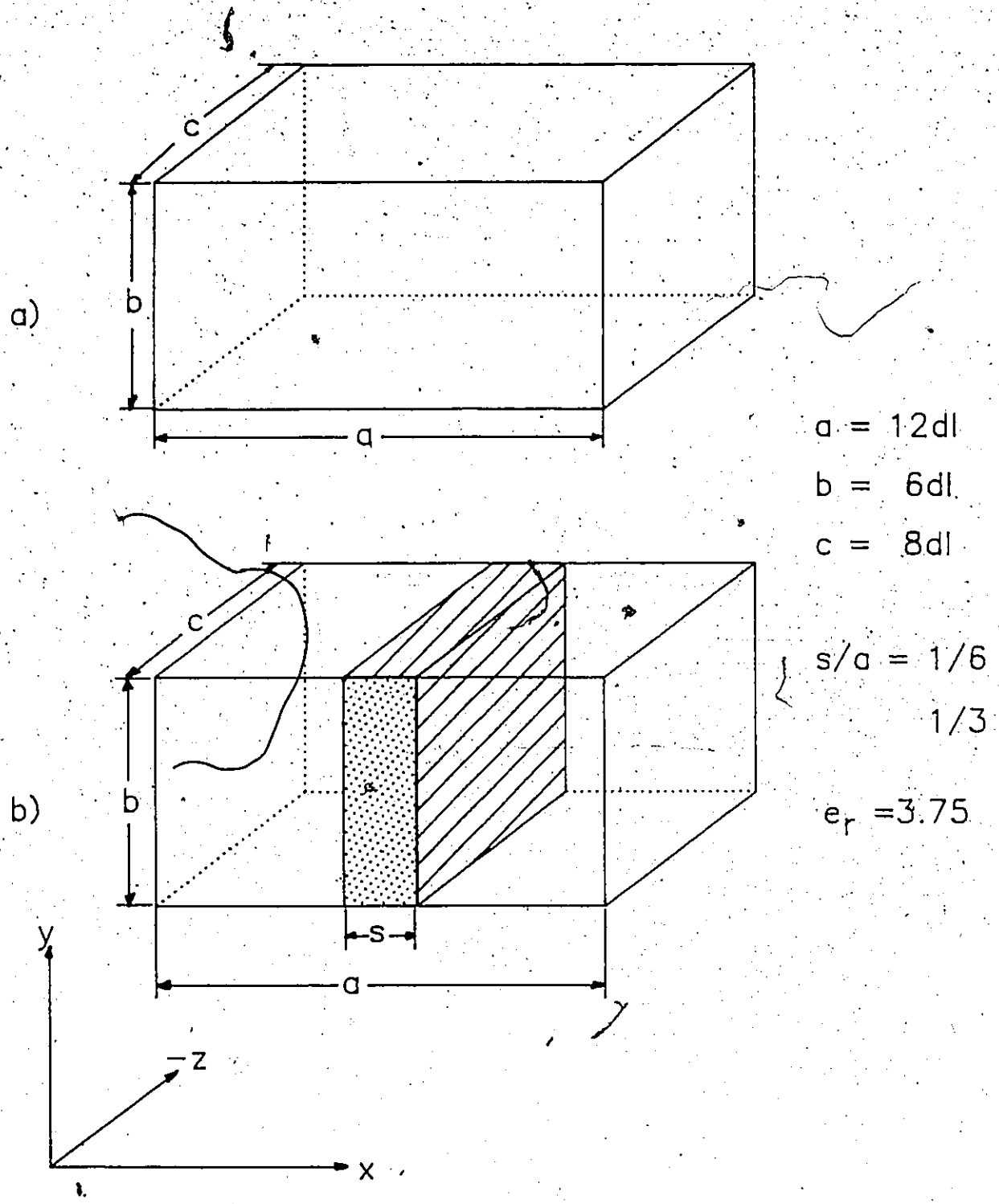

Fig. 4.6 Rectangular cavities evaluated with the scalar TLM method.

	analytic value	scalar TLM (error %)	original TLM (error %)
TE_{101}	0.07511	0.07480 (0.40)	0.07480 (0.40)
TM_{110}	0.09317	0.09299 (0.18)	0.09249 (0.72)
TM_{201}	0.10417	0.10379 (0.36)	0.10337 (0.76)
TE_{111}	0.11219	0.11199 (0.18)	
TM_{210}	0.11785	0.11759 (0.22)	
CPU- time on AMDAHL 470/v78		1 minute	7 minutes

Table 4.3 Comparison of the first five normalized resonant frequencies of a homogeneously filled rectangular cavity with values obtained by the scalar and the original TLM methods.

The geometry is given in Fig. 4.6 a).

mode	s/a	analytic value	scalar TLM	error (%)
LSE_{101}	1/6	0.0522	0.0516	1.15
	1/3	0.0445	0.0440	1.12
LSE_{201}	1/6	0.0988	0.0985	0.3
	1/3	0.0776	0.0759	2.19

Table 4.4 Normalized resonant frequencies of the first two LSE modes in a dielectric slab–loaded cavity evaluated with the scalar TLM method.

The geometry is given in Fig. 4.6.b)

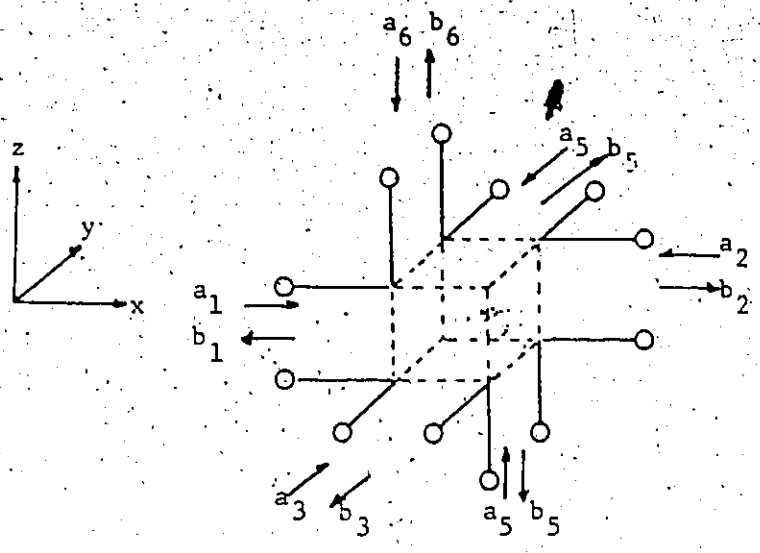

a) One possible series node of series unit cells.

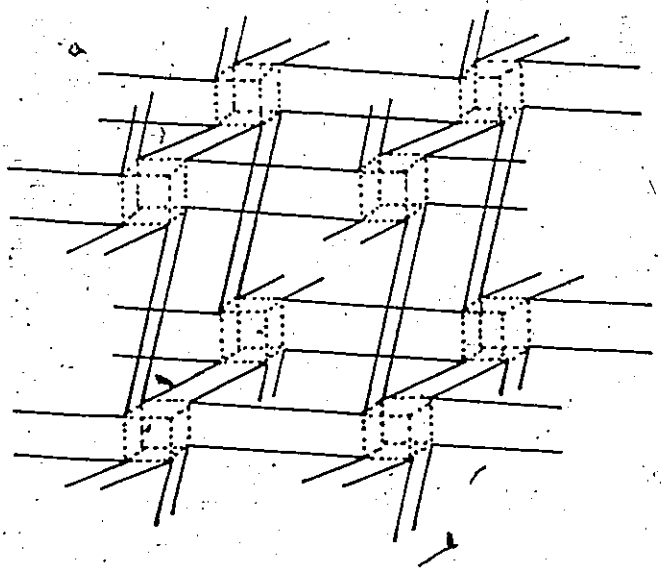

b) Series-connected scalar network utilizing unit cell as in a)

Fig. 4.7 Series- connected scalar TLM network

4.6 DISCUSSION AND FURTHER WORK

In this chapter, a simplified three-dimensional scalar TLM network has been presented and analyzed. It can simulate any quatity that satisfies the scalar homogeneous wave equation and is subject to totally reflecting boundaries. This quantity may be any component of an electric or magnetic field when the EM fields are separable into TE or TM fields. If a geometry is complex, two different potentials are coupled, and can not be handled by the scalar TLM. This is the limitation of this method.

The scalar nature of the simulated quantity simplifies the network structure of the TLM model, reduces the required memory size by four times and the CPU time seven times as compared with the conventional formulation.

A further advantage resides in the fact that the propagation velocity is less dispersive in the scalar network than in the conventional three-dimensional mesh. Finally, all methods proposed to reduce time and memory requirements of the conventional TLM method such as variable mesh size and window optimization can be applied to the scalar method as well, thus maintaining its inherent advantage.

In the future, it is hoped that this concept could be extended to include coupled potential situations, then this method will be a completely general method like the conventional TLM with far less complexity.

Chapter V

UNIFORM FD-TD TECHNIQUE

5.1 INTRODUCTION

In previous chapters, several improvements to the original TLM method were discussed, and their additional requirements for numerical simulations were briefly examined. However, in spite of several advantages gained over the original TLM by these improvements, the application of these improved TLM algorithms to the practical situation still involves considerable computer resources.

Even though the graded mesh algorithm reduces memory space requirements, it demands far more iterations than the original TLM method for equal frequency resolution[23]. This is especially obvious in the case of three-dimensional simulations where the graded ratio N requires an additional N^2-1 iterations. These requirements of large computer resources may critically limit the practical applicability of the TLM technique.

In view of these requirements, Saguet and Pic [24] have proposed a simplified node which reduces the number of variables to be processed by one third. However, this modifica-

tion makes each node unsymmetrical and results in increased velocity error. also this method still requires 15 real memory spaces per node. The major reason for the large CPU memory demand of this technique resides in the basic three-dimensional TLM concept. In order to represent each electromagnetic field component, each three-dimensional unit cell requires 26 real memory spaces; 12 for pulse storage and 14 for additional network parameters. Therefore, each operation on a node involves a lage number of variables, requiring considerable computer CPU space and time. Furthermore, experience has shown that the number of iterations increases with the complexity of the structure under study. For example, the analysis of a finline requires easily over 1000 iterations. These massive requirements have motivated the author to find an alternative numerical technique which possesses the advantages of the TLM approach but needs less computer resources. As a results, the author proposes a new algorithm based on both the Finite Difference-Time Domain (FD-TD) method and the TLM method.

The Finite Difference Time Domain (FD-TD) method was first formulated by Yee[27], and has been extensively applied to scattering and coupling problems with open boundaries[28]-[35], i.e. to the solution of deterministic problems. The author noted the similarity between this method and the TLM method which has been widely used in the numerical solution of electromagnetic eigenvalue problems in the time domain.

The three-dimensional dielectric scattering problem was treated by Taflove and Brodwin[29]. Other workers investigated electromagnetic pulse interaction with metallic bodies of revolution, and with detailed models of aircraft[33]. Recently Taflove and Umashankar have made a comparison study on this method and the method of moments. They showed a high level of agreement on the near and far field results for three-dimensional problems.

All the applications so far treated have been directed towards the time domain analysis of the scattering structure by imposing a plane incident wave which is pulse-shaped or a sinusoidal waveform of known frequency. In this thesis, the author has developed a novel procedure which increases the numerical efficiency of the time domain approach without sacrificing its advantages[61]. The method differs from the classical FD-TD method in the assignment of initial field values and the application of the Fourier transform to the time domain solution.

Concerning numerical accuracy, Taflove and Brodwin has utilized a mesh size of 20x20x10 with 10 % error for the solution of time domain scattering problems[29]. Later, for the cylindrical metal cavity scattering problem, they achieved 1db accuracy relative to known analytical data . However, in our application of this method to the solution of problems in the frequency domain, much improved accuracy

i.e. within 2 % , has been obtained even with a much smaller number of nodes employed.

In the following sections, the main concept of the FD-TD technique and the procedure of computer simulation will be described and some numerical results will also be presented in the last section.

5.2 THE THREE-DIMENSIONAL FD-TD MODEL

5.2.1 General form of Maxwell's equations

The behavior of electromagnetic fields in the presence of material media is governed by Maxwell's equations of macroscopic electrodynamics:

$$\nabla \times \vec{E}(r,t) = -\partial \vec{B}(r,t)/\partial t$$

$$\nabla \times \vec{H}(r,t) = \vec{J} + \partial \vec{D}(r,t)/\partial t \qquad (5.1)$$

$$\nabla \cdot \vec{B}(r,t) = 0$$

$$\nabla \cdot \vec{D}(r,t) = \rho$$

Implicit in the Maxwell's equations is the continuity equation for charge density and current density,

$$\nabla \cdot \vec{J} + \partial \rho/\partial t = 0 \qquad (5.2)$$

This follows from combining the time derivative of the fourth equation (5. 1) with the divergence of the second equation. The field vectors must also satisfy the appropriate boundary conditions.

Maxwell's equations do not take into account the properties of media, which must be included in the solution of electromagnetic phenomena. A description of the media is provided by the constitutive relations which describe functional dependance among field vectors. The most general form of the constitutive relations can be written as

$$\begin{bmatrix} \bar{D} \\ \bar{B} \end{bmatrix} = \begin{bmatrix} C \end{bmatrix} \begin{bmatrix} \bar{E} \\ \bar{H} \end{bmatrix} \tag{5.3}$$

$$\begin{bmatrix} C \end{bmatrix} = \begin{bmatrix} \varepsilon & w \\ z & \mu \end{bmatrix}$$

where ε, w, z and μ are all 3x3 matrices. Their elements are called constitutive parameters. In this form, each field vector $\bar{D}$, $\bar{B}$, $\bar{E}$ and $\bar{H}$ forms a single tensor in four-dimensional space and time, and the constitutive relations are Lorentz-covariant. When w and z are not equal to zero, the media are called "Tellegen" or bianisotropic media.

Under time harmonic excitation the constitutive matrix C is usually complex and frequency dependent. In source-free regions where $\bar{J} = \bar{0}$, the time average of the divergence of Poynting's vector is

$$\begin{aligned} \langle \nabla \cdot S \rangle &= 1/2 \, \mathrm{Re}[j\omega(\bar{B} \cdot \bar{H}^* - \bar{E} \cdot \bar{D}^*)] \\ &= 1/4[\{j\omega(\bar{B} \cdot \bar{H}^* - \bar{E} \cdot \bar{D}^*)\} + \{j\omega(\bar{B} \cdot \bar{H}^* - \bar{E} \cdot \bar{D}^*)\}^*] \\ &= 1/4j\omega[\bar{E}^* \cdot (\varepsilon - \varepsilon^\dagger)\, \bar{E} + \bar{H}^* \cdot (\mu - \mu^\dagger)\, \bar{H} \end{aligned}$$

$$+ \bar{E}^* (w+z^\dagger) \bar{H} - \bar{H}^* (w^\dagger+z) \bar{E}] \qquad (5.4)$$

where the superscript † denotes a transpose complex conjugate, and the * symbol denotes the complex conjugate.

For lossless media, we obtain from (5. 4) the lossless condition:

$$\begin{aligned} \varepsilon &= \varepsilon^\dagger \\ \mu &= \mu^\dagger \\ w &= z^\dagger \end{aligned} \qquad (5.5)$$

When there is no coupling between electric and magnetic fields, i.e. $w = z = 0$, the general constitutive relation of (5. 3) can be conveniently reduced to two 3x3 submatrices for ε and μ called permittivity and permeability tensors. In practice, most important anisotropic media are described as follows

$$\varepsilon = \begin{bmatrix} exx & exy & 0 \\ exy^* & eyy & 0 \\ 0 & 0 & ezz \end{bmatrix} \qquad (5.6)$$

and

$$\mu = \begin{bmatrix} uxx & uxy & 0 \\ uxy^* & uyy & 0 \\ 0 & 0 & uzz \end{bmatrix}$$

The media characterized by (5. 6) are also called bidirectional or electrically gyrotropic and magnetically gyrotropic respectively.

For the lossless case, the matrices ε and μ can always be transformed into a diagonal form

$$\varepsilon = \begin{bmatrix} exx & 0 & 0 \\ 0 & eyy & 0 \\ 0 & 0 & ezz \end{bmatrix} \qquad \mu = \begin{bmatrix} uxx & 0 & 0 \\ 0 & uyy & 0 \\ 0 & 0 & uzz \end{bmatrix} \qquad (5.7)$$

where the diagonal elements of ε and μ are the eigenvalues of the corresponding matrices, and their directions constitute the principal axis or optical axis. Therefore, the elements exy ,exy* may represent misalignment of the medium coordinate system with respect to that of wave propagation.

In general, the values of all diagonal elements are distinct, in which case the medium is called biaxial, Then the general constitutive relation (5. 3) can be written $\overline{D} = \varepsilon_o \varepsilon_r \overline{E}$ and $\overline{B} = \mu_o \mu_r \overline{H}$. With the aid of these relations, source-free Maxwell's equations can be written in the rectangular system as

$$\begin{aligned} \partial E_z/\partial y - \partial E_y/\partial z &= -\mu_o uxx\, \partial H_x/\partial t \\ \partial E_x/\partial z - \partial E_z/\partial x &= -\mu_o uyy\, \partial H_y/\partial t \\ \partial E_y/\partial x - \partial E_x/\partial y &= -\mu_o uzz\, \partial H_z/\partial t \end{aligned}$$

and (5. 8)

$$\begin{aligned} \partial H_z/\partial y - \partial H_y/\partial z &= \varepsilon_o exx\, \partial E_x/\partial t \\ \partial H_x/\partial z - \partial H_z/\partial x &= \varepsilon_o eyy\, \partial E_y/\partial t \\ \partial H_y/\partial x - \partial H_x/\partial y &= \varepsilon_o ezz\, \partial E_z/\partial t \end{aligned}$$

We note that satisfying the curl equations automatically ensures that the divergence equations of (5. 1) are also satisfied. Equation (5. 8) will be employed in the following section for modelling time-dependent electromagnetic propagation.

The boundary conditions satisfied by the field vectors of interest for this modelling, can be categorized into two forms depending on the properties of the media on either side of the boundary or on the symmetric features of the given structure. These are

1. For a boundary between two lossless dielectric media, the tangential components of the electric and magnetic field intensity vectors must be continuous across the boundary,

$$\hat{n} \times (\overline{E}_2 - \overline{E}_1) = 0$$
$$\hat{n} \times (\overline{H}_2 - \overline{H}_1) = 0 \qquad (5.9)$$

2. For a boundary between a perfect conductor and a dielectric medium, the tangential components of the electric field must vanish at the boundary.
   A surface having this boundary condition is said to be an "electrical wall". For an electrical wall, therefore,

$$\hat{n} \times \overline{E}_2 = 0 \qquad (5.10)$$

On an electric wall, the tangential magnetic field is

discontinuous.

A magnetic wall can be defined as a surface on which the tangential magnetic field vanishes.

$$\hat{n} \times \vec{H}_2 = \vec{0} \qquad (5.11)$$

On a magnetic wall the tangential electric field is discontinuous. Note that a magnetic wall may be a plane of symmetry that might be used when the geometry of the structure exhibits symmetrical properties about certain planes. On the other hand, an electrical wall is a real physical wall of the structure in a form of a conducting boundary.

5.2.2 The Finite Difference - Time Domain model

In a rectangular coordinate system, Maxwell's equations given in (5. 8) can be written as first order hyperbolic equations.

$$|\varepsilon| dE/dt = |A_x|' dH/dx + |A_y|' dH/dy + |A_z|' dH/dz$$
$$|\mu| dH/dt = -|A_x|' dE/dx - |A_y|' dE/dy - |A_z|' dE/dz \qquad (5.12)$$

where $E = (E_x, E_y, E_z)^t$, $H = (H_x, H_y, H_z)^t$

$$|Ax|' = \begin{bmatrix} 0 & 0 & 0 \\ 0 & 0 & -1 \\ 0 & 1 & 0 \end{bmatrix} \quad |Ay|' = \begin{bmatrix} 0 & 0 & 1 \\ 0 & 0 & 0 \\ -1 & 0 & 0 \end{bmatrix} \quad |Az|' = \begin{bmatrix} 0 & -1 & 0 \\ 1 & 0 & 0 \\ 0 & 0 & 0 \end{bmatrix}$$

After multiplying both sides of (5.12) by $|\varepsilon|$ and $|\mu|$ respectively we get

$$d\bar{E}/dt = |A_x|d\bar{H}/dx + |A_y|d\bar{H}/dy + |A_z|d\bar{H}/dz$$

$$d\bar{H}/dt = |C_x|d\bar{E}/dx + |C_y|d\bar{E}/dy + |C_z|d\bar{E}/dz \qquad (5.13)$$

where

$$|Ax| = \begin{bmatrix} 0 & 0 & 0 \\ 0 & 0 & -1/eyy \\ 0 & 1/ezz & 0 \end{bmatrix} \quad |Ay| = \begin{bmatrix} 0 & 0 & 1/exx \\ 0 & 0 & 0 \\ -1/ezz & 0 & 0 \end{bmatrix} \quad |Az| = \begin{bmatrix} 0 & -1/exx & 0 \\ 1/eyy & 0 & 0 \\ 0 & 0 & 0 \end{bmatrix}$$

$$|Cx| = \begin{bmatrix} 0 & 0 & 0 \\ 0 & 0 & 1/uyy \\ 0 & -1/uzz & 0 \end{bmatrix} \quad |Cy| = \begin{bmatrix} 0 & 0 & -1/uxx \\ 0 & 0 & 0 \\ 1/uzz & 0 & 0 \end{bmatrix} \quad |Cz| = \begin{bmatrix} 0 & 1/uxx & 0 \\ -1/uyy & 0 & 0 \\ 0 & 0 & 0 \end{bmatrix}$$

Each of these scalar equations can be expressed in finite difference form. Yee [27] introduced a set of finite difference equations for the system of (5.13). Following Yee's nomenclature, any function of space and time is discretized.

$$F^n(i,j,k) = \bar{F}(i\Delta x, j\Delta y, k\Delta z, n\Delta t)$$

where $\Delta x = \Delta y = \Delta z = \Delta$ is the space increment and Δt is the time increment. By positioning the field components of E and H on the mesh in the way that is shown in Fig.5.1, and evaluating E and H at alternate half-time steps, we obtain the components of Maxwell's equations.

$$H_x^{n+1/2}(i,j+1/2,k+1/2) = H_x^{n-1/2}(i,j+1/2,k+1/2)$$
$$+ s/uxx(i,j+1/2,k+1/2)[E_y^n(i,j+1/2,k+1)$$
$$- E_y^n(i,j+1/2,k) + E_z^n(i,j,k+1/2) - E_z^n(i,j+1,k+1/2)]$$

(5.14.a)

$$H_y^{n+1/2}(i+1/2,j,k+1/2) = H_y^{n-1/2}(i+1/2,j,k+1/2)$$
$$+ s/uyy(i+1/2,j,k+1/2)[E_z^n(i+1,j,k+1/2)$$
$$- E_z^n(i,j,k+1/2) + E_x^n(i+1/2,j,k) - E_x^n(i+1/2,j,k+1)]$$

(5.14.b)

$$H_z^{n+1/2}(i+1/2,j+1/2,k) = H_z^{n-1/2}(i+1/2,j+1/2,k)$$
$$+ s/uzz(i+1/2,j+1/2,k)[E_x^n(i+1/2,j+1,k)$$
$$- E_x^n(i+1/2,j,k) + E_y^n(i,j+1/2,k) - E_y^n(i+1,j+1/2,k)]$$

(5.14.c)

$$E_x^{n+1}(i+1/2,j,k) = E_x^n(i+1/2,j,k) + s/exx(i+1/2,j,k)$$
$$[H_z^{n+1/2}(i+1/2,j+1/2,k) - H_z^{n+1/2}(i+1/2,j-1/2,k)$$
$$+ H_y^{n+1/2}(i+1/2,j,k-1/2) - H_y^{n+1/2}(i+1/2,j,k+1/2)]$$

(5.14.d)

$$E_y^{n+1}(i,j+1/2,k) = E_y^n(i,j+1/2,k) + s/eyy(i,j+1/2,k)$$
$$[H_x^{n+1/2}(i,j+1/2,k+1/2) - H_x^{n+1/2}(i,j+1/2,k-1/2)$$
$$+ H_z^{n+1/2}(i-1/2,j+1/2,k) - H_z^{n+1/2}(i+1/2,j+1/2,k)]$$

(5.14.e)

$$E_z^{n+1}(i,j,k+1/2) = E_z^n(i,j,k+1/2) + s/ezz(i,j,k+1/2)$$
$$[H_y^{n+1/2}(i+1/2,j,k+1/2) - H_y^{n+1/2}(i-1/2,j,k+1/2)$$
$$+ H_x^{n+1/2}(i,j-1/2,k+1/2) - H_x^{n+1/2}(i,j+1/2,k+1/2)]$$

(5.14.f)

where the stability factor $s = c\,\Delta t/\Delta$ and c is the velocity of light. In these expressions, $\overline{E}$ and $\overline{H}$ are normalized such that the characteristic impedance of space is unity. With the system of (5.14), the new value of a field vector component at any lattice point depends only on its previous value

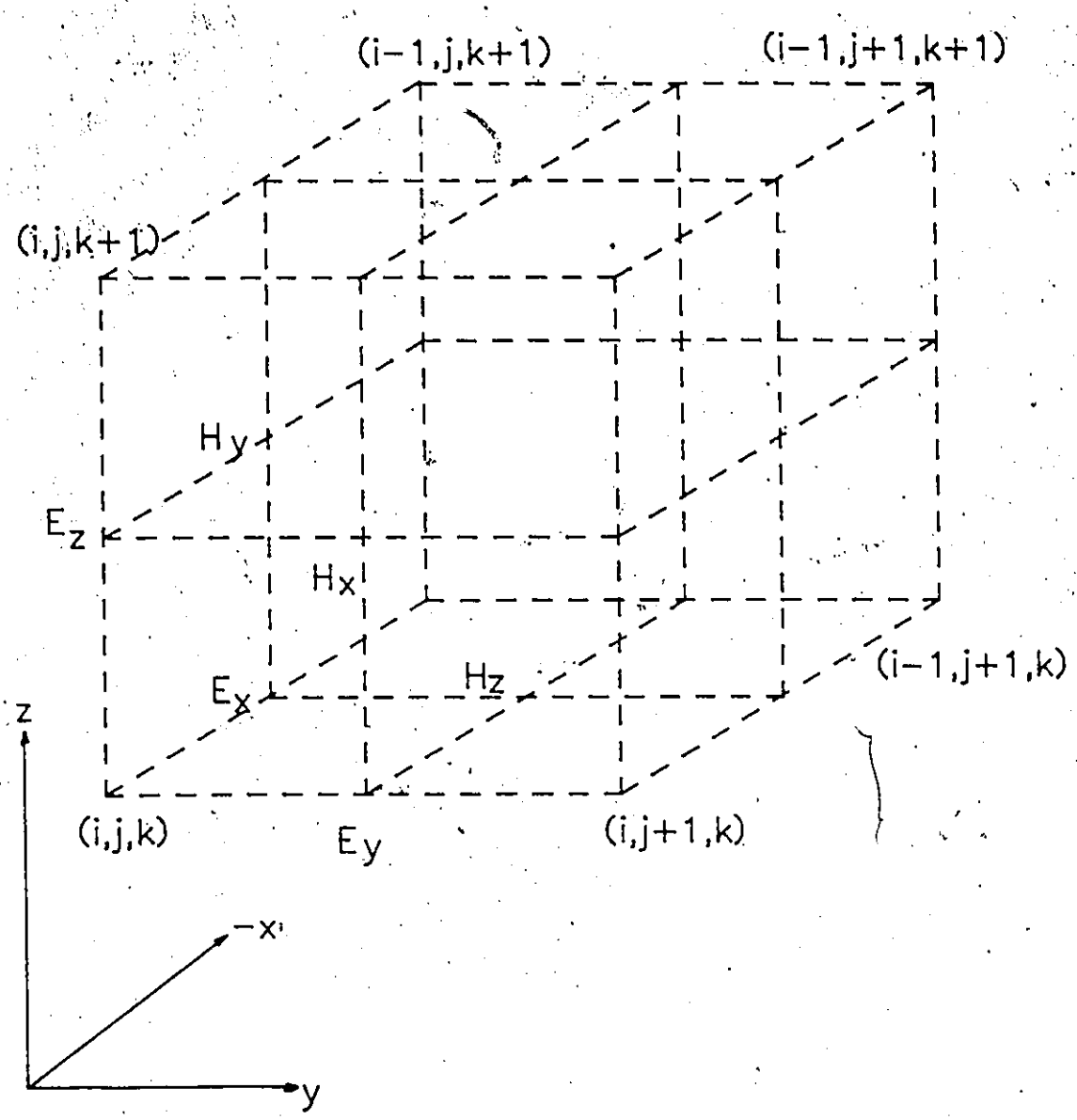

Fig. 5.1 The position of the field components in Yee's mesh

and on the other field vectors at adjacent points. Therefore, at any given time step, the computation of a field vector may proceed one point at a time. Computer storage must be provided for 12 quantities at each unit cell of the lattice if a completely general anisotropic medium is simulated by this algorithm.

5.2.3 The boundary condition

So far, a space-time mesh has been introduced, and Maxwell's equations have been replaced by a system of finite difference equations. Difficulties arise when the domain in which the field must be computed is unbounded. Since no computer can store an unlimited amount of data, a special technique must be used to limit the domain where the numerical computation is made, by introducing so-called "absorbing" or "truncating" boundary conditions.

These conditions have been described by Taylor et al[28], who use a simple extrapolation method, and by Taflove and Brodwin[29], who simulate the outgoing waves and use an averaging process in an attempt to account for all possible angles of propagation of the outgoing waves. Kunz and Lee[31] use the radiation condition at large distance from the center of the scatterer to obtain an absorbing boundary condition. Mur[32] employs a second order radiation condition to improve the accuracy of the results. Although these

schemes have been used in scattering problems in the past, no ideal reflection-free boundary condition has been proposed so far.

However, in the formulation of eigenvalue problems, only "hard boundaries" - usually represented by conducting walls - occur. At these boundaries, the tangential electric and the normal magnetic field components are maintained at zero. For example, on a perfectly conducting wall in the plane i = 1 (see Fig.5.1) we must have

$$\left.\begin{aligned} E_y^n(1,j+1/2,k) &= 0 \\ E_z^n(1,j,k+1/2) &= 0 \\ H_x^n(1,j+1/2,k+1/2) &= 0 \end{aligned}\right\} \quad \text{for all } n$$

The third condition is implicit in the previous two, but its implementation reduces numerical errors.

Another method of imposing "hard boundary" conditions may be obtained by linear extrapolation techniques as follows. Suppose a conducting plane is situated in (1,j,k) of Fig.5.1. Then, each component of the fields on this plane can be expressed by neighbor components. For example, the fifth equation of (5. 8) in that plane is:

$$\partial E_y(1,j,k)/\partial t = \partial H_x(1,j,k)/\partial z - \partial H_z(1,j,k)/\partial x \qquad (5.15)$$

The left hand terms of (5.15) may be expressed through Taylor series as:

$$H_z(2)=H_z(1) + \Delta x \partial H_z/\partial x|_1 + \Delta x^2 \partial^2 H_z/(2\partial x^2) + O(\Delta x^2)$$

(5.16)

$$H_z(3)=H_z(1) +2\Delta x\partial H_z/\partial x|_1 + 4\Delta x^2\partial^2 H_z/(2\partial x^2)+ O(\Delta x^2)$$

After multiplying the first equation of(5.16) by four and subtracting the second equation from the first, we get

$$\partial H_z/\partial x|_1 = [4H_z(2) - H_z(3) - 3H_z(1)]/(2\Delta x) \qquad (5.17)$$

The first term of the left side of (5.17) can be replaced by a central difference expression at (1,j,k), which is:

$$\partial H_z/\partial z|_1 = [H_x(1,j,k+1) - H_x(1,j,k-1)]/(2\Delta z) \qquad (5.18)$$

By substituting (5.17) and (5.18) into (5.15), we obtain finally,

$$E_y(1,j,k,n+1) =E_y(1,j,k,n) - s[4H_z(2,j,k,n)-H_z(3,j,k,n)-3H_z(1,j,k,n)+H_x(1,j,k+1,n)-H_x(1,j,k-1,n)]$$

--------(5.19)

All other components can be obtained by a similar procedure.

Although this latter technique can be applied equally to boundary value problems, this procedure requires more algorithm steps in programming and some numerical error occurss due to extrapolation in the calculation of the field values at the boundaries. Therefore the previous method will be employed in calculation.

5.2.4 Initial value condition

In most scattering problems, an impulsive or sinusoidal plane wave is injected at the bigining of the computation. Yee[27] directly utilized a sinusoidal plane wave type, and Taflove and Brodwin[29] used the modified form of sinusoidal waveform as an example of a soft plane wave source condition.

However, in eigenvalue problems, the direction of the propagation vector is usually not known and depends on the space coordinates and on the eigenvalue which is to be found. In these cases, the logical choice is an isotropic pulse which propagates in radial direction. The spatial pulse envelope should be smooth enough with respect to the mesh size not to accumulate numerical error due to overshoot and ringing as it propagates through the space lattice.

A better way to start the computation is to first estimate the field distribution of the desired mode in the structure and then choose the initial value accordingly. The experienced researcher usually has a good idea of the approximate modal field distributions in a structure and is therefore able to make an educated guess of the steady-state field pattern for a particular eigenmode. This procedure is equivalent to the excitation of a TLM mesh with a weighted impulse distribution, and is somewhat similar to the way in which one chooses appropriate basis functions in the spectral domain approach.

5.2.5 Outline of the numerical procedure

The application of this FD-TD method will be discussed using a rectangular resonator as an example. We replace a continuous medium with a three-dimensional uniform mesh. To solve the system of equations (5.14) in this mesh, initial values must be assigned first as described in the last section. For a rectangular type resonator, a simple sinusoidal function is an appropriate choice for the dominant mode eigenvalue.

As n increases, the discrete time functions for E and H fields evolve towards the steady state which is characteristic of the desired mode in the geometry. In this way, the evolution of all six field components is obtained simultaneously at any discrete time points $n\Delta t$. The final steady state time solution may be calculated by taking the time average of the time domain solution at each mesh point. Thus, the steady state solution is given by

$$F(i_o, j_o, k_o) = \sum_n |F^n(i_o, j_o, k_o)| / N \qquad (5.20)$$

where N is the number of iterations.

This simple procedure to obtain the final field distribution is another advantage over the TLM method which requires a second simulation for finding the fields of a given mode.

In eigenvalue problems, the steady-state solution is a time-harmonic function from which the eigenvalues can be extracted by discrete Fourier transform, as in the TLM method.

$$S(f) = \sum_{n} F^{n}(i_o, j_o, k_o)\exp(-j2\pi snf) \qquad (5.21)$$

In order to test this algorithm for validity, we have applied it to a simple rectangular cavity with sides 12x6x8. We have assumed a dominant TE_{101} mode in the initial value assignment. The time domain solution is given in Fig. 5.2.a). Discontinuous field figures are due to the numerical error caused by the finite difference form of (5.14). Fig. 5.2.b) compares the frequency responses obtained with the FD-TD and TLM methods under identical conditions. The responses are not distinguishable. 500 iterations have been used and the peak of the solution is located at dl/λ = 0.0750 in both methods. The exact analytical solution is 0.07511. Even though a small number of meshes is used in this algorithm when compared with the scattering problems in [28]-[30], it is noted that the accuracy in the solution of the eigenvalue problems is better than that of the scattering problems by one order of magnitude. From equation (5.21) we note that the spectrum of the solution is strongly influenced by a constant s as well as N. This stability factor s will be discussed in the following section.

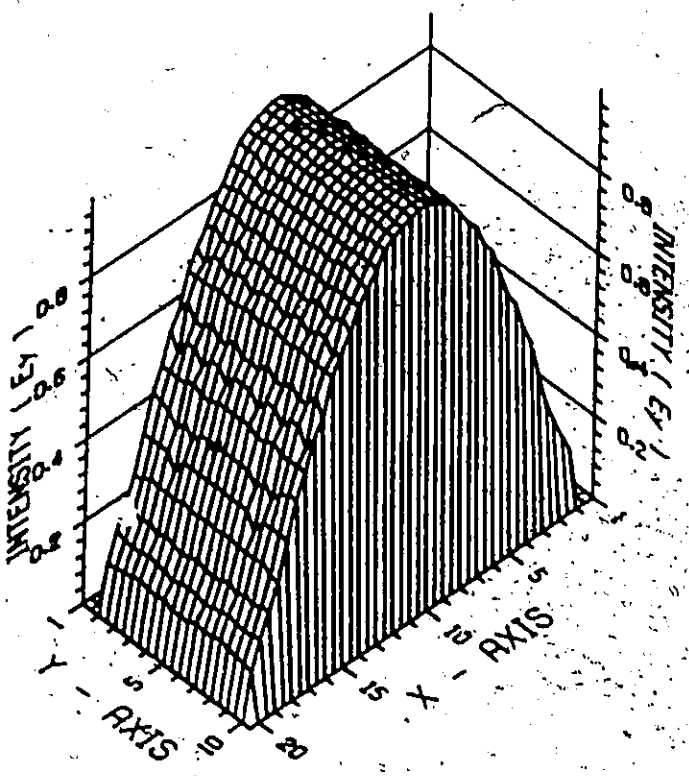

a) Field distribution in an empty rectangular resonator

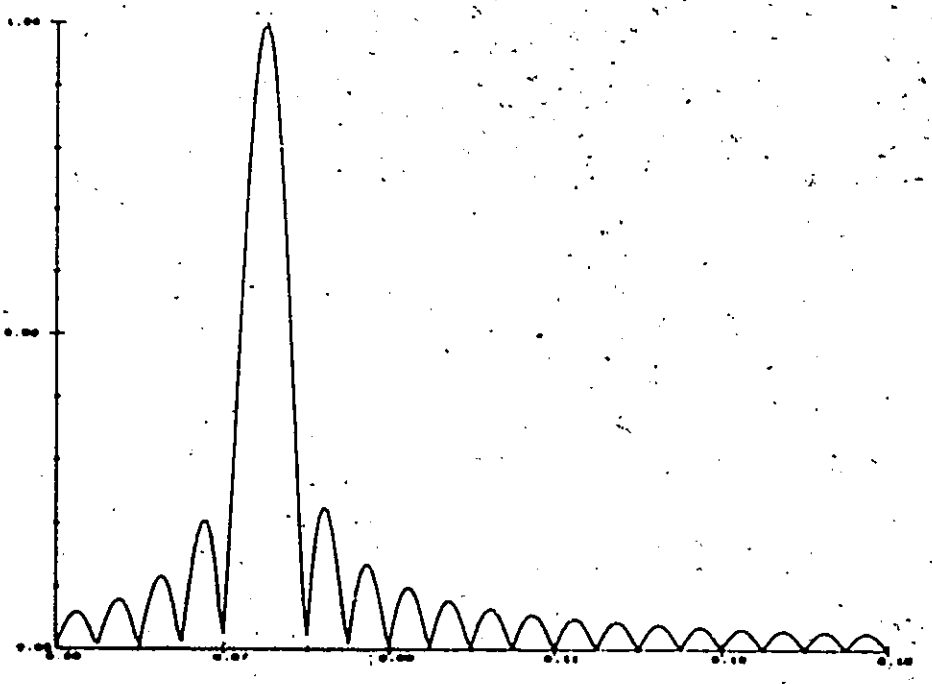

b) Output spectrum obtained with both the TLM and FD-TD methods under identical conditions

Fig. 5.2 Time and frequency responses

5.3 STABILITY FACTOR

A rigorous stability condition for the FD-TD method has been derived by Taflove and Boldwin[29] in free space media. The stability study has been carried out by the author in homogeneous dielectric media with a different approach using the von Neuman condition[71]. A detailed derivation is given in Appendix C. The final form of the condition is:

$$s = cdt/dx \leq \sqrt{\varepsilon_r \mu_r} / 3 \qquad (5.22)$$

The condition (5.22) reduces to

$$s \leq 1/\sqrt{3} \qquad (5.23)$$

in free-space. Therefore 0.5 is used in our algorithm for s. This stability condition has been proved necessary and sufficient condition for this algorithm to be absolutely stable [62].

This condition (5.22) can be derived by the following simple method. Although this may not be rigorous as the others, this qualitative way is very realistic and instructive.

In the unit cell shown in Fig.5.1, any perturbation of E's and H's propagate with the group velocity c in free space. In the algorithm after a time dt the perturbation reaches the adjacent mesh. It requires dt, 2dt, and 3dt from the mesh (i,j,k) to the mesh (i,j+1,k), (i,j+1,k+1) and

(i+1,j+1,k+1) respectively. Thus the velocity of propagation in the algorithm is not smaller than

$V_1 = dx/dt$: longitudinal direction

$V_2 = \sqrt{2}\, dx/2dt$: diagonal direction (plane)

and $V_3 = \sqrt{3}\, dx/3dt$: diagonal direction (cubic)

To assure the proper functioning of the algorithm, the smallest among the velocities V_1, V_2 and V_3 must be greater than the free space velocity c. Therefore,

$$\sqrt{3}\, dx/3dt \geq c \quad \longrightarrow \quad s \leq 1/\sqrt{3}$$

which is identical to (5.23).

5.4 NUMERICAL ERROR ANALYSIS

There are some errors involved in this proposed method. They are due to the following sources:

1. The finite difference form employed to express the differential Maxwell's equations.
2. The finite time truncation of the discrete Fourier transform of the equation (5.21).
3. The numerical round-off error.
4. The assumption of a steady state in the time and frequency domain.

5.4.1 Space resolution error

To analyze the first cause of error, let us consider the following. We have replaced the differential equation (5.8) by the finite difference form (5.14). The error resulting from this discretization is called local resolution error. Let us introduce the difference between the exact solutions of the differential and difference equations at the grid point (p, q, r, n) as

$$Z(p,q,r,n) = u(p,q,r,n) - U(p,q,r,n)$$

where u and U represent the exact and approximate solutions for any component of E and H. Since we have utilized central difference formulae in both time and space in (5.14), we can write:

$$\partial u(p,q,r,n)/\partial t=\Delta U(p,q,r,n)/\Delta t+\Delta t^2\partial^3 U/(24\partial t^3)+ \cdots$$

and

$$\partial u(p,q,r,n)/\partial x=\Delta U(p,q,r,n)/\Delta x+\Delta x^3\partial^3 U/(24\partial x^3)+ \cdots \qquad (5.24)$$

Therefore, each scalar Maxwell equation can be represented in the following general form:

$$Z(p,q,r,n)=\partial u/\partial t - \partial u/\partial x - \partial u/\partial y + (\Delta x^3 + \Delta y^3)/24 + \Delta t^2/24+ \cdots$$

$$= u(p,q,r,n) - U(p,q,r,n) = O(\Delta x^3 + \Delta t^2)$$

Since dt and dx are bounded by the stability condition (5.22), the resulting error will decrease as dx decreases.

Typically, dx is a small fraction of the wavelength of the dominant mode. In this case, the error caused by the approximation may be minor. With this concept in mind, it is clear that for higher order mode calculations, the step size dx must be reduced accordingly if the same solution accuracy is to be maintained.

5.4.2 Time truncation error

The time truncation error is due to the finite computation time in the evaluation of the steady state. It can be reduced by increasing the number of iterations, as in the TLM procedure. In order to show the convergence of the steady state solution of this method, the variation of the resonant frequency of a finline cavity is shown in Fig.5.3 with the results obtained by the TLM method. After 500 iterations, both methods converge to the desired values, but this method shows slightly faster convergence over the TLM.

It may be convenient to decide how many iterations are needed for a given structure. As a general rule, more complex structures require more iterations. One way to determine the proper number of iterations is to terminate the calculation automatically based on the probability of the occurence of the same output result. But it may be too time-consuming a process. After extensive simulation of various structure, we propose the following empirical formula to obtain the number of time steps.

$$A = C \times p \times q \times r$$

where C : shape factor

p : number of mesh cells in x direction

q : number of mesh cells in y direction

r : number of mesh cells in z direction

C = 1/3 : empty resonator

1/2 : resonators containing planar circuit inserts with narrow strips and/or slots on thin substrates.

Another variable quantity in this algorithm is the stability factor s which must be chosen as large as possible but must be smaller than the value given by the stability condition. In the TLM method, if the peaks corresponding to the higher modes are too close to the desired mode in frequency spectrum, influence of sidelobes may cause a shift in the location of the main peak. The better the initial field distribution corresponds to the desired solution, the smaller is the effect of this error since other modes are not strongly excited.

5.4.3 Other errors

The computer roundoff error generally increases as the mesh size decreases or the number of iterations increases. It also depends on the specific computer system employed.

Therefore it is difficult to estimate roundoff error without knowing the specific operating system in use. We have tested our system indirectly for the estimation of the roundoff error. On a loss-free rectangular cavity, we excited one single node with a unit field value and calculated the sum of dispersed pulse amplitudes by adding the field values at every time step. After 600 iterations this summation gave a value different from unity by only 0.1 %. This confirms that our roundoff error is negligible compared with other errors.

Another error occurs at the interface of two different dielectric media. If this technique is applied to a inhomogeneous structure, we may encounter boundary ambiguity error due to the step change of dielectric constant. As shown in Fig. 5.4, step-wise boundary is approximated by smooth change in the dielectric constants. This error can be minimized by reducing step size or irregularly spaced mesh technique which is discussed in the next chapter.

5.5 PROGRAM DISCRIPTION

A general three-dimensional program has been written to implement the FD-TD analysis. The basic structure of this program, as listed at the end of this thesis, is similar to the three-dimensional TLM program. The program based on the proposed method basically requires 6 real memory spaces per

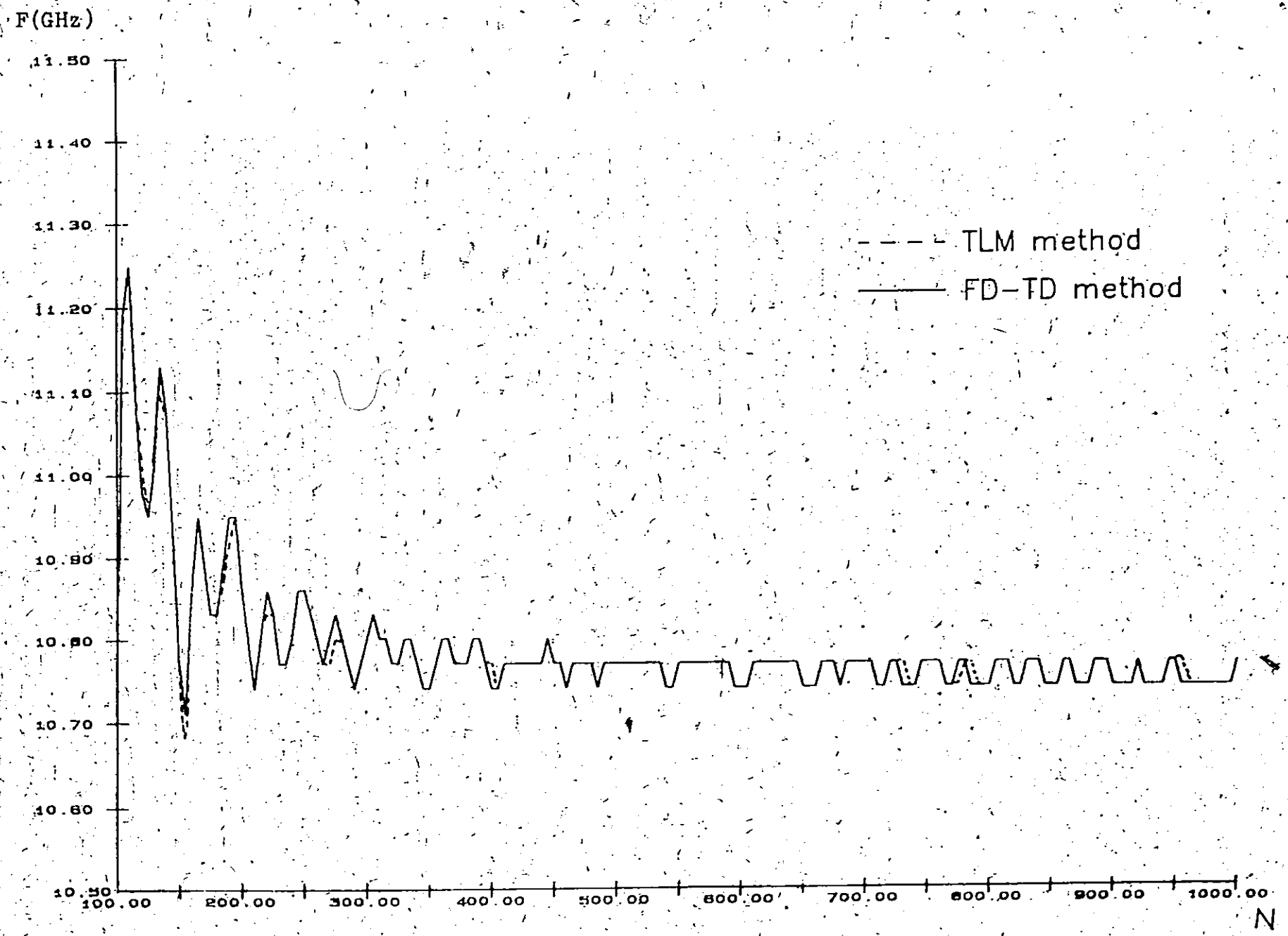

Fig. 5.3 Stability and convergence of the TLM and FD-TD methods as a function of the number of iterations.

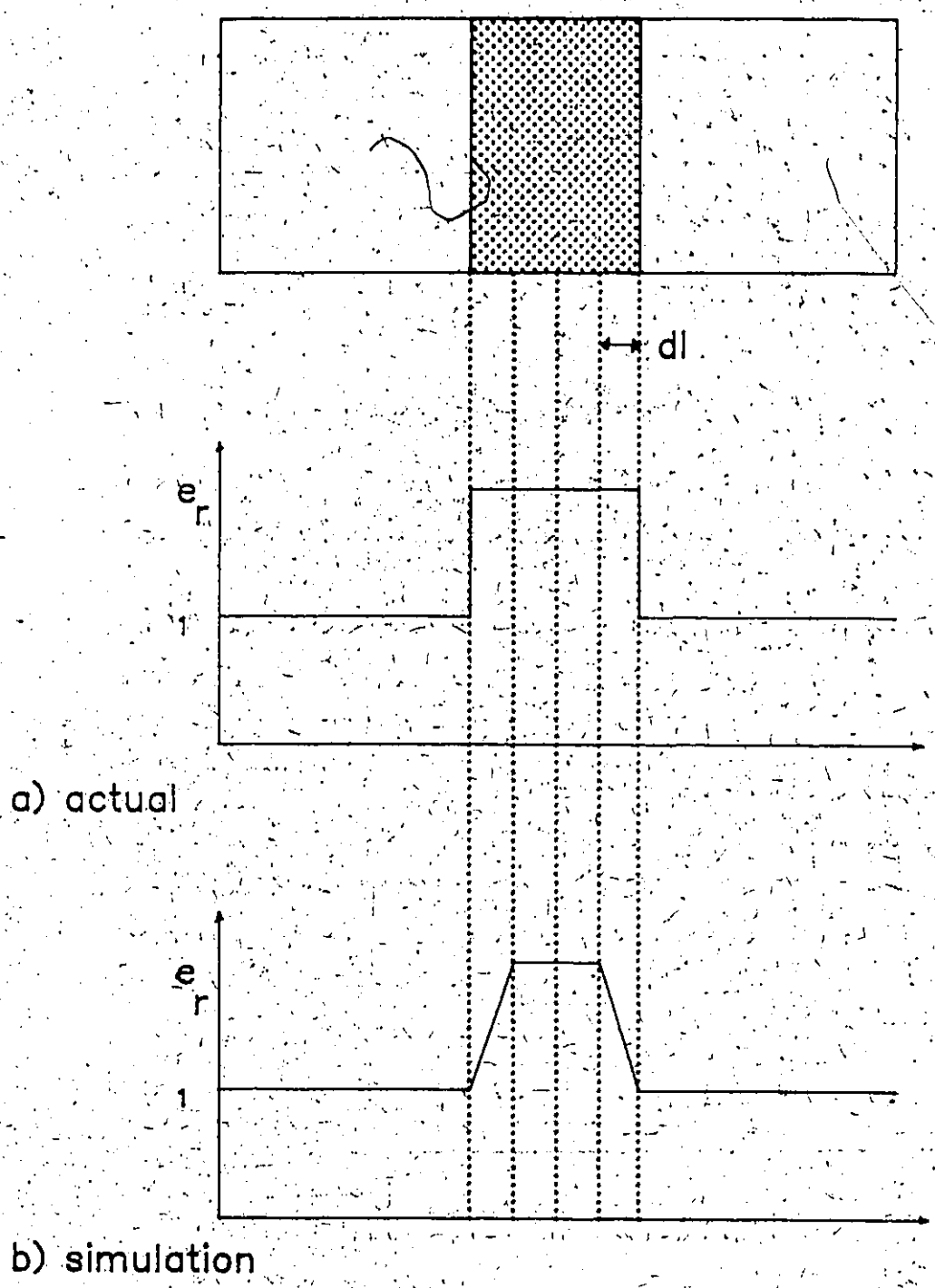

Fig. 5.4 Simulation error caused by a step change in dielectric constant

3-D node. However, a maximum of 12 memory spaces is needed if a complete electric and magnetic anisotropic medium is simulated, i.e. all exx, eyy, ezz, uxx, uyy, and uzz are functions of space. In practice, isotropic inhomogeneous media, of which most practical system are made, require 8 memory spaces, one of which contains the initial field value. This requirement is almost one third of those of the original TLM which requires at least 22 memory spaces.

One additional store per node and per field component is required for the computation of field distribution if desired. This program has been written in about 130 lines of Fortran, including one subroutine. This subroutine calculates the Fourier transform of the time-domain solution obtained in the main program. The Flow chart of the program is given in Fig. 5.5.

5.6 NUMERICAL EXAMPLES

We have applied this technique to most examples described in the TLM literature and obtained practically identical results. The method requires less than one-half of the CPU time spent by the equivalent TLM program under identical conditions, including the initial excitation distribution. Some examples are given in this section.

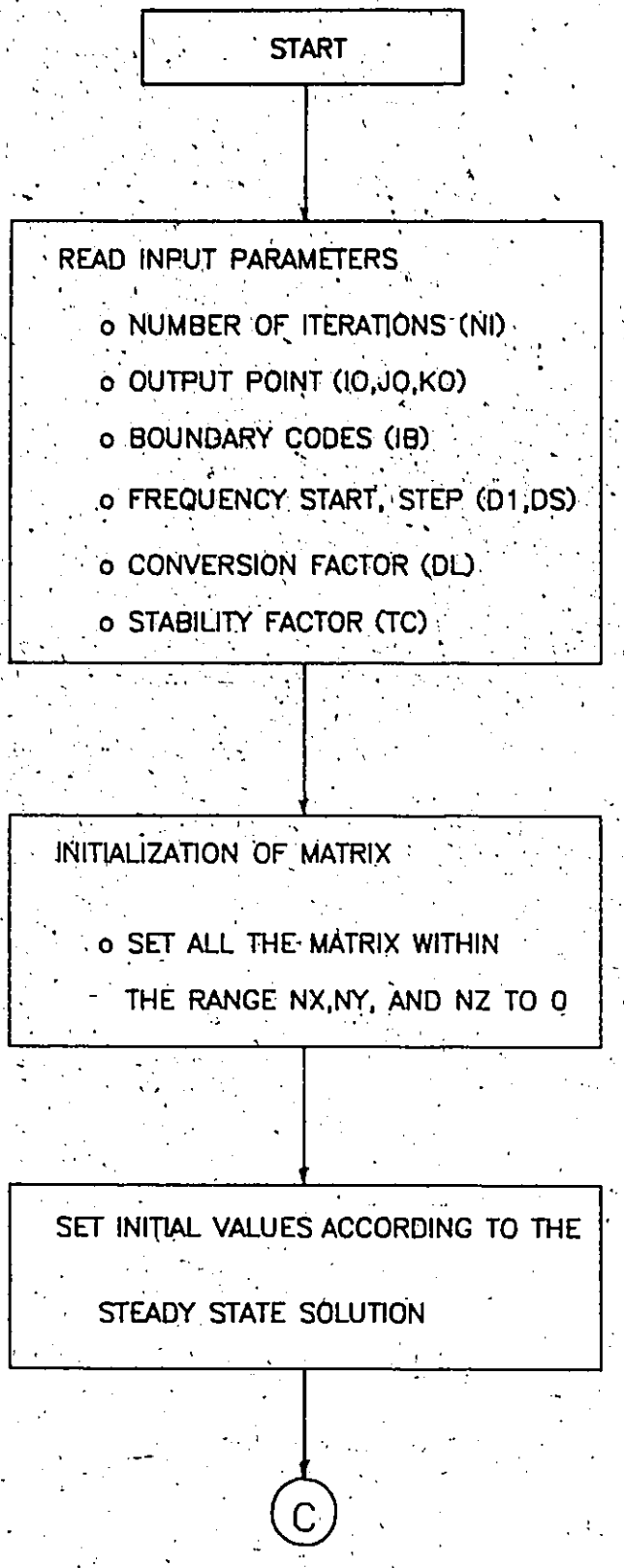

Fig. 5.5 The flow chart of the FD-TD program

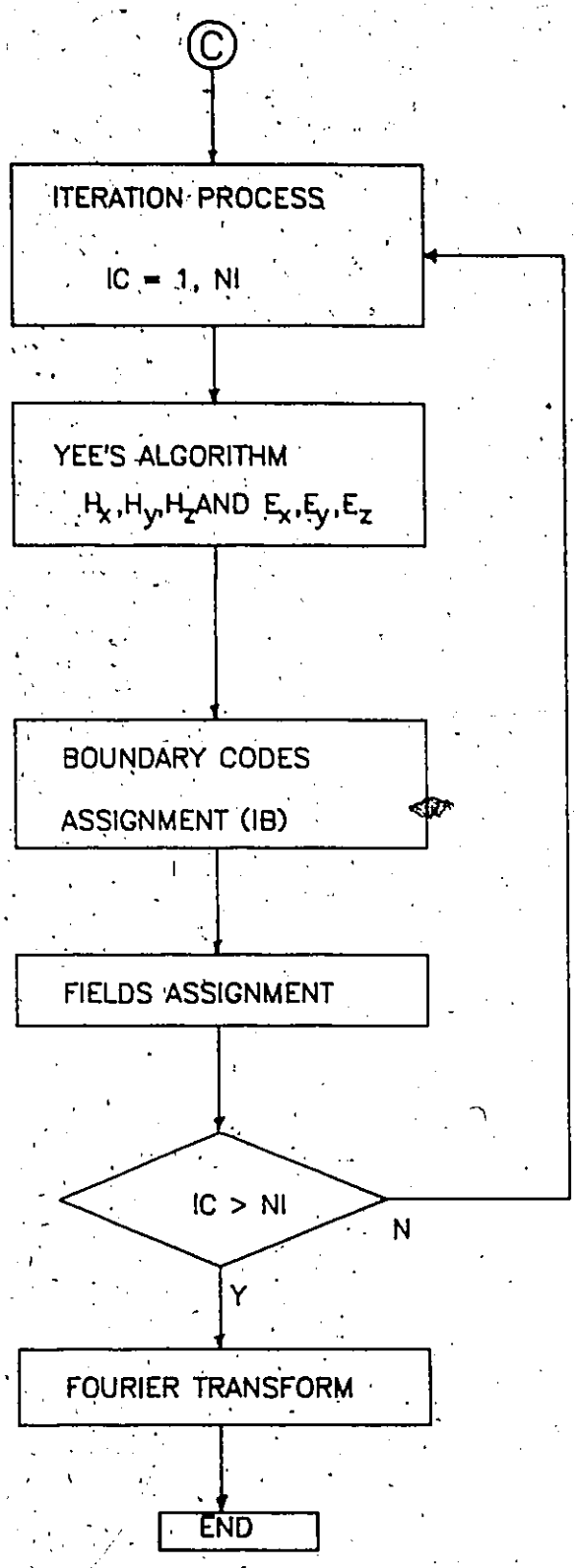

Fig.5.5 continued

5.6.1 Inhomogeneous resonator

Fig. 5.6, shows structures for which solutions have been computed with this method. Dominant resonant frequencies of those structures are given and compared with TLM solutions in Table 5.1. The inhomogeneous rectangular cavity of Fig.5.6.b and c illustrates the capability of this algorithm to solve hybrid field problems. The number of nodes chosen in each problem is the same as that employed in the TLM solution. Note that the CPU time requirement is much smaller than that for TLM. Fig. 5.7 shows the time domain solution of the same structure in Fig. 5.6.a.

5.6.2 Finline structure

We have computed the resonant frequency of a finline resonator shown in Fig. 5.8 treated previously by Saguet[25]. The mesh size is chosen in such a way that only one node is located in the dielectric region. Even though accurate results are not available in the literature, we can confirm the accuracy of these data using other methods. As discussed earlier, we also noted that the employment of variable mesh techniques in the TLM method usually reduces accuracy of the result.

In order to compare the convergence of both time-domain methods, solutions obtained after every fifth iteration are drawn in Fig. 5.3. The results show virtualy identical con-

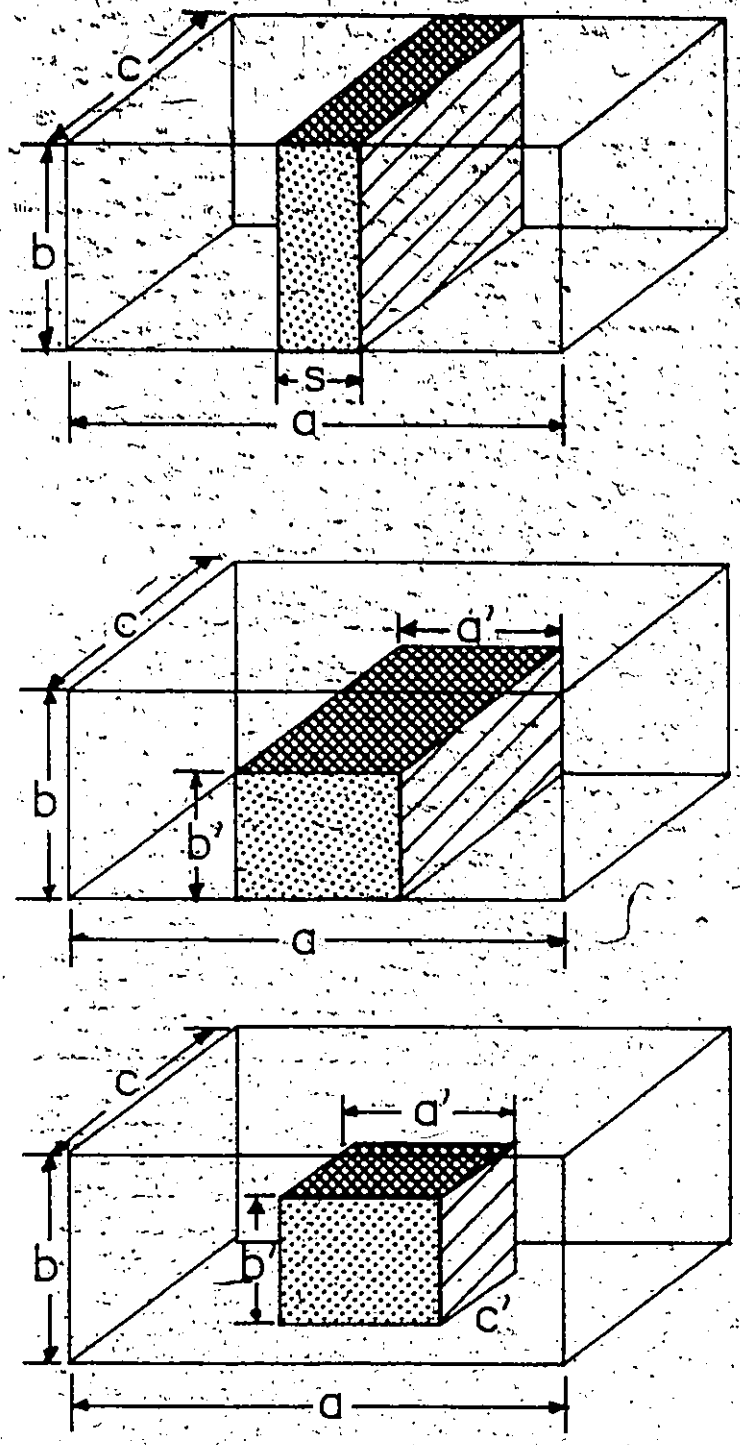

Fig. 5.6 3-D inhomogeneous resonators analyzed in this study

	Mode	s/a	TRM	TLM (CPU time)	FD-TD (CPU time)
a)	LSE	1/6	0.05220	0.0516 (144)	0.0517 (51)
		1/3	0.0445	0.0440 (145)	0.0442 (51)
b)	Hybrid			0.0278 (357)	0.0278 (117)
c)	Hybrid			0.0405 (357)	0.0405 (117)

Table 5.1 Comparison of normalized frequencies (dl/λ) obtained with the TLM and FD-TD methods under identical simulation conditions for the geometries in Fig. 5.6

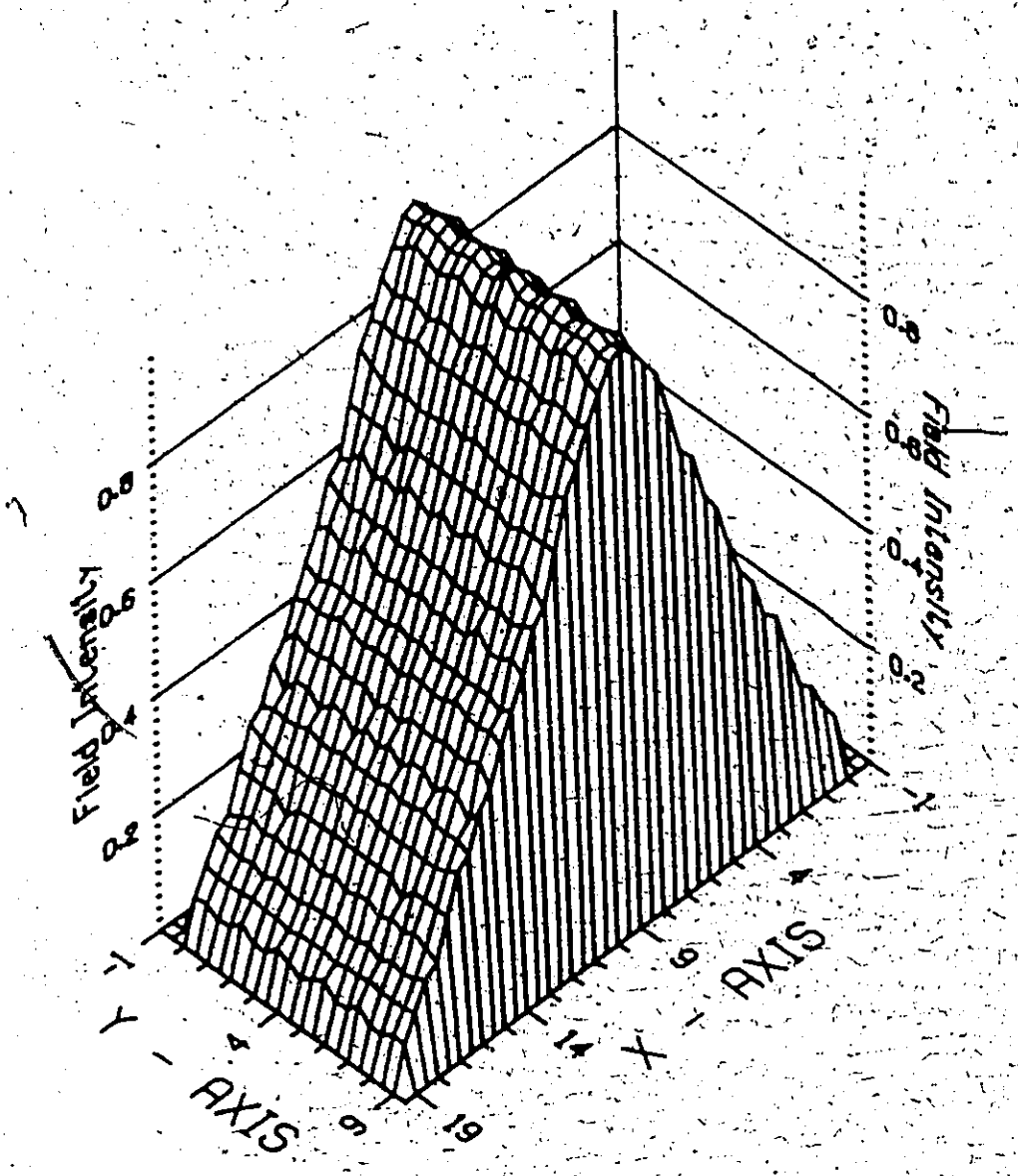

Fig. 5.7 A time domain solution of the structure given in Fig. 5.6 a)

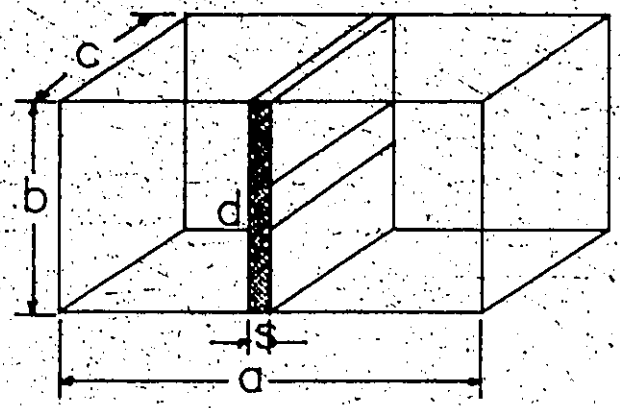

a : 20 mm
b : 10 mm
c : 15 mm
d : 4 mm
s : 1 mm
e_r : 2.22

a) a finline cavity

	Saguet [24]		This method	
	S.D.A	Variable mesh TLM	FD-TD	TLM
Resonant Freq. (GHz)	10.77	10.14	10.74	10.74
Number of Iteration		1000	600	600
CPU time (s)			155	380

b) Resonant frequencies of the unilateral finline of a)

Fig. 5.8 A finline resonator and resonant frequencies obtained by both methods

vergence. Fig. 5.9 shows the dispersion characteristics of a finline with the same cross-section as that used by Saguet, computed with our method. The results obtained by both methods show no difference. A comparison has been made with the results obtained with the spectral domain method. The stability factor used in this case was 0.3.

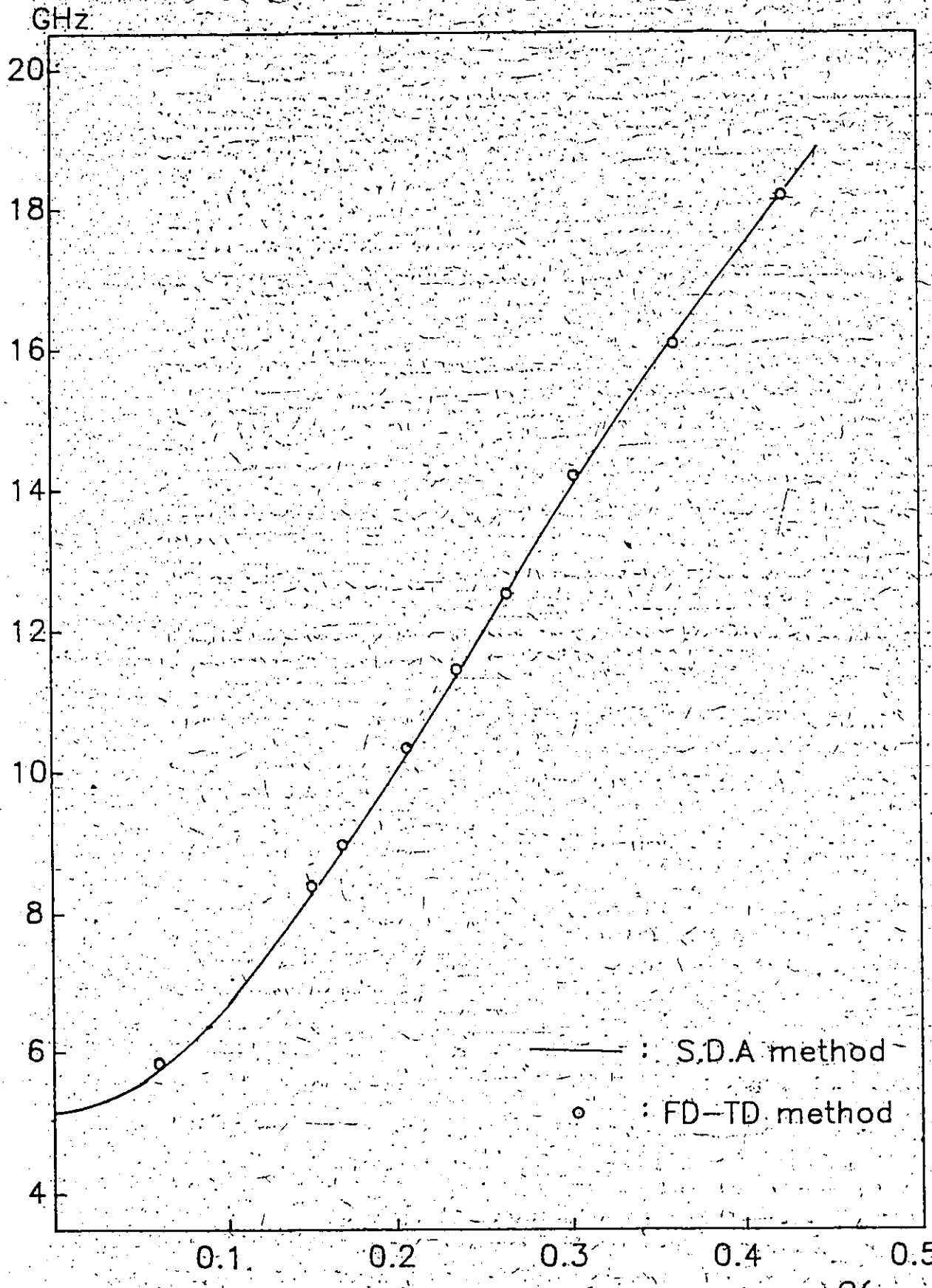

Fig. 5.9 Dispersion diagram of unilateral finline with the cross-sectional geometry given in Fig. 5.8.a)

Chapter VI

DEVELOPEMENT OF IRREGULAR MESH FD-TD TECHNIQUE

6.1 INTRODUCTION

The discussion of the last chapter has shown that the FD-TD technique yields the time domain field distributions and frequency domain solutions in a similar way as the TLM method. A simple and efficient routine to solve electromagnetic eigenvalue problems for three-dimensional geometries has been established, using the former method.

However, this new technique still requires comprehensive computer resources in some practical applications where a large number of meshes is required. Especially, the application of this method to a finline or general types of E-plane circuit may require unnecessarily high discretization in areas of relatively constant fields due to their highly localized inhomogeneous nature. The finer the mesh, the more computer resources are required.

This can be best illustrated with some numerical examples: the completely general FD-TD model capable of representing all the anisotropic medium properties would require 12 real-number storage places per node. If for a particular

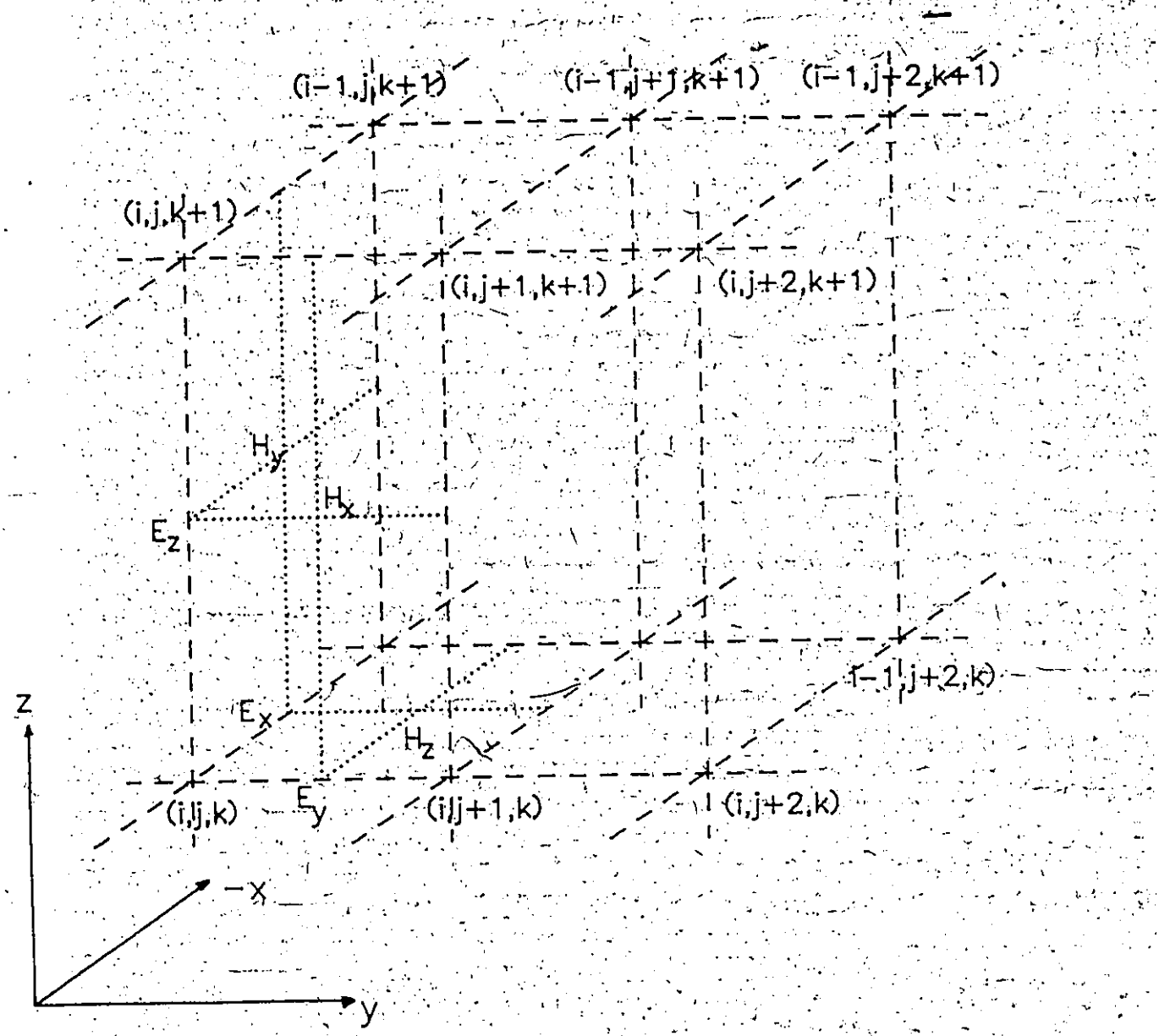

o Grading technique is employed to the y-direction only (grading ratio 1 : 0.5)

Fig. 6.1 The variable mesh FD-TD network

case the dimensions needed are 12x6x15 the storage requirement is about 24K words in most computer systems. If the size increases to 13x7x16 the storage requirement jumps to 35K words, and to 46K words if the dimensions are extended to 14x8x17. These considerable increases in storage demands for the increase by one unit node, may seriously limit the range of application.

Since most planar structures have a highly inhomogeneous geometry, it may be proper to employ different mesh sizes in different regions such that the areas of highly nonuniform fields contain a large number of nodes. Because the programming of FD-TD method of numerical analysis is very similar to that of the TLM method, it seems logical to apply the irregular mesh technique which has been used in the TLM method and assess the results from the point of view of additional complexity versus the increase in efficiency obtained. The outline of the extension procedure is given in the present chapter.

The basic program structure of the irregular mesh FD-TD algorithm will be similar to that of the original FD-TD. The difference is that instead of using everywhere the same unit cubic cell, i.e $dx = dy = dz$, a basic mesh element can now have arbitrary dimensions(dx_i, dy_j, dz_k). A schematic diagram of a basic element is given in Fig. 6.1. The relative magnitudes of each space mesh dl with respect to the refer-

ence mesh length dl_o are incorporated into the difference equation (5.14). This reference mesh length dl_o is required to compute the exact frequency in the Fourier transform procedure.

The set of equations thus contains a scaling factor which changes locally and can be programmed in a similar way as material parameters (i.e., permeability and permittivity). Therefore the effect of irregular mesh on isotropic media becomes equivalent to the wave propagation on the anisotropic media. This concept is elaborated on in the next section.

6.2 IRREGULAR MESH FD-TD MODEL

6.2.1 Modelling

Since the basic concept of the variable FD-TD technique is similar to that in section (5.2.2), only an outline is given here. Irregular space step size can be implemented by altering the difference equations (5.14). In these equations, dx, dy and dz can all be different. Then the H_x and E_x components of the set of difference equations will be of the following form:

$$H_x^{n+1/2}(i,j+1/2,k+1/2) = H_x^{n-1/2}(i,j+1/2,k+1/2)$$
$$+1/uxx(i,j+1/2,k+1/2)Z_o[cdt/dz_k\{E_y^n(i,j+1/2,k+1)$$
$$-E_y^n(i,j+1/2,k)\}+cdt/dy_j\{E_z^n(i,j,k+1/2)-E_z^n(i,j+1,k+1/2)\}] \qquad (6.1.a)$$

$$E_x^{n+1}(i+1/2,j,k) = E_x^n(i+1/2,j,k) + Z_o/exx(i+1/2,j,k)$$
$$[cdt/dy_j\{H_z^{n+1/2}(i+1/2,j+1/2,k)-H_z^{n+1/2}(i+1/2,j-1/2,k)\}$$

$$+cdt/dz_k\{H_y^{n+1/2}(i+1/2,j,k-1/2)-H_y^{n+1/2}(i+1/2,j,k+1/2)\}] \quad \ldots\ldots\ldots (6.1.b)$$

where $Z_o = \sqrt{\mu_o/\varepsilon_o}$ and $dx_i \neq dy_j \neq dz_k$. All other components can be expressed in a form similar to (6.1). All integer arguments are identical to those of the finite difference equation in (5.14), and are therefore supressed for the sake of simplicity in (6.1).

Suppose dx_i, dy_j and dz_k are smaller than the unit mesh dx, dy, and dz which are equal to the unit reference length such that

$$dx_i = p \times dx$$

$$dy_j = q \times dy \qquad (6.2)$$

$$dz_k = r \times dz, \text{ and}$$

$$0 < p, q, r \leq 1 \quad , \quad dx = dy = dz$$

Then by substituting dx_i, dy_j and dz_k of (6.2) into (6.1), we obtain:

$$H_x^{n+1/2}(i,j+1/2,k+1/2) = H_x^{n-1/2}(i,j+1/2,k+1/2) +$$
$$sxx'[\{E_y^n(i,j+1/2,k+1) - E_y^n(i,j+1/2,k)\}/p$$
$$+ \{E_z^n(i,j,k+1/2) - E_z^n(i,j+1,k+1/2)\}/q]$$
$$(6.3.a)$$
$$H_y^{n+1/2}(i+1/2,j,k+1/2) = H_y^{n-1/2}(i+1/2,j,k+1/2) +$$
$$syy'[\{E_z^n(i+1,j,k+1/2) - E_z^n(i,j,k+1/2)\}/p$$
$$+ \{E_x^n(i+1/2,j,k) - E_x^n(i+1/2,j,k+1)\}/r]$$

(6. 3.b)

$$H_z^{n+1/2}(i+1/2,j+1/2,k) = H_z^{n-1/2}(i+1/2,j+1/2,k) +$$
$$szz'[\{E_x^n(i+1/2,j+1,k) - E_x^n(i+1/2,j,k)\}/q$$
$$+ \{E_y^n(i,j+1/2,k) - E_y^n(i+1,j+1/2,k)\}/r]$$

(6. 3.c)

$$E_x^{n+1}(i+1/2,j,k) + E_x^n(i+1/2,j,k) + sxx$$
$$[\{H_z^{n+1/2}(i+1/2,j+1/2,k) - H_z^{n+1/2}(i+1/2,j-1/2,k)\}/q$$
$$+ \{H_y^{n+1/2}(i+1/2,j,k-1/2) - H_y^{n+1/2}(i+1/2,j,k+1/2)\}/r]$$

(6. 3.d)

$$E_y^{n+1}(i,j+1/2,k) = E_y^n(i,j+1/2,k) + syy$$
$$[\{H_x^{n+1/2}(i,j+1/2,k+1/2) - H_x^{n+1/2}(i,j+1/2,k-1/2)\}/r$$
$$+ \{H_z^{n+1/2}(i-1/2,j+1/2,k) - H_z^{n+1/2}(i+1/2,j+1/2,k)\}/p]$$

(6. 3.e)

$$E_z^{n+1}(i,j,k+1/2) = E_z^n(i,j,k+1/2) + szz$$
$$[\{H_y^{n+1/2}(i+1/2,j,k+1/2) - H_y^{n+1/2}(i-1/2,j,k+1/2)\}/p$$
$$+ \{H_x^{n+1/2}(i,j-1/2,k+1/2) - H_x^{n+1/2}(i,j+1/2,k+1/2)\}/q]$$

(6. 3.f)

where $sxx' = cdt/(uxxZ_o dx)$ $\quad sxx = Z_o cdt/(exxdx)$

$syy' = cdt/(uyyZ_o dy)$ $\quad syy = Z_o cdt/(eyydy)$

$szz' = cdt/(uzzZ_o dz)$ $\quad szz = Z_o cdt/(ezzdz)$

The final equations (6. 3) are the basic form which represents the irregular mesh algorithm, at each mesh element, in terms of its physical dimensions and physical properties. If p, q, and r are all unity, (6. 3) reduces to the uniform mesh algorithm set of (5.14).

6.2.2 Programming procedure and flow chart

The difference between the uniform mesh FD-TD and the irregular mesh FD-TD lies only in the additional storage requirement for the geometrical mesh size information p, q, and r. In order to perform the Fourier transformation correctly, we need a reference mesh size. All other different size meshes can be normalized to this specific reference value. Then, irregularly graded portions of the geometry, which could at the same time be situated in regions of higher dielectric constant, must have space parameters p, q, and r smaller than unity.

Before iteration of the algorithm starts, the geometry of the grid meshes for the structure under study should be determined properly. The relative size of the mesh elements with respect to x, y, and z directions are stored in three one-dimensional arrays, XD(NX+1), YD(NY+1), and ZD(NZ+1). NX, NY, and NZ are the total number of meshes in the three orthogonal directions. These arrays are then substituted into equation (6. 3). All remaining procedures follow the regular mesh algorithm. The flow chart is given in Fig. 6.2.

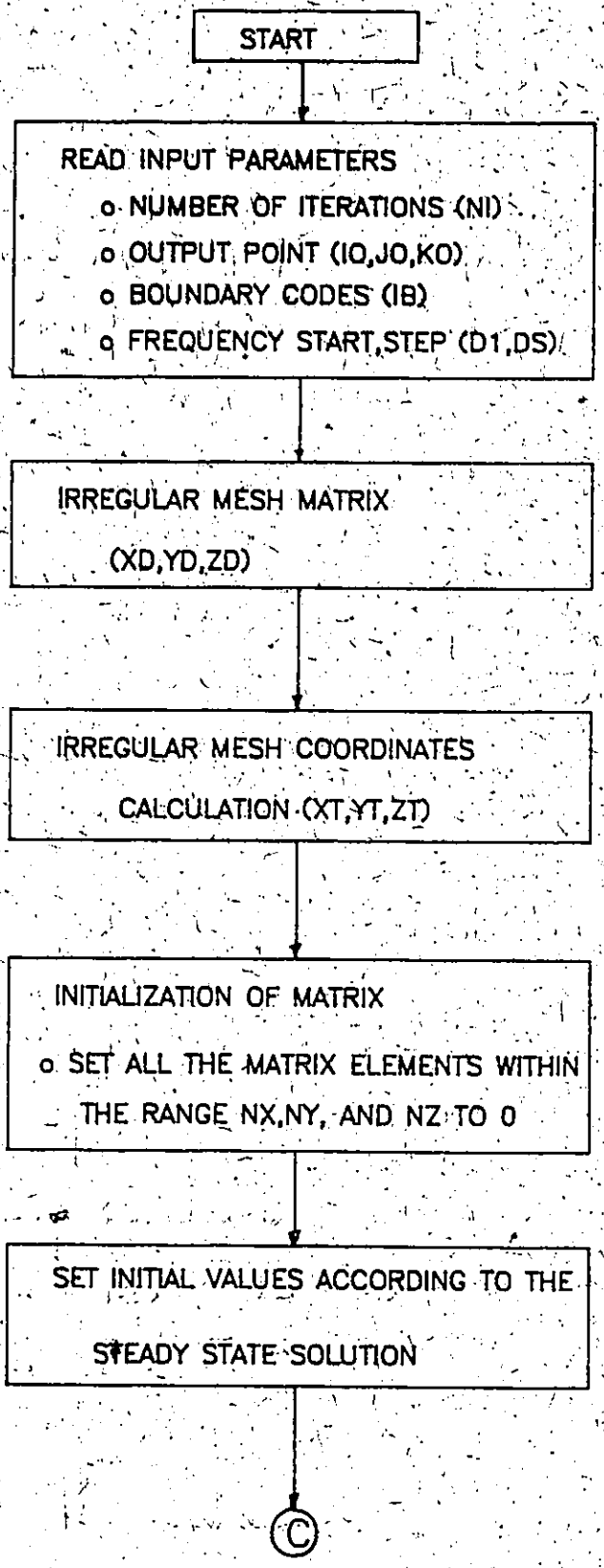

Fig. 6.2 The flow chart of the irregular FD–TD program

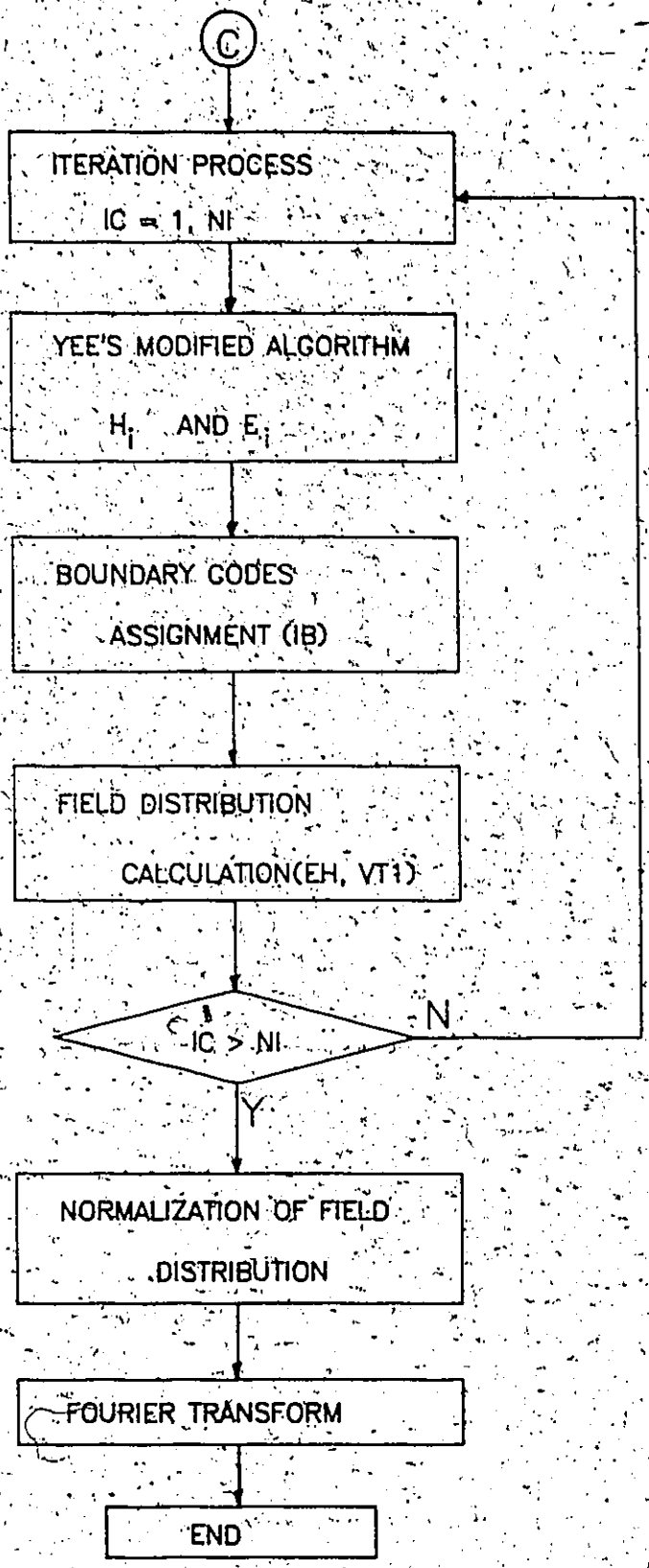

Fig. 6.2 continued

6.3 NUMERICAL EXAMPLE

6.3.1 Long empty rectangular cavity

This example is used to demonstrate an application of the technique. Fig. 6.3 shows the type of cavity under consideration and the number of mesh elements needed when it is subdivided into cubic mesh elements. The comparison of these cases gives an idea about the reduction achieved in the total number of nodes and hence the computer storage and processing time. Results for the dominant mode TE_{101} are shown in Table 6.1. Agreement with the analytical results is good for a wide range of frequencies and grading ratio.

6.3.2 Dielectric slab loaded cavity

The dielectric slab loaded cavity is a section of a very useful type of guiding structure known for its lower cutoff frequency and characteristic impedance compared with an ordinary waveguide.

Furthermore, a dielectric loaded cavity, unlike a ridged waveguide cavity, does not reduce the air gap, and consequently has a higher power handling capacity because of the dielectric material located in the region where breakdown is most likely. In addition to the above advantages, the slab loaded guide is used as a phase-shifting structure such as a phase shifter or a delay line.

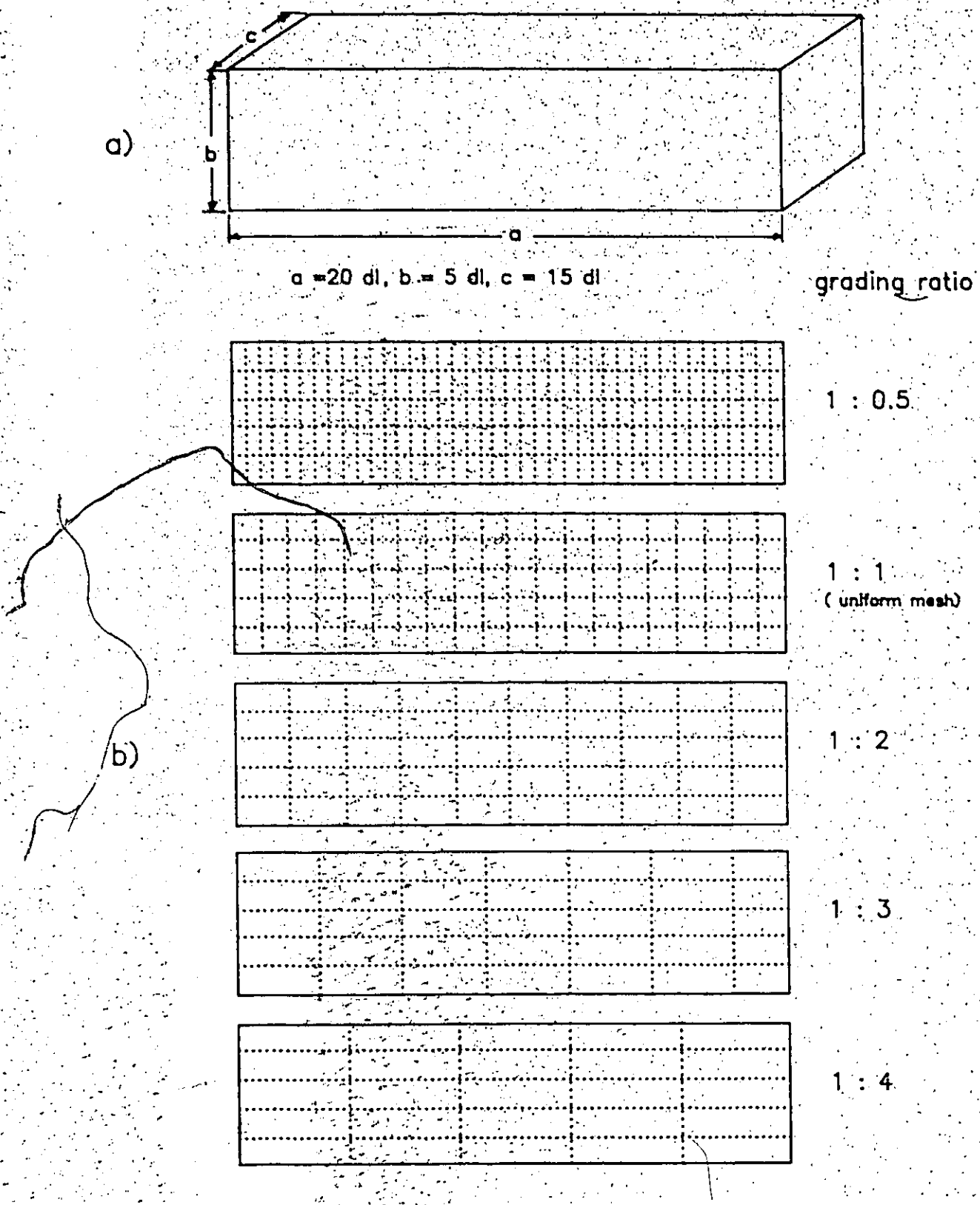

Fig. 6. 3 A long rectangular cavity and variable mesh scheme to calculate resonant frequency.

grading ratio	FD-TD method (error %)	CPU time (s)
1 : 0.5	0.04168 (0.02)	223.1
1 : 1	0.04170 (0.07)	143.2
1 : 2	0.04162 (0.12)	88.1
1 : 3	0.04160 (0.16)	72.0
1 : 4	0.04140 (0.64)	60.1
exact solution	0.041667	

Table 6.1 Normalized resonant frequencies of TE_{101} mode obtained by employing different grading ratios given in Fig. 6.3

This structure was evaluated with the following mesh configurations:

1) A uniform mesh with cubic elements throughout the cavity. This mesh is considered the reference mesh in the following configurations with variable mesh size.

2) A mesh with two different element sizes, one being equal to the reference size, and the other being four times as fine. In two consecutive computation, the finer mesh part was placed

   a) in the dielectric region.

   b) in the air-filled region.

Fig.6.4 shows these different arrangements. The results are compared in Table 6.2. It appears clearly that the irregular mesh technique is advantageous only when the finer mesh is in the region of higher field intensity.

The stability factor s must be reduced in proportion to the grade ratio. However, reduction of the stability factor does not necessarily reduce the accuracy of the computation as long as the output spectrum does not contain other modes sidelobes of which could interfere with the cavity solution under study.

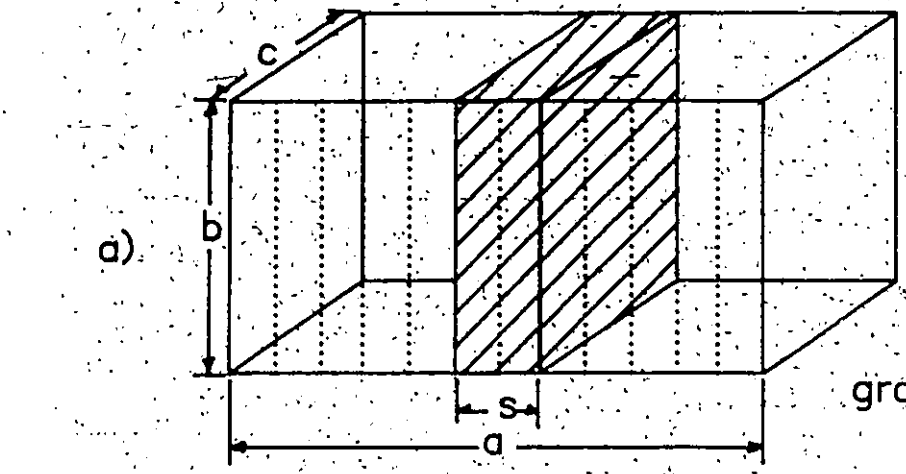

a = 12dl
b = 6dl
c = 8dl
e_r = 3.75

grading ratio =1:1

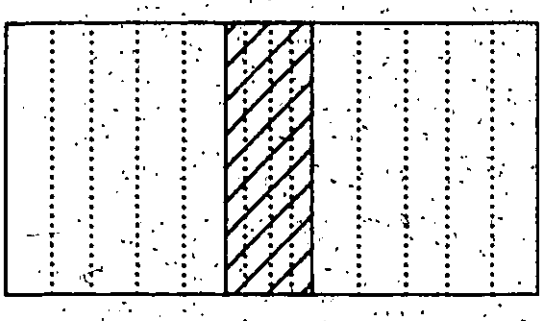

grading ratio = 1 : 0.5

b)

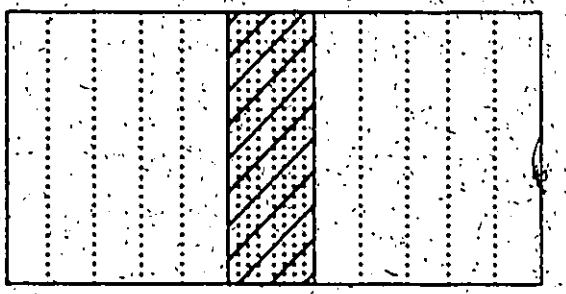

grading ratio = 1 :0.25

c)

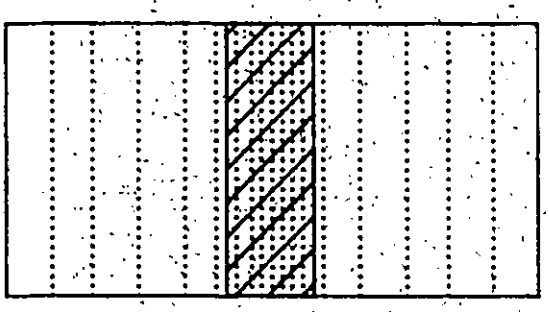

grading ratio = 1 :0.25

d)

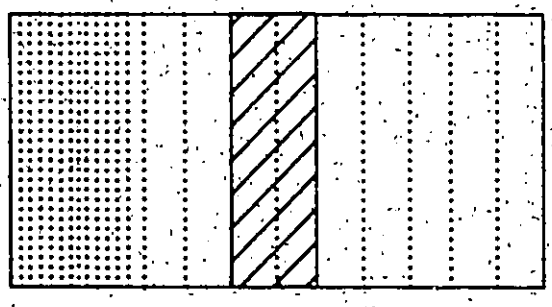

grading ratio = 1 :0.25

e)

Fig. 6.4 Employment of different mesh sizes.

grading ratio (Fig. #)	graded TLM		variable FD-TD	
	(error %)	CPU (s)	(error %)	CPU (s)
1 : 1 (a) uniform mesh	0.0516 (0.77)	144	0.0516 (0.77)	51
1 : 0.5 (b)	0.0517 (0.58)	155	0.0519 (0.19)	59
1 : 0.25(c,d)	0.0518 (0.38)	170	0.0520 (0)	68
1 : 0.25 (e)	0.0516 (0.77)	170	0.0516 (0.77)	67
exact value	0.0520			

Table 6.2 Resonant frequencies of LSE mode obtained by employing different grading ratios given in Fig. 6.4

6.3.3 A Time Domain Solution of a Unilateral finline

The field distribution of a finline structure given in Fig. 5.9 is calculated by taking the time average of the time domain solution at each mesh point. Because of the inherent inaccuracy of time domain solutions of the FD-TD technique compared to those in the frequency domain mentioned in chapter V, it is essential to use the graded mesh technique to ensure the highest possible accuracy.

The y-component of the electric field at the cross-sectional plane is shown in Fig 6.5. The numerical data obtained by this scheme also demonstrates the versatility of this method.

6.4 A COMPARISON OF THE GRADED MESH TLM AND FD-TD METHODS

Although the TLM and the FD-TD methods differ conceptually, they lead to very similar algorithms. A qualitative comparison of the requirements for computer memory and algorithm steps for the purpose of computing eigenvalues of resonant structures has been made in Table 6.3. A general inhomogeneous wave propagating medium is assumed in this comparison.

From this comparison, the irregular mesh FD-TD algorithm is definitely superior in obtaining eigenvalues to the other as far as computer resource requirements are concerned. Fur-

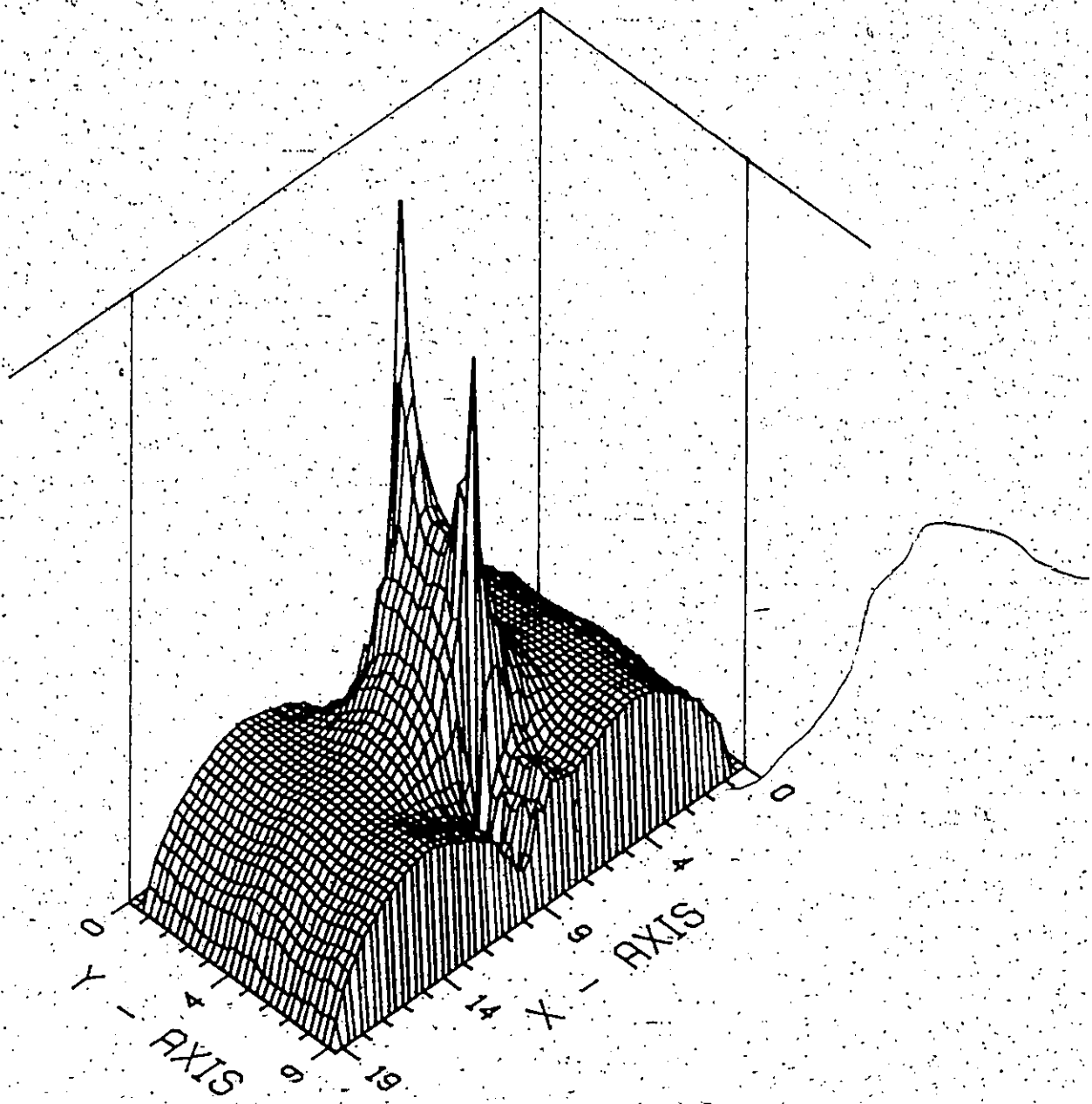

Fig. 6.5 The field distribution (E_y) of a finline given in Fig. 5.8.a)

	GRADED TLM [24]		VARIABLE MESH FD-TD	
REAL NUMBER PLACE REQUIRED PER NODE	PULSES ON THE LINK LINE AND PERMITTIVITY , PERMEABILITY STUBS	18	COMPONENTS OF ELECTROMAGNETIC FIELD	6
	OPEN CIRCUIT STUB ADMITTANCE	3	VALUES OF PERMITTIVITY AND PERMEABILITY	2
	SHORT CIRCUIT STUB IMPEDANCE	3		
	SHUNT CIRCUIT SCATTERING PARAMETER COEFFICIENT	3		
	PARALLEL CIRCUIT SCATTERING PARAMETER COEFFICIENT	3		
	VALLUES OF PERMITTIVITY AND PERMEABILITY	2		
	TOTAL	32	TOTAL	8
ALGORITHM STEPS PER ITERATION PER EACH COMPONENT	ADDITION (4 REAL NUMBERS)	1	ADDITION AND SUBSTRACTION	1
	MULTIPLICATION (2 REAL NUMBERS)	1		
	REPLACEMENT	5	MULTIPLICATION	1
	TOTAL	7	TOTAL	2

Table 6.3 A comparison of computer storage requirement and algorithm steps required in graded TLM and variable mesh FD-TD methods

thermore, before iteration begins, the TLM method requires that six variables of stub impedance and admittance must be calculated which are not included in this comparison. Therefore, this comparison may explain the considerable difference in CPU time spent in both algorithms.

6.5 DISCUSSION

In this chapter, the graded mesh technique was developed and its advantages are illustrated by applications to inhomogeneous resonators. The uniform mesh algorithm has been extended such that different mesh sizes could be applied separately to different regions under study. Therefore, unnecessarily fine mesh deployment in an air-filled space where field variations are relatively small, can be avoided. The advantage of this variable mesh technique is evident because most microwave planar circuits exibit regions of highly inhomogeneous field distribution. Especially in a finline structure, maximum field strength and field derivative exist in the gap along the dielectric interface. Therefore, it is logical to employ a small mesh size in those areas, while the reference mesh in the air-filled space is several times larger than the fine mesh.

It is also noted that higher grading ratios require smaller values of the stability factor s. This means that a higher number of iterations is needed to obtain an identical

frequency spectrum. However, the reduction ratio of s is not necessarily proportional to the grading ratio. For example, in our simulation, a grading ratio of four requires only half of the original stability factor s. With an identical number of iterations, this doubles the width of the frequency spectrum. To obtain an identical frequency spectrum, the number of iterations must thus be doubled.

A specific example may illustrate the advantage of this technique over the uniform mesh technique. As shown in section (5.4.2), the CPU time is linearly proportional to the number of mesh cells in one dimension. Suppose we employ the grading technique in one dimension only, which is usual in a planar structure analysis, and have ten mesh cells in that direction. If one of these ten cells is subdivided into four, (grading ratio 1 : 0.25), the CPU time is increased by 30 %. Since the mesh size has been reduced in one part of the structure, the stability factor s must be reduced, in this case by 50 %. This increases the CPU-time by a factor of 2.6 if the same resolution in the spectral domain is desired.

Chapter VII

NUMERICAL ANALYSIS OF VARIOUS MILLIMETER WAVE PLANAR CIRCUITS

7.1 INTRODUCTION

In this chapter the general three-dimentional FD-TD program is used to analyze a wide variety of three-dimensional millimeter wave cavity structures. The results presented here include the cutoff frequencies of the groove waveguide (two-dimensional problem), the resonant frequencies of empty and partially filled cavities. In particular, cavities containing finlines have been studied, and the resonant frequencies of cavities of various length are used to plot frequency versus dispersive phase constant curves.

The finline solutions include unilateral and bilateral finlines with a step change in gap width. In all cases, whenever possible, the results obtained by this method have been compared with those obtained with other methods. In addition to the frequency solution, steady state field distributions have been obtained in selected cross-sections of the structures. This has been done by calculating average field values at each point in the mesh. This feature represents an advantage of this method over the TLM. Because

the TLM requires two simulation runs , i.e. one for the resonant frequency and one for the field calculation, double amount of CPU time is required. In this case, this algorithm may be six times faster than that of TLM.

7.2 RECTANGULAR CAVITY

The method is first applied to the simplest form of a three-dimensional problems with and without dielectric slab (see Fig. 7.1). Table 7.1 shows the resonant frequencies of the TE_{101} mode in such a cavity obtained with TLM and FD-TD. They are also compared with results obtained with the transverse resonant method in the case of a dielectric loaded cavity. As shown in this simple example, the results of both methods are virtually identical. The frequency step used is 0.5.

7.3 CUTOFF FREQUENCY OF A GROOVE GUIDE

Groove guide is one of a group of waveguiding structures proposed some 20 or more years ago for use at millimeter wavelengths. Those waveguides were not investigated beyond some initial basic studies because they were not yet needed, and no adequate sources for millimeter waves were available. Today, such sources are readily available, and the many advantages of millimeter waves are being increasingly exploited.

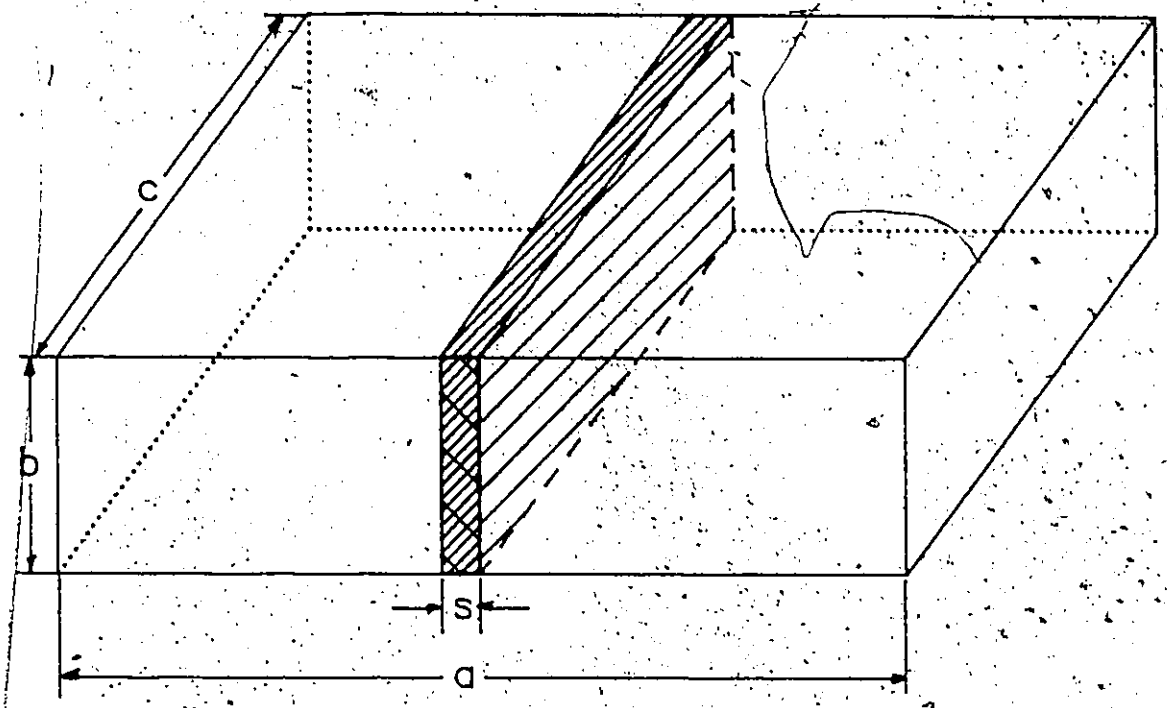

a = 20 dl

b = 5 dl

c = 15 dl

s = dl

e_r = 1 or 2.22

Fig. 7.1 A slab loaded rectangular resonator

	e_r \ c/dl	8	10	12	14	16	18	22
FD–TD	1.0	20.13	16.74	14.55	13.05	12.03	11.22	10.14
	2.22	18.84	15.72	13.68	12.30	11.31	10.59	9.57
TLM	2.22	18.95	15.75	13.71	12.30	11.30	10.59	9.52
S.D.A	2.22	18.75	15.63	13.62	12.30	11.30	10.60	9.58

Table 7.1 Resonant frequencies (GHz) obtained by different methods for a rectangular cavity given in Fig. 7.1

The cross-section of a groove guide is shown in Fig. 7.2.a), and an indication of the dominant mode electric field in its cross-section is given in Fig. 7.2.b). The main attractiveness of the groove guide resides in its low losses. This is so because the electric field is parallel to the metal walls, and the attenuation associated with those walls decreases as the frequency is increased; conversely, the attenuation increases with increasing frequency when the electric field is perpendicular to the walls.

The first theoretical study of the propagation constant and cutoff frequency of the dominant mode was carried out by Nakahara and Kurauchi[63], resulting in first order result by taking only the dominant transverse mode in each region of the cross section. The procedure, however, neglects the presence of all higher order transverse modes. Recently, Oliner and Lampariello[64] have proposed an improved equivalent network approach which includes higher order mode effects, and presents results which are closer to measured data.

The FD-TD technique was applied to this structure to obtain normalized cutoff frequencies, and very close agreement with previous result[64] was obtained as shown in Fig. 7.3. Deviations are only noticeable for very small and very large ratio of a'/a. The discrepancies can be explained as follows. In the case of large a'/a ratio, the number of mesh

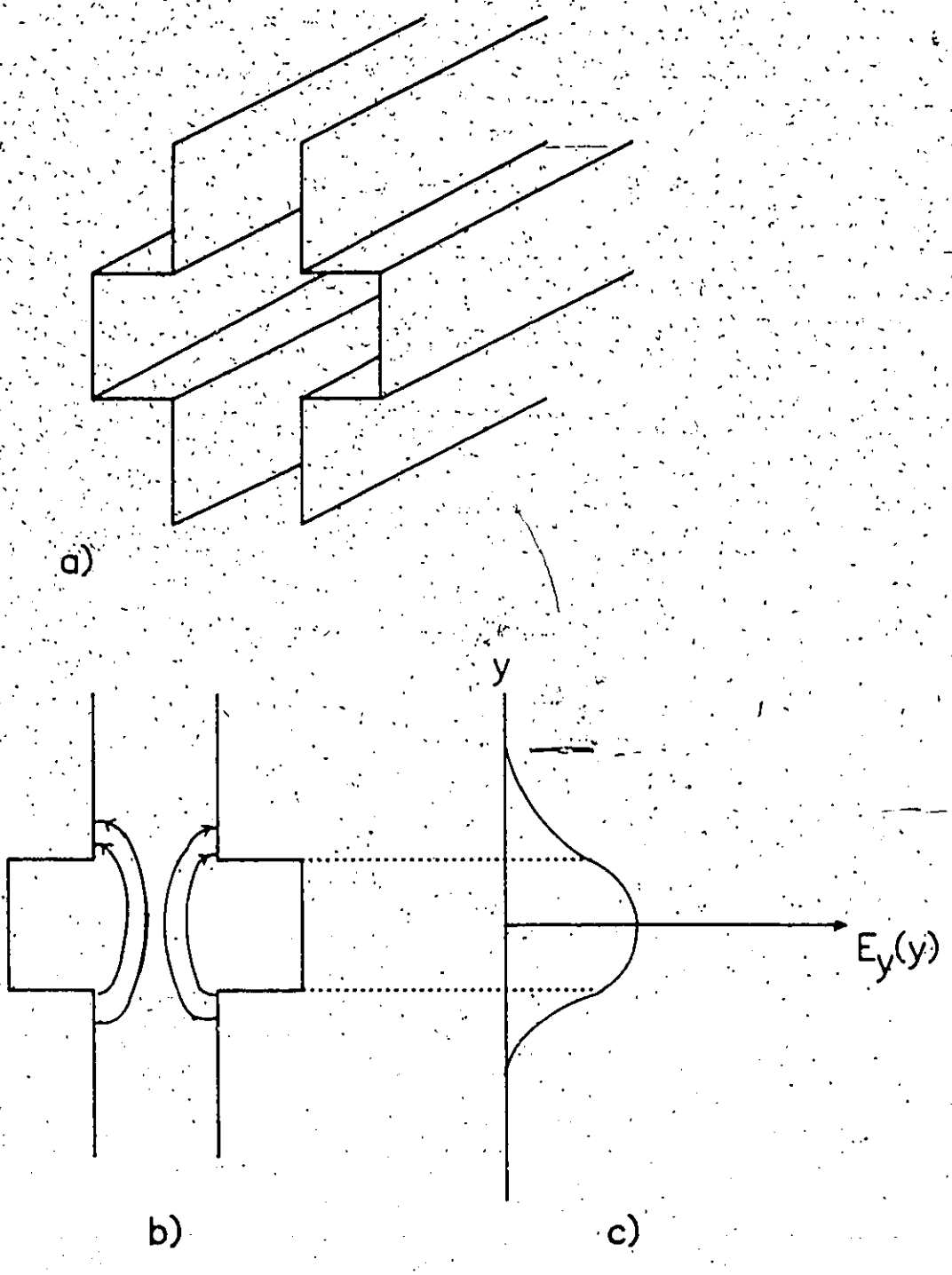

Fig. 7.2 A groove guide and its field distribution

a) A groove waveguide
b) Electric field lines in the cross-section.
c) Approximate plot of the vertical component E_y as a function of vertical position y.

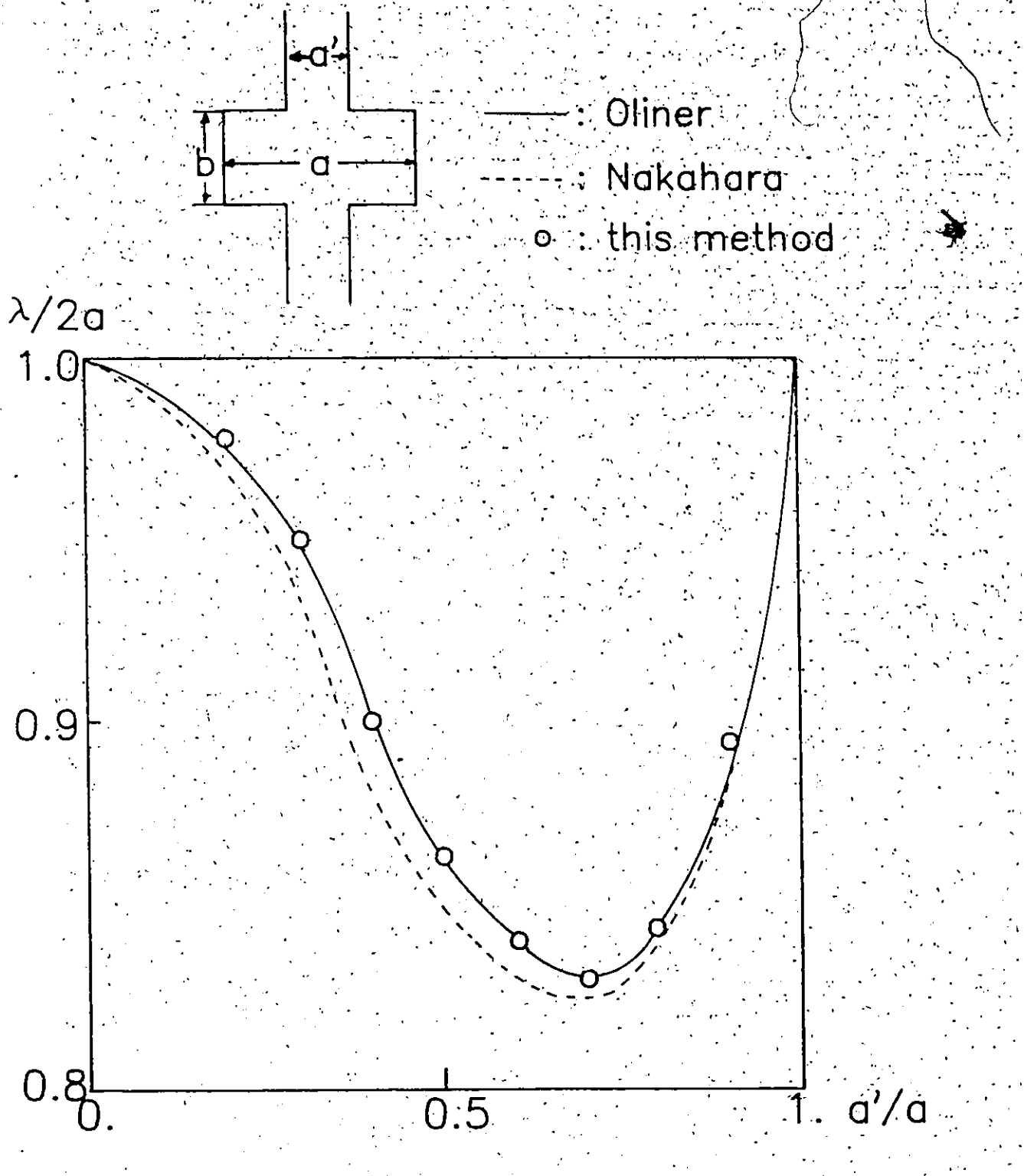

Fig. 7.3 Normalized cut off frequencies of a groove guide

elements in the narrow section becomes too small, resulting in increasing spatial resolution error. In the opposite case, the higher order modes decay only very slowly in the lateral part of the structure. Since in the FD-TD model, the groove guide is short-circuited on both sides, the effect of these walls alter the result quite noticeably. In our case, both extreme cases are of no practical interest.

7.4 DIELECTRIC LOADED WAVEGUIDE

E-plane circuits are almost exclusively suspended in the center of a waveguide enclosure because only modes with even symmetry about the center will be affected in this case. Furthermore, maximum interaction with the dominant TE_{10} mode is achieved which, in turn, maximizes the single mode bandwidth of the circuit.

The electric characteristics of a waveguide containing E-plane slabs of dielectric have been investigated by many authors[65]-[67]. Although the dominant mode in such a structure is clearly the distorted TE_{10} mode, it is not at all obvious, as Gardiol[67] has pointed out, that the first higher order mode will be the distorted TE_{20} mode. In fact, for very thin substrates the LSE and LSM modes are found to limit the single mode bandwidth.

Preliminary to analysis of the finline the dispersion characteristics of the dielectrics are obtained in this sec-

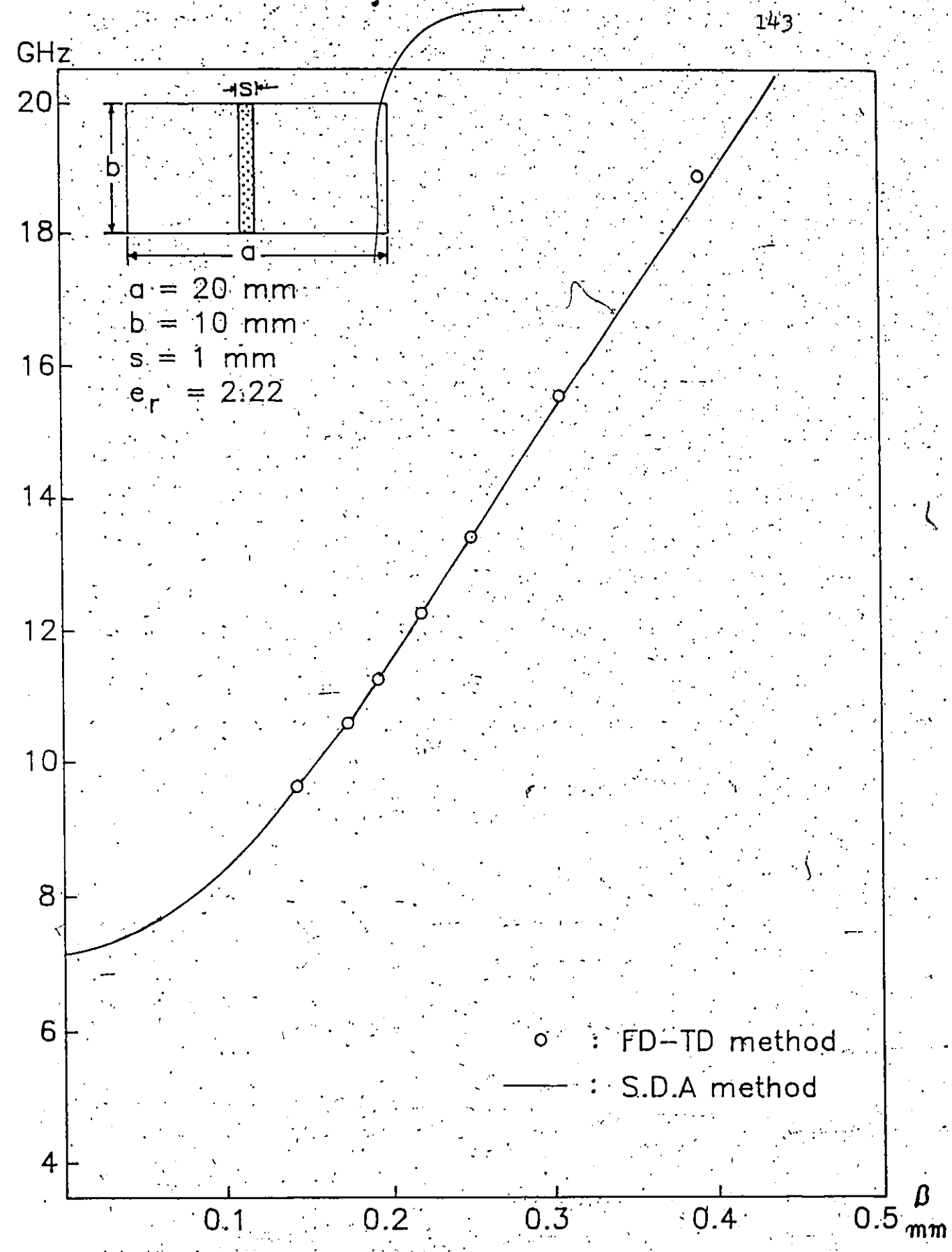

Fig. 7.4 Dispersion diagram of slab loaded waveguide

tion. The dispersion characteristics of such a waveguide are obtained with the use of a half wavelength three-dimensional cavity. The curves also are compared with the results of the spectral domain analysis. Fig.7.4 shows this example.

7.5 DISPERSION CHARACTERISTICS OF FINLINES

Saguet[25] has applied a variable mesh TLM method to the three-dimensional finline resonator. In this example, we have applied both graded mesh FD-TD and graded TLM methods to find resonant frequencies of the various finline resonators. In most cases, it was found that the results of the graded mesh TLM and graded mesh FD-TD are virtually identical. Therefore, only FD-TD results will be used in the following characteristic curves.

Like in the TLM technique, the resonant frequency corresponding to various lengths L of the cavity was computed to plot the frequency versus phase constant curves shown in Fig. 7.5, and Fig. 7.6. All the results are compared with those obtained by spectral domain analysis. Those Figures show dispersion curves of unilateral and bilateral finlines with different gap width.

The curves of Fig. 7.5 and Fig. 7.6 demonstrate the high accuracy of the results obtained by this method, even though only two nodes were placed inside the dielectric slab. As

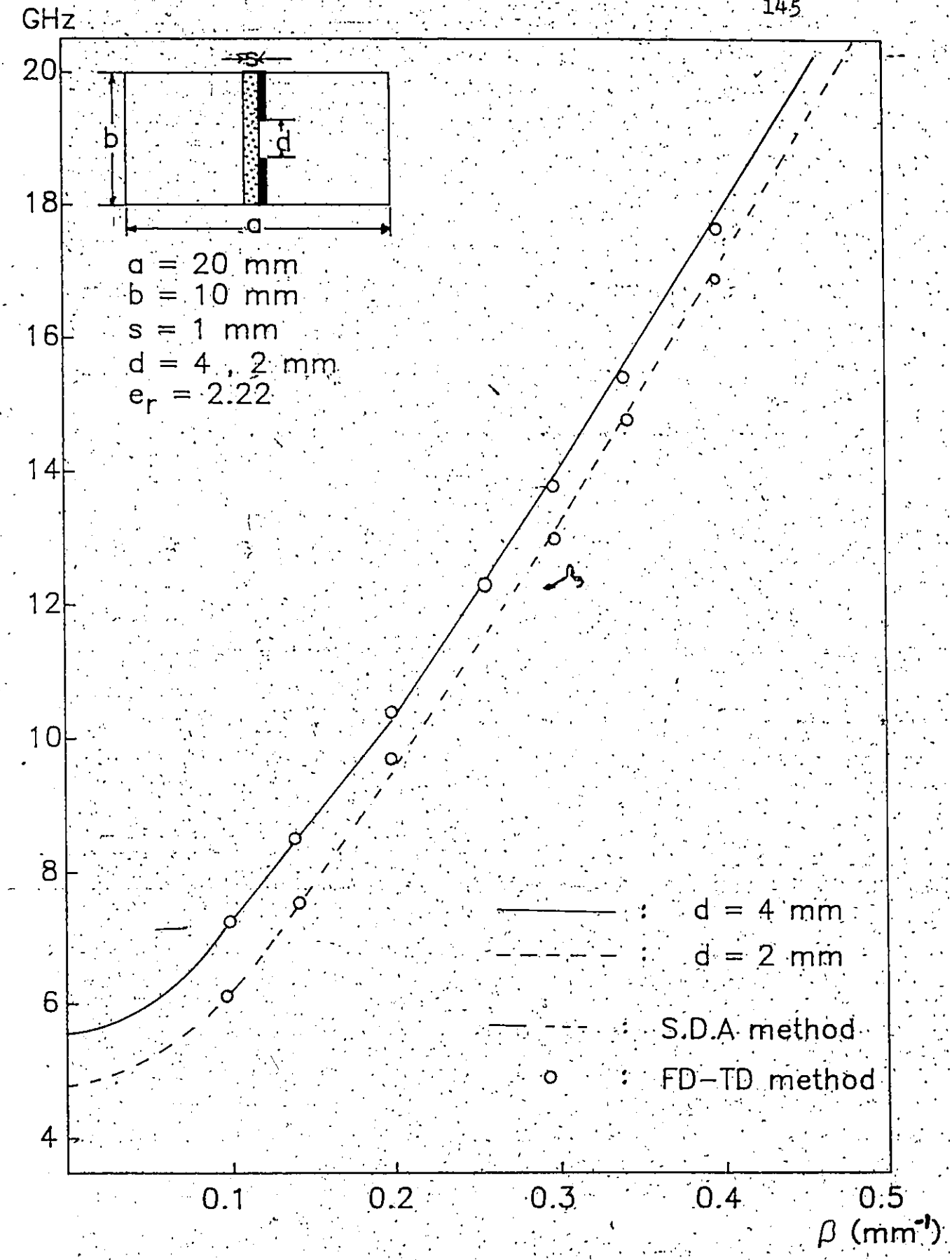

Fig. 7.5 Dispersion diagram of unilateral finline

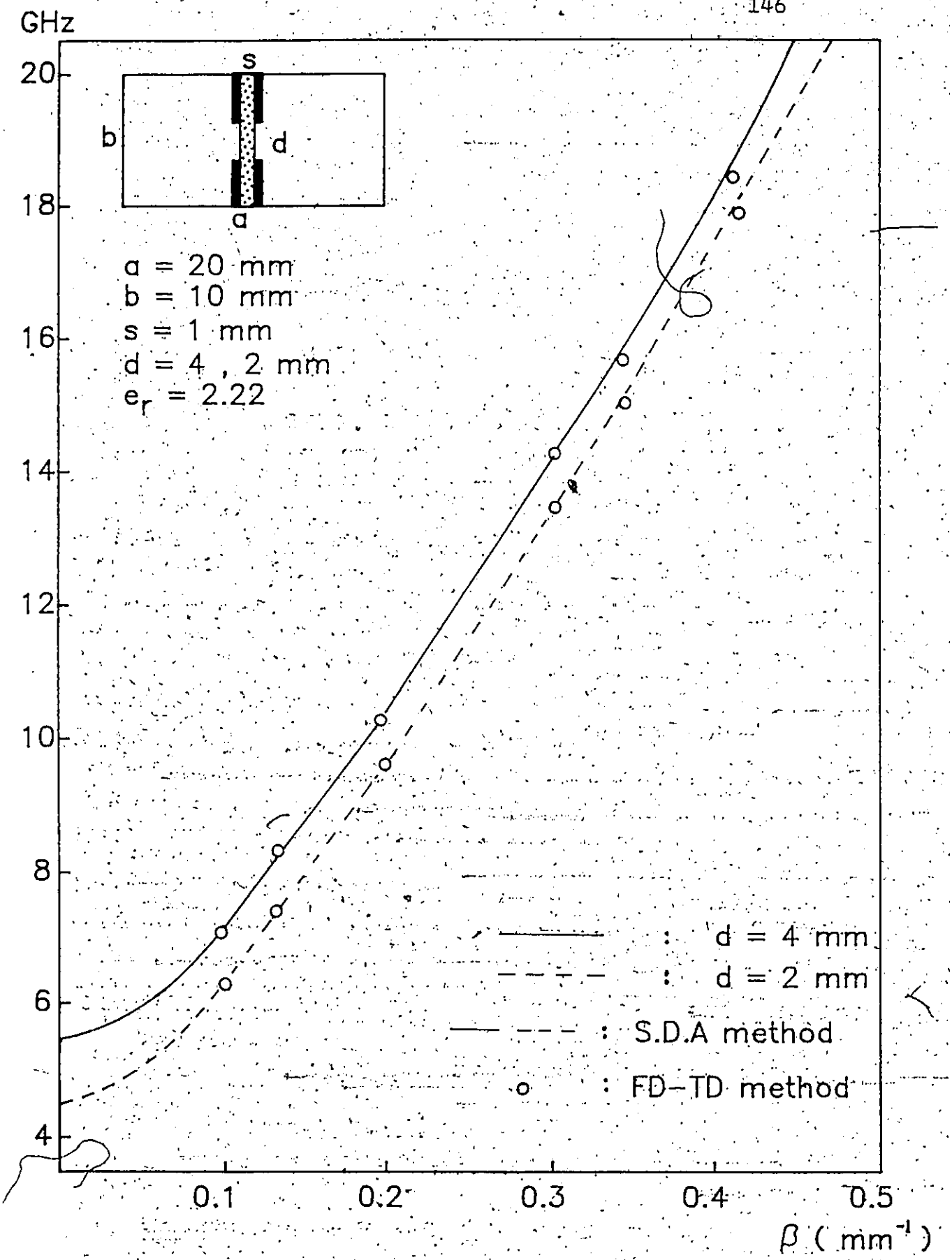

Fig. 7.6 Dispersion diagram of bilateral finline

pointed out already, the CPU time of the FD-TD was about one third of that of the graded mesh TLM.

7.6 FINLINE DISCONTINUITIES

As discussed in chapter II, finline filters contain inductive strips. A discontinuity element closely related to these is the finline short circuit. Konishi and Matsumura have presented a rigorous field expansion approach for this problem when no dielectric substrate is present[68]. Hoefer and Pic[72] have carried out a series of resonator measurements to determine the elements of an appropriate equivalent circuit for the short circuit end effect when a dielectric substrate is present.

A more rigorous approach was taken by Knorr[69] who has computed the eigenfrequencies of finline resonators using the spectral domain method and has deduced equivalent circuit descriptions for the short circuit from those calculations. Koster and Jansen[70] have solved the more general problem of an inductive strip of finite width of which the short circuit is a limiting case. They also used a spectral domain method approach and arrived at equivalent circuit descriptions for the discontinuity.

In the first example (Fig.7.7), the dispersion curve of a finline discontinuity has been obtained by using the same procedure applied to the uniform finline. The second exam-

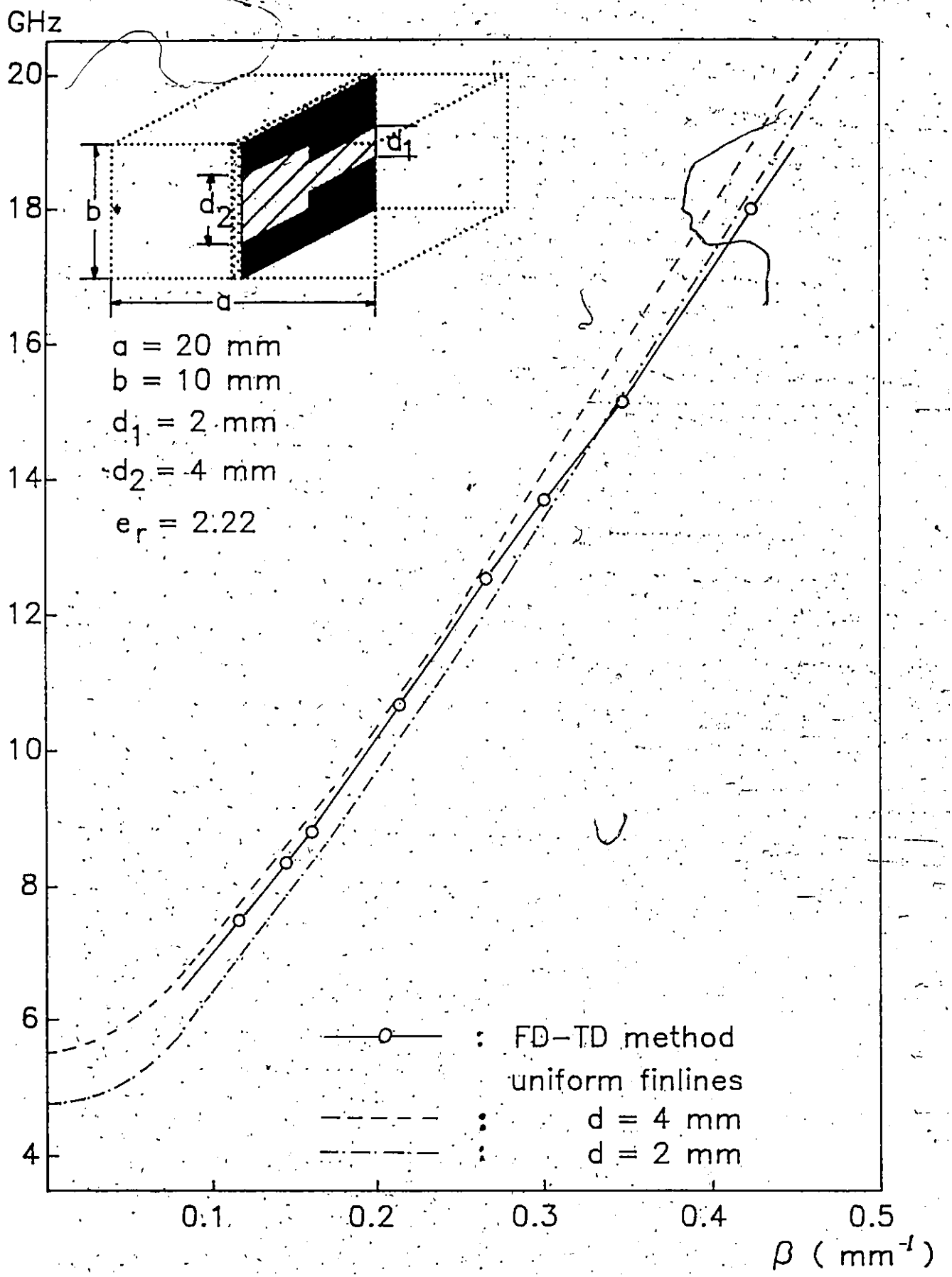

Fig. 7.7 Dispersion diagram of finline discontinuity

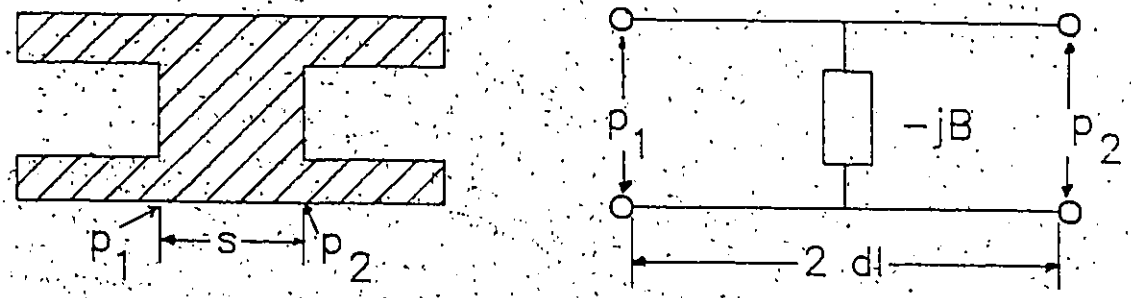

o Finline strip to longitudinal direction

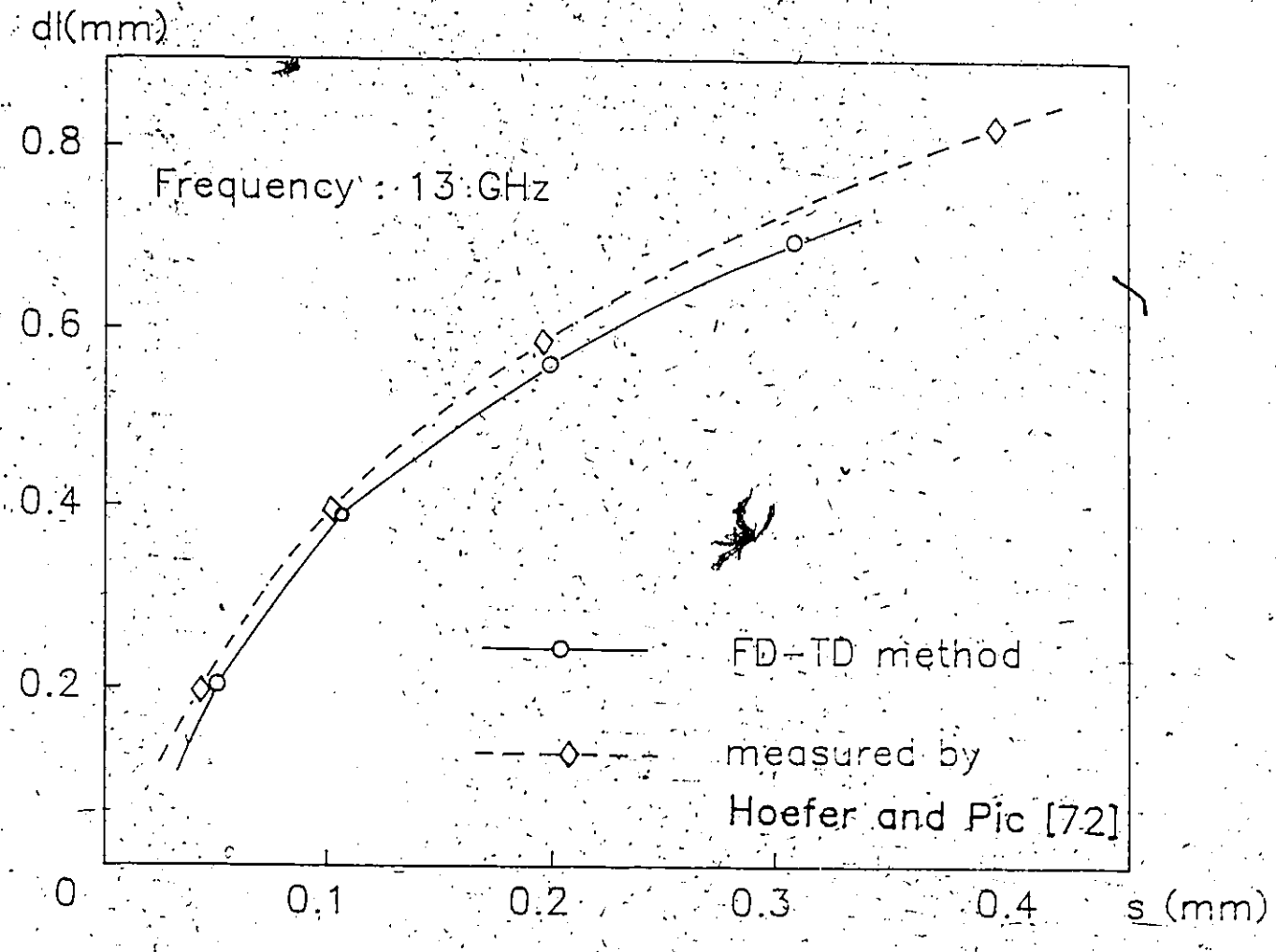

Fig. 7.8 Finline parameters obtained by this method

ple in Fig.7.8 shows the versatility of the FD-TD in calculating the resonant frequency of a finline structure measured by Hoefer and Pic[72] to obtain equivalent circuit parameters. From these data, it can be seen that numerical results confirm the accuracy of the empirical design curves obtained by the measurment technique.

7.7 ANALYSIS OF ANISOTROPIC MEDIA

To show the versatility of this method, the characteristics of a microstrip resonator on an anisotropic substrate are computed in the last example, shown in Fig. 7.9. Several different resonant frequencies obtained by changing the length c are tabulated in Table 7.2. It is well known[13] that the TLM simulation of three-dimensional inhomogeneous planar structures involves dielectric interface ambiguity. The best way to resolve this error is to employ two dielectric substrate thicknesses differing by one Δl. In our case, 3 and 4 nodes were placed successively inside the substrate. The final result is obtained by taking the average of the solutions obtained for the two cases where c is equal to $10\Delta l$. This is shown in Fig.7.10. The solution obtained with the FD-TD method is also drawn in the same figure. As expected, the latter solution is located exactly between the two values obtained with the TLM method. This clearly illustrates the accuracy and convenience of the FD-TD method in such situations. Fig.7.11 shows the disper-

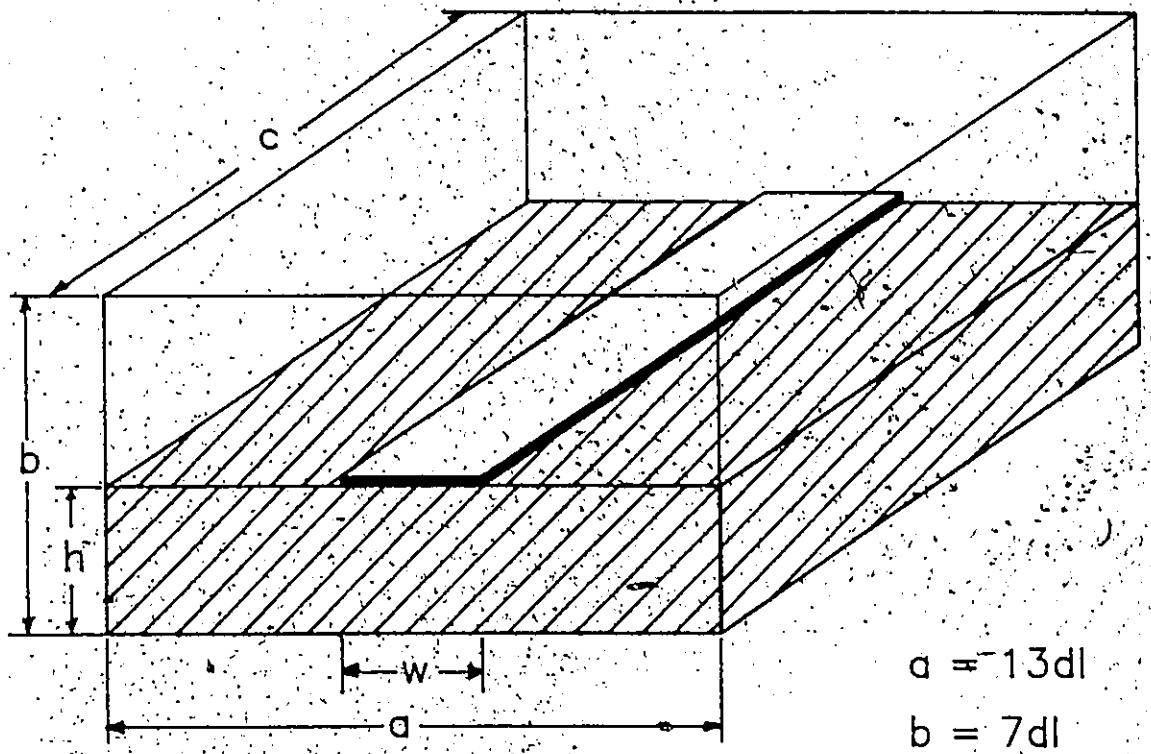

$e_{xx} = e_{yy} = 9.4$

$e_{zz} = 11.6$

a = 13dl

b = 7dl

h = 3dl

w = 3dl

dl = 0.5 mm

Fig. 7.9 A microstrip resonator on anisotropic substrate

c/dl / h		6	8	10	15	20
TLM (GHz)	3dl	15.72	12.24	10.14	7.14	5.46
	4dl	14.22	11.16	9.18	6.36	4.98
	average	14.97	11.70	9.66	6.75	5.22
FD-TD (GHz)		14.64	11.52	9.54	6.78	5.28

Table 7.2 Dominant resonant frequencies obtained by both the TLM and the FD-TD methods for the structure given in Fig. 7.9

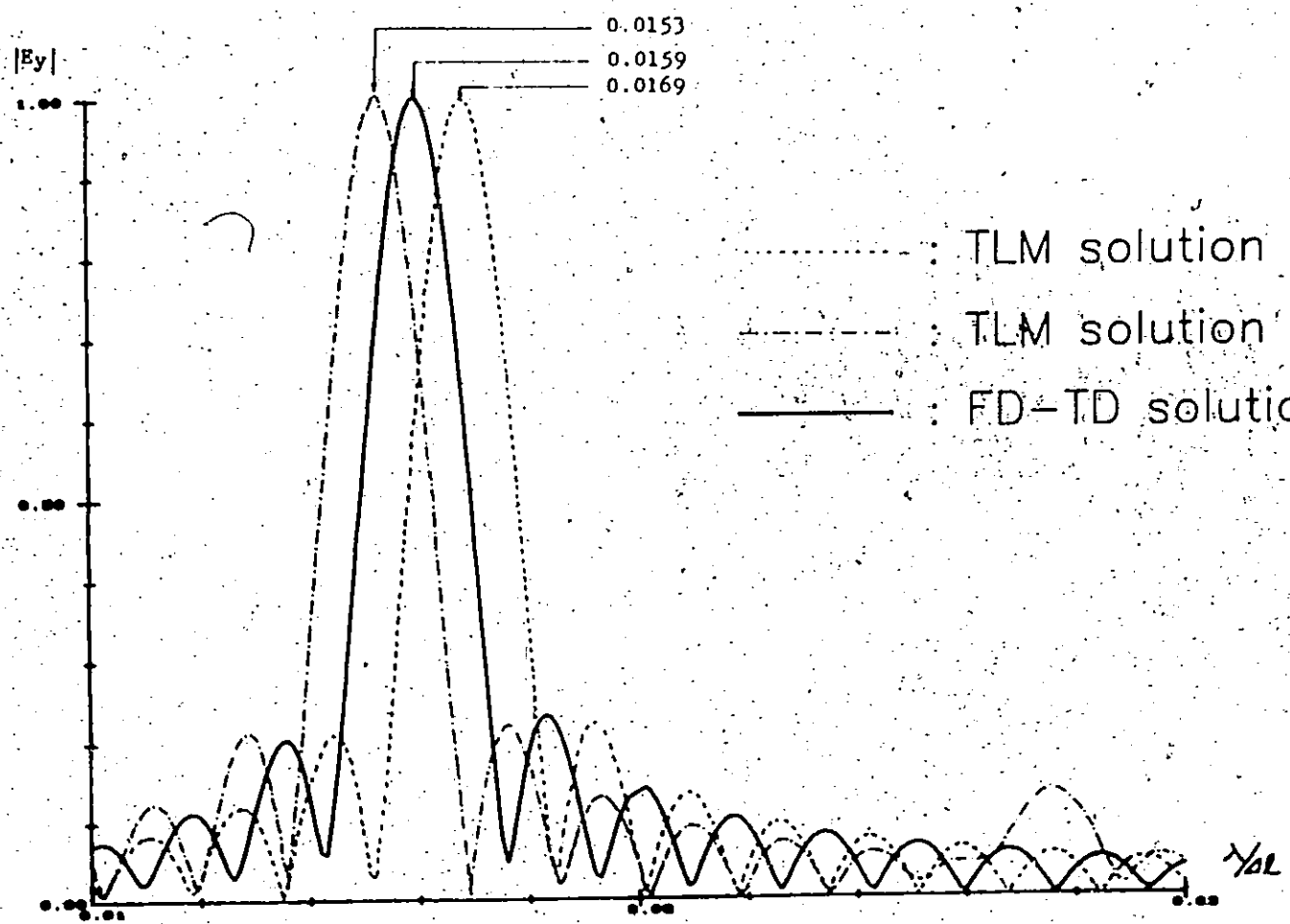

Fig. 7.10 Frequency spectra for the microstrip in Fig. 7.9, showing the effect of dielectric interface error in the TLM solution.

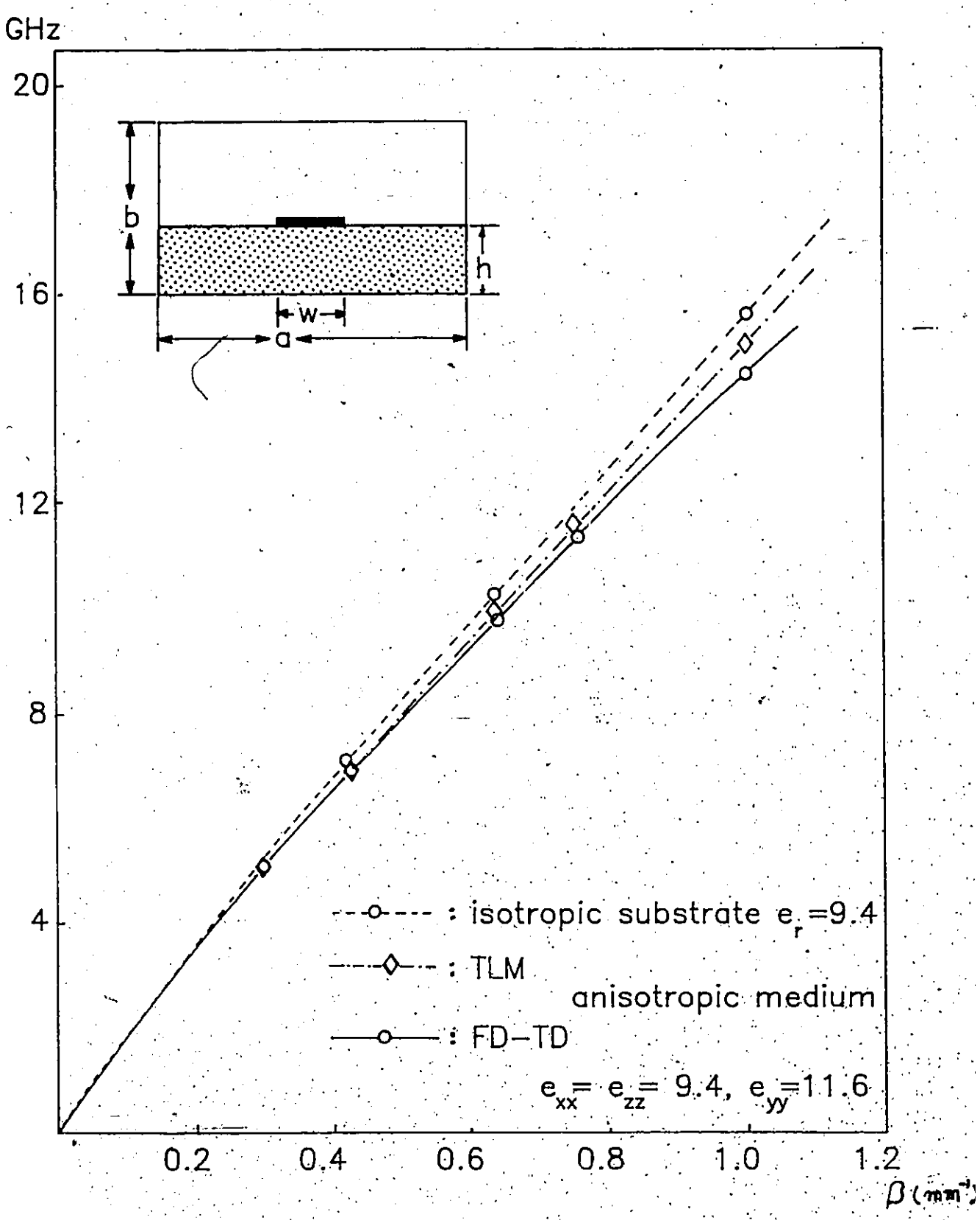

Fig. 7.11 Dispersion diagram of the anisotropic microstrip

sion characteristics of the microstrip which has the same cross-section as that in Fig.7.9. Again, both TLM and FD-TD methods give very similar results except at higher frequencies.

Chapter VIII

CONCLUSION

The capability of two time domain numerical techniques - the TLM and FD-TD methods - has been enhanced without sacrificing their advantages, i.e. generality and simplicity as compared with other methods. Firstly, by employing the Hertzian potential concept instead of voltage and current network variables used in the original TLM method, the scalar TLM method was developed, and its application to simple microwave structures was demonstrated. Numerical results show that only about one third of the CPU memory and time required by the original TLM procedure was spent to obtain identical results. However, it has been found that the scalar nature of this method does not allow its application to hybrid field problems.

In order to develop a method which is general enough to treat the case of hybrid mode wave propagation, the Finite Difference Time Domain algorithm, which has been used previously for the time domain analysis of scattering problems, was extended in order to handle anisotropic wave propagation and eigenvalue problems. Additional features developed in this thesis include initial field value assignment and Fourier transform. Numerical results show that the accuracy of

this algorithm is comparable to or better than that of the TLM while the required CPU memory and time are one third of the TLM. Especially, this method is not affected by ambiguity errors caused by the dielectric interface in three-dimensional structures. An additional advantage of this method is its capability to obtain the field distribution corresponding to an eigen solution in one single simulation, whereas the TLM requires two runs, one for the computation of the eigenvalue, and one for the field distribution.

Even though the basic concept of this method is quite different from that of the TLM, the computer algorithms of both methods are very similar. The program using this new technique was inspired by the three-dimensional TLM code which has proved its efficiency and versatility. Like the TLM, all the information relating to a three-dimensional cavity, such as conducting boundaries, strip patterns, permeability and permittivity at different points, are simply fed into the computer as an input data file. The output is printed in a separate output file which can be reproduced in graphical form.

The developed uniform mesh FD-TD algorithm has been extended further to irregular mesh size in order to maximize the efficiency of space discretization. This irregular mesh FD-TD concept is also similar to the irregular mesh TLM method, but the computer algorithm is much simpler than that

of the TLM because the irregular mesh TLM requires additional calculation of stub impedances and admittances. Since the number of iterations in the irregular mesh TLM increases in proportion to the grading ratio, the advantage of our algorithm becomes more pronounced as the complexity of the field problem increases.

In chapter VII, a wide range of millimeter wave cavities has been analyzed using the irregular mesh FD-TD program. The results presented include the resonant frequencies of partially filled cavities, and the dispersion characteristics for unilateral and bilateral finlines. Also, some results for the equivalent parameters of the finline discontinuities, and the characteristics of microstrip on anisotropic substrate are given. In all cases where comparisons could be made, there has been excellent agreement.

Finally, there are other waveguiding structures that may be analyzed by this technique in the future. For example, applications to irregular cylindrical structures for which analytical solutions are not available, may be investigated with a slight modification of the program.

In conclusion, the work presented in this thesis is a step towards more efficient numerical computations of general electromagnetic problems in the time domain. It represents not only an enhancement and an extension of previously known methods, but also paves the way to the solution of

nonlinear inhomogeneous, anisotropic problems with possible time-dependent material parameters, i.e. the most general electromagnetic problems that can be encountered. Possible future application include the simulation of complete monolithic circuits for microwave and millimeter wave frequencies in the time domain. It may also form the basis for an enhanced computer-aided design technique by allowing the generation of multi-dimensional lookup tables for fast interpolation.

Appendix A

SIMPLIFIED NODE CHARACTERISTICS

The eigen-network of the simplified node can be obtained through modification of the conventional TLM network as shown in Fig.A.1 and Fig. A.2.

If $\theta = \omega dl/c$ and

$$T = \begin{bmatrix} \cos\theta/2 & j\sin\theta/2 \\ j\sin\theta/2 & \cos\theta/2 \end{bmatrix}$$

Then the voltage and current propagation, taking the permittivity stub into account, is described:

$$\begin{bmatrix} V_i \\ I_i \end{bmatrix} = T \cdot \begin{bmatrix} 1 & 0 \\ j\{\tan\theta + Y_o \tan(\theta/2)\} & 1 \end{bmatrix} \begin{bmatrix} 1 & j\tan\theta/2 \\ 0 & 1 \end{bmatrix} \cdot T \begin{bmatrix} V_{i+1} \\ I_{i+1} \end{bmatrix}$$

$$= \begin{bmatrix} A_{11} & A_{12} \\ A_{21} & A_{22} \end{bmatrix} \cdot \begin{bmatrix} V_{i+1} \\ I_{i+1} \end{bmatrix} \qquad (A.1)$$

If the waves on the periodic structure have a propagation constant $r_n = a_n + b_n$ then:

$$\begin{bmatrix} V_i \\ I_i \end{bmatrix} = \begin{bmatrix} \exp(r_\eta dl) & 0 \\ 0 & \exp(r_\eta dl) \end{bmatrix} \begin{bmatrix} V_{i+1} \\ I_{i+1} \end{bmatrix} \qquad (A.2)$$

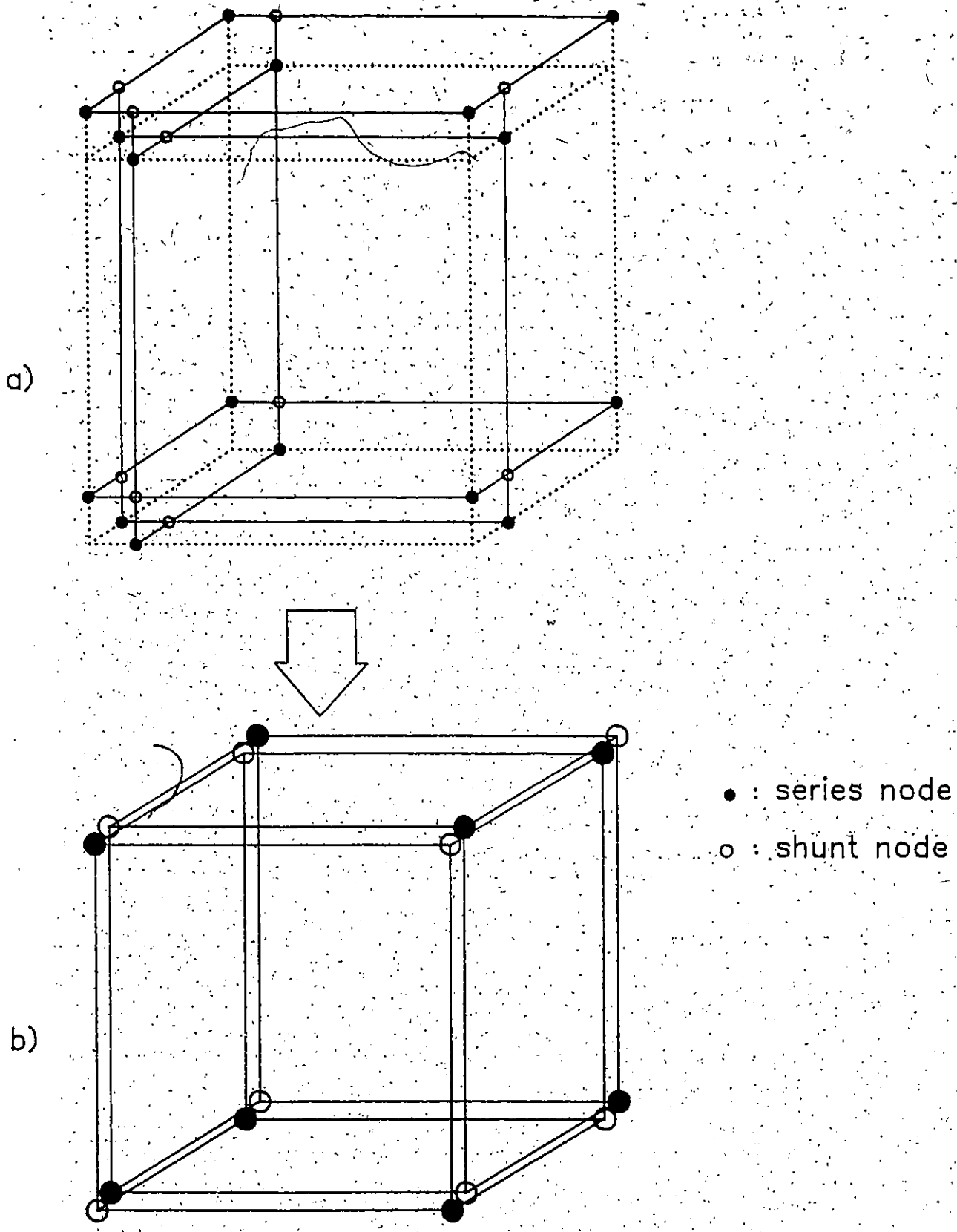

Fig. A.1 Evolution of the original TLM network leading to the simplified TLM network

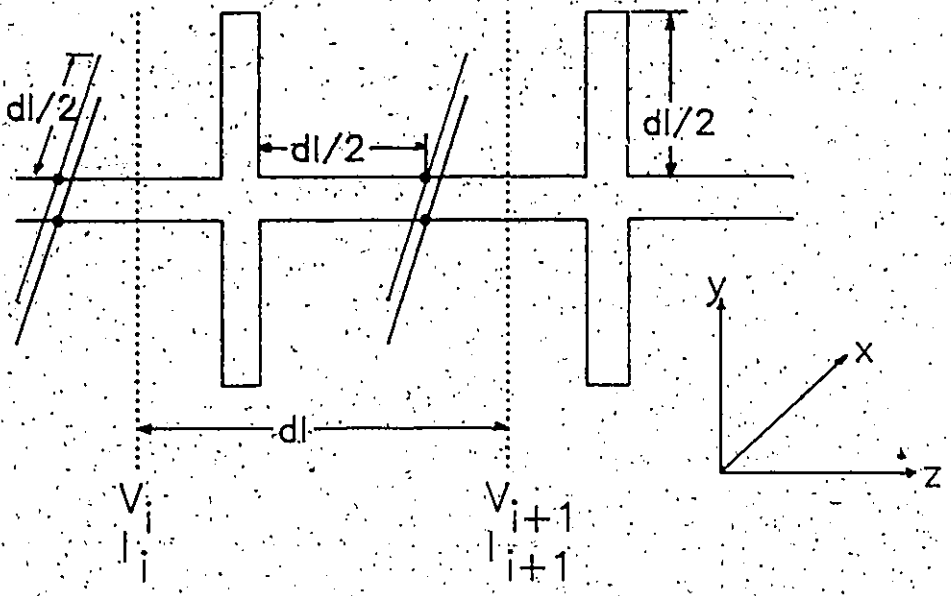

a) Equivalent network of the original TLM

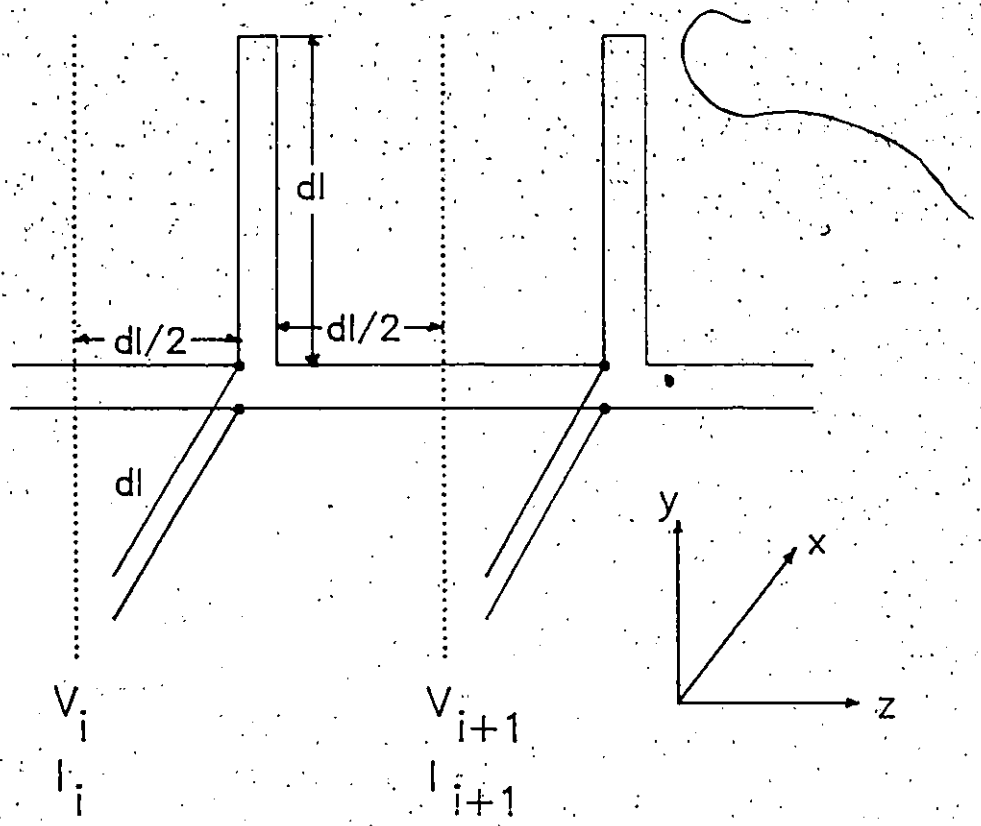

b) Equivalent network of the simplified node TLM

A.2 Equivalent network of two different TLM methods for the waves propagationg in the z-direction

Solution of equations (A. 1), (A. 2) gives the following eigen value equation:

$$\cos(r_n dl) = (A_{11} + A_{22})/2$$

$$= \cos\theta - 3/2 \sin\theta\tan\theta - 2Y_o \sin^2(\theta/2) \qquad \text{(A. 3)}$$

which for the low frequency passband reduces to

$$\sin\beta\, dl/2 = \sqrt{1+Y_o}\, \sin\theta/2 \sqrt{1+3\cos^2(\theta/2)/\{(1+Y_o)\cos\theta\}} \qquad \text{(A. 4)}$$

(A. 4) has been used to obtain the dispersion characteristics of the simplified node TLM network given in (3.14).

Appendix B

PROPERTIES OF THE SCALAR TLM NETWORK

Like the TLM matrix, the scalar TLM network of Fig.4.1.a) is a slow wave structure whose slow wave properties may be understood by considering the propagation of plane waves along it. All three different propagation directions and corresponding networks are shown in Fig.4.2. The first case to be considered is the propagation of a plane wave along the main axis representing direction A. All the transfer matrix parameters are based on the travelling wave representation instead of voltage and current representation.

i) Case A

If $\theta = \omega dl/c$ and

$$T = \begin{bmatrix} \exp(j\theta/2) & 0 \\ 0 & \exp(-j\theta/2) \end{bmatrix} \qquad (B.1)$$

then the incident and reflected wave are described by:

$$\begin{bmatrix} a_i \\ b_i \end{bmatrix} = T \cdot \left| 1/2 \begin{bmatrix} 2+j\tan(\theta/2) & j\tan(\theta/2) \\ -j\tan(\theta/2) & 2-j\tan(\theta/2) \end{bmatrix} \right|^4 \cdot T \cdot \begin{bmatrix} b_{i+1} \\ a_{i+1} \end{bmatrix}$$

$$= \begin{bmatrix} \exp(j\theta)\{1+2j\tan(\theta/2)\} & 2j\tan\theta/2 \\ -2j\tan(\theta/2) & \exp(-j\theta)\{1-2j\tan(\theta/2)\} \end{bmatrix} \cdot \begin{bmatrix} b_{i+1} \\ a_{i+1} \end{bmatrix}$$

----------(B. 2)

If the waves on the periodic structure have a propagation constant $r_n = a_n + b_n$ then

$$\begin{bmatrix} a_i \\ b_i \end{bmatrix} \quad \begin{bmatrix} \exp(r_n dl) & 0 \\ 0 & \exp(-r\ dl) \end{bmatrix} \begin{bmatrix} a_{i+1} \\ b_{i+1} \end{bmatrix} \qquad \text{(B. 3)}$$

The solution of equation (B. 2) and (B. 3) gives the following eigenvalue equation:

$$\cos(r_n dl) = \cos\theta - 2\tan(\theta/2)\sin\theta$$
$$= \cos\theta - 4\sin^2(\theta/2)$$

which for the low frequency pass-band reduces to

$$\sin(\beta\, dl/2) = \sqrt{3}\, \sin(\theta/2) \qquad \text{(B. 4)}$$

ii) Case B

For the propagation direction B, transfer matrix will be:

$$\begin{bmatrix} a_i \\ b_i \end{bmatrix} = T \cdot \left| 1/2 \begin{bmatrix} 2+j\tan(\theta/2)/2 & j\tan(\theta/2)/2 \\ -j\tan(\theta/2)/2 & 2-j\tan(\theta/2)/2 \end{bmatrix} \right|^2 T \cdot \begin{bmatrix} b_{i+1} \\ a_{i+1} \end{bmatrix}$$

$$= \begin{bmatrix} \exp(j\theta)(1+1/2j\tan\theta/2) & 1/2j\tan\theta/2 \\ -1/2j\tan\theta/2 & \exp(-j\theta)(1-1/2j\tan\theta/2) \end{bmatrix} \begin{bmatrix} b_{i+1} \\ a_{i+1} \end{bmatrix}$$

then, the eigenvalue equation is:

$$\cos(r_n dl) = \cos\theta - \sin^2(\theta/2) \quad \text{or}$$

$$\sin(\beta\, dl/2) = \sqrt{3/2}\, \sin(\theta/2) \qquad \text{(B. 5)}$$

iii) Case C

As can be seen in Fig.4.2, all three lines are matched at the junction. Therefore eigensolution is:

$$\beta\, dl = \theta \qquad \text{(B. 6)}$$

Note that β's of equation (B. 5) and (B. 6) represent propagation constants along the transmission lines not in the direction of the propagation wavefront. Therefore the real propagation constants of (B. 5) and (B. 6) must be modified as:

$$\begin{aligned} \beta &\text{ ---------> } \beta/\sqrt{2} \mid \text{case B} \\ \beta &\text{ ---------> } \beta/\sqrt{3} \mid \text{case C} \end{aligned} \qquad \text{(B. 7)}$$

By substituting (B. 7) into (B. 5) and (B. 6), the final set of dispersion relations become:

$$\begin{aligned} \sin(\beta dl/2) &= \sqrt{3}\,\sin(\theta/2) \mid \text{case A} \\ \sin(\beta dl/2\sqrt{2}) &= \sqrt{3/2}\,\sin(\theta/2) \mid \text{case B} \\ \beta/\sqrt{3} &= \theta \mid \text{case C} \end{aligned} \qquad \text{(B. 8)}$$

Equation (B. 8) is depicted in Fig.4.4 and used to obtain corresponding phase velocity characteristics of (4.10).

Appendix C

DERIVATION OF THE STABILITY CONDITION

The stability condition employed in this thesis can be derived by applying the von Neumann method[71] to the explicit finite difference form of (5.14). This form is obtained by substituting the equations involving Hx(n+1/2), Hy(n+1/2), and Hz(n+1/2) of (5.14) into the other set of Maxwell's equations.

After some mathematical simplification, the right hand side of the two sets of Maxwell's equation contains only n, n-1/2 terms in time and various i, j, k terms in space. This substitution could have been started after properly shifting 1/2 in time and space, resulting in all n in time and i, j, k in space for the left side terms. But the final results are the same as for the present derivation but with more mathematical involvement. The arranged vectorial form is:

$$\begin{bmatrix} \overline{H}(n+1/2) \\ \\ \overline{E}(n+1) \end{bmatrix} = \begin{bmatrix} \\ \sum_{\ell} A_{\ell} + \sum_{k} A_{k} \\ \\ \end{bmatrix} \begin{bmatrix} \overline{H}(n-1/2) \\ \\ \overline{E}(n) \end{bmatrix} \qquad \text{(C. 1)}$$

where $\overline{E} = (E_x, E_y, E_z)^t$, $\overline{H} = (H_x, H_y, H_z)^t$. Note that the components of E and H are located with half integer shifts relative to each other as shown in Fig.5.1. 1 represents single

index i-1, i+1, j-1, j+1, k-1, and k+1. k represents double index (i+1, j-1), (i+1, k-1), (j+1, i-1), (j+1, k-1), (k+1, i-1), and (k+1, j-1).

A_1 and A_k are 6x6 matrices containing elements $s = cdt/dx$ and s^2 and -1, +1. (C. 1) can be expressed more simply as:

$$\bar{U}(i,j,k,n+1) = \sum_{\ell}^{*} A_{\ell}\bar{U}(i,j,k,n) \qquad \text{(C. 2)}$$

where $\bar{U}(i,j,k,n+1)$ is a vector containing all elements of E and H. Let us define an error vector $\bar{Z}(i,j,k,n)$ which is a difference between the true solution $\bar{u}(i,j,k,n)$ and approximate solution $\bar{U}(i,j,k,n)$ of (C. 1). Then,

$$\bar{Z}(i,j,k,n) = \bar{u}(i,j,k,n) - \bar{U}(i,j,k,n) \qquad \text{(C. 3)}$$

The von Neuman method require that error vector be decomposed by a series of harmonic functions as

$$Z(i,j,k,n)=\sum_{i}\sum_{j}\sum_{k}A(i,j,k,n)\exp(j\beta idx)\exp(j\gamma jdy)\exp(j\delta kdz) \qquad \text{(C. 4)}$$

where in general $|\beta|$, $|\gamma|$ and $|\delta|$ are arbitrary and A(i,j,k,n) denotes the error magnitude at the n-th time interval.

It can be shown that the error function (C. 4) or each element of (C. 4) satisfies the original finite difference equation (C. 2). For convenience, suppose that the time level being considered corresponds to t = ndt. To find the error propagation as t increases, A solution of the finite

difference equation is found which reduces to $\exp(j\beta idx)\exp(j\gamma jdy)\exp(j\delta kdz)$ when $t = ndt$. By substituting one element of (C. 4), say

$$\bar{Z}(i,j,k,n) = \bar{U}_o \exp(\alpha ndt)\exp(j\beta idx)\exp(j\gamma jdy)\exp(j\delta kdz),$$

into (C. 1) and rearranging it, we obtain

$$\bar{U}_o \exp(\alpha dt) = [\,G\,]\,\bar{U}_o$$

with:

$$[\,G\,] = \begin{bmatrix} 1 & 0 & 0 & 0 & p & -p \\ 0 & 1 & 0 & -p & 0 & p \\ 0 & 0 & 1 & p & -p & 0 \\ 0 & q & -q & 1-2pq & pq & pq \\ -q & 0 & q & pq & 1-2pq & pq \\ q & -q & 0 & pq & pq & 1-2pq \end{bmatrix}$$

where $p = 2j\exp(j\theta)\sin(\theta)s/(Z_o\mu_r)$

$q = -2j\exp(-j\theta)\sin(\theta)sZ_o/\varepsilon_r$

$\theta = \beta dx/2$

and $s = c\Delta t/\Delta$

$\bar{U}_o$ denotes the error vector at ndt and $\bar{U}_o\exp(\alpha dt)$ is the propagated error vector after one time step. The matrix [G] is known as the amplification matrix and we have assumed that $dx = dy = dz = \Delta$ for simplicity of derivation.

The von Neuman condition requires that if $||G|| \leq 1$, then the original error component $\exp(j\beta dx)\exp(j\gamma dy)\exp(j\delta dz)$ will not grow. The norm of $||G||$ may be obtained from the maximum eigenvalue of [G]. After some algebraic manipulations, the eigenvalues of [G] are computed to be:

$$1, \quad \pm\sqrt{[-3pq+2+((3pq-2)^2-4)^{1/2}]/2}$$

Clearly if $(3pq - 2)^2 \leq 4$, then $|\lambda| = 1$ for all the eigenvalues of [G], and hence the difference scheme is numerically stable. Thus $(3pq - 2)^2 \leq 4$ is a condition for stability. Substituting pq, finally we have

$$s^2\sin^2\theta/(\varepsilon_r\mu_r) \leq 1/3 \quad \text{or} \quad s \leq \sqrt{\varepsilon_r\mu_r/3} \qquad \text{(C. 6)}$$

REFERENCES

1. G.Kron,"Equivalent circuit of the field equations of Maxwell - I", Proc.IRE, vol.32, pp.289-299, May 1944.

2. G.Kron,"Numerical solution of ordinary and partial differential equations by means of equivalent circuits", J.of App. Physics, vol.16, pp.172-186, Mar. 1945.

3. G.Kron,"Electric circuit models of partial differential equations", Electrical Eng. vol.67 pp.672-684, 1948.

4. J.R.Whinnery and S.Ramo, "A new approach to the solution of high-frequency field problems", Proc. IRE, vol.32, pp 284- 288, may 1944

5. J.R.Whinnery, C.Concordia, W.Ridgway, and G.Kron, "Net work analyzer studies of electromagnetic cavity resonators", Proc. IRE, vol.32, pp.289-299, may 1944.

6. P.B.Johns and R.L.Beurle, "Numerical solution of 2-dim ensional scattering problems using a transmission line matrix', Proc. Inst. Elec. Eng., vol.118, no.9, pp 1203-1208, Sep. 1971.

7. P.B.Johns, "Application of the transmission-line matrix method to homogeneous waveguides of arbitrary cross-section", Proc. Inst. Elec. Eng., vol.119, no.8, pp. 1086-1091, Aug. 1972.

8. P.B.Johns, "The solution of inhomogeneous waveguide problems using a transmission-line matrix", IEEE Trans., Microwace Theory Tech., vol. MTT-22, pp.209-215, Mar. 1974.

9. P.B.Johns, "A new mathematical model to describe the physics of propagation", Radio Electron. Eng., vol. 44, no. 12, pp. 657-666, Dec. 1974.

10. S.Akhtarzad and P.B.Johns, "Solution of 6-component electromagnetic fields in three space dimensions and time by the TLM method", Electron Lett., vol.10, no.25/26 pp. 535-537, Dec. 12, 1974.

11. S.Akhtarzad and P.B.Johns, "TLM analysis of the dispersion characteristics of microstrip lines on magnetic substrates using 3-dimensional resonators", Electron. Lett., vol.11, no.6, pp.130-131, mar. 20 1975.

12. S.Akhtarzad and P.B.Johns, "Dispersion characteristic of a microstrip line with a step discontinuity", Electron Lett., vol. 11, no.14, pp.310-311, july 10, 1975.

13. S.Akhtarzad, "Analysis of lossy microwave structure and microstrip resonators by the TLM method", Ph.D dissertation, Univ. of Nottingham, England, July 1975.

14. S.Akhtarzad and P.B.Johns, "3-dimensional TLM computer analysis of microstrip resonators", IEEE Trans., Microwave Theory Tech., vol. MTT-23, pp.990-997, Dec. 1975.

15. S.Akhtarzad and P.B.Johns, "Solution of Maxwell's equation in three space dimensions and time by the T.L.M. method of analysis", Proc. Inst. Elec. Eng., vol.122, no.12, pp.1344-1348, Dec. 1975.

16. S.Akhtarzad and P.B.Johns, "Generalized elements for TLM method of numerical analysis", proc. Inst. Elec. Eng., vol.122 no. 12, pp.1349-1352, Dec. 1975.

17. G.E.Mariki, "Analysis of microstrip lines on inhomogeneous anisotropic substrates by the TLM numerical technique", Ph.D. thesis, Univ. of California, Los Angeles, June 1978.

18. P.B.Johns, "A simple explicit and unconditionally stable numerical routine for the solution of the diffusion equation", Int. J. for Num. methods in Eng., vol.11, pp.1307-1328, 1977.

19. W.J.R.Hoefer and A.Ros, "Fin line parameters calculated with the TLM method", IEEE MTT-S Int. Microwave Symp. Dig. (Orlando, FL), Apr. 28-May 2, 1979.

20. P.Saguet and E.Pic, "An improvement for the TLM method", Electron. Lett., vol.16, no. 7, pp.247-248, Mar. 27, 1980.

21. Y.C.Shih and W.J.R.Hoefer, "Dominant and second-order mode cutoff frequencies in finlines calculated with a two- dimensional TLM program", IEEE Trans., Microwave Theory Tech., vol. MTT-28, pp.1443-1448, Dec. 1980.

22. P.Saguet and E.Pic, "Le maillage rectangulaire et le changement de maille dans la methode TLM en deux dimensions", Electron. Lett., vol.17, no.7, pp.277-278, Apr. 2, 1981.

23. D.A.Al-Mukhtar and J.E.Sitch, "Transmission line matrix method with irregularly graded space", Proc. Inst. Elec. Eng., vol.128, pt.H, no. 6, pp. 299-305, Dec. 1981.

24. P.Saguet and E.Pic, "Utilisation dun nouveau type de noeud dans la methode TLM en 3 dimensions", Electron. Lett., vol.18 no.11, pp.478-480, May 1982.

25. P.Saguet, "Le maillage parallelepipedique et le changement de maille dans la methode TLM en trois dimensions", Electron. Lett., vol. 20, no. 5, pp.222-224, Mar. 15,1984.

26. D.H.Choi and W.J.R.Hoefer, "The simulation of three dimensional wave propagation by a scalar TLM model", IEEE MTT-S Int. Microwave Symp. Dig., May 1984.

27. K.S.Yee, "Numerical solution of initial boundary value problems involving Maxwell's equations in isotropic media", IEEE Trans. vol. AP-14, pp.302-307, May 1966.

28. C.D.Taylor, D.H.Lam, and T.H.Shumpert, "Electfomagnetic pulse scattering in time-varying inhomogeneous media", IEEE Trans. vol. AP-17, pp.585-589, Sep. 1969.

29. A.Taflove and M.E.Brodwin, "Numerical solution of steady state electromagnetic scattering problems using the time- dependent Maxwell's equations", IEEE Trans., Microwave Theory Tech., vol. MTT-23, pp. 623-630, Aug. 1975.

30. R.Holland, "Threde: A free-field EMP coupling and scattering code", IEEE Trans. Nucl.Sci., vol. NS-24, pp:2416-2421,Dec.1977.

31. K.S.Kunz and K.M.Lee, "A three-dimensional finite difference solution of the external response of an aircraft to a complex transient EM environment:Part I-The method and its implementation", IEEE Trans. vol. EMC-20, pp. 328-333, May 1978.

32. G.Mur, "Absorbing boundary conditions for the finite difference approximation of the time-domain electromagnetic-field equations", IEEE Trans. vol. EMC-23, pp.377-382, Nov. 1981.

33. A.Taflove and K.R.Umashankar, "A hybrid moment method/ finite difference time domain approach to electromagnetic coupling and aperture penetration into complex geometries", IEEE Trans. vol. AP-30, pp. 617-627, July 1982.

34. K.R.Umashankar and A.Taflove, "A novel method to analyze electromagnetic scattering of complex objects", IEEE Trans., vol. EMC-24, pp. 397-405, Nov. 1982.

35. A.Taflove and K.Umashankar, "Radar cross section of general three-dimensional scatterers", IEEE Trans., vol. EMC-25, no. 4, Nov. 1983.

36. P.J.Meier, "Two new integrated-circuit media with special advantages at millimeter wavelengths", IEEE MTT-S Int. Microwave Symp. Dig., pp. 221-223. 1972.

37. S.D.Robertson,"The ultra-bandwidth fin-line coupler", IRE Trans. Microwave Theory Tech., vol. MTT-3, pp. 45-48, 1955.

38. P.J.Meier, "New developments with integrated fin-line and related printed millimeter circuits", IEEE MTT-S Int. Microwave Symp. Dig., pp.143-145, 1975.

39. H.Hofmann, H.Meinel, and B.Adelseck, "New integrated millimeter wave components using fin-lines", IEEE MTT-S Int. Microwave Symp. Dig., pp. 21-23. 1978.

40. "Solid-state switch from 75 to over 100 GHz", Product feature, Microwave J., vol. 22, no.4, p. 108, Apr. 1979.

41. H.Meinel,and H.Callsen, "Fin-line PIN diode attenuators and switches for 94 GHz range", Electronics letters vol.18, no.13, pp:541-542, June 1982.

42. R.N.Bates, M.D.Coleman, S.J.Nightingale, and R.Davies, "E-planes drop millimeter costs", Microwave System News, pp. 74-80, Dec. 1980.

43. P.J.Meier, "Integrated fin-line/A versatile and proven millimeter transmission line", Microwave J., pp. 24-25, Nov. 1976.

44. U.Gysel, "A 26.5-40 GHz planar balanced mixer", in 5th Eur. Microwave Cong. Dig., (Hamburg), pp. 491-495, 1975.

45. P.M.Ballard, "Waveguide-bandwidth millimeter mixer with IF to 18 GHz", Electronics letters, vol. 19, no. 2, pp. 46-47, Jan. 1983.

46. W.Menzel,and H.Callsen, "140 GHz fin-line components", IEEE Trans. Microwave Theory Tech., vol. MTT-33, pp. 53-56, Jan. 1985.

47. F.Arndt,J.Bornemann,D.Grauerholz, and R.Vahldieck, "Theory and design of low-insertion loss fin-line filters", IEEE Trans., Microwave Theory Tech., vol. MTT-30, pp. 155-163, Feb. 1982.

48. W.Menzel, H.Callsen, and K.Solbach, "An integrated receiver front end for a 94 GHz dual polarization radar", Proc. of 13th European Micrwave Conf., pp. 142-147, Sept. 1983.

49. A.K.Sharma and W.J.R.Hoefer, "Empirical analytical expressions for fin-line design", IEEE MTT-S Int. Microwave Symp. Digest, pp. 102-104, 1981.

50. A.M.K.Saad and K.Schunemann, "A simple method for analyzing fin-line structures", IEEE Trans. Microwave Theory Tech., vol. MTT-26, pp. 1002-1007, Dec. 1978.

51. H.Hofmann, "Fin-line dispersion", Electron. Lett., vol. 12, no. 17, pp. 428-429, Aug. 1976.

52. C.Chang and T.Itoh, "Spectral domain analysis of dominant and higher order modes in fin-lines", IEEE MTT-S Int. Microwave Symp. Dig., (Orlando) 1979.

53. R.Mittra and T.Itoh, "A new technique for the analysis of the dispersion characteristics of microstrip lines", IEEE Trans., Microwave Theory Tech., vol. MTT-19, pp. 47-56, Jan. 1971.

54. L.P.Schmidt and T.Itoh, "Spectral domain analysis of dominant and higher order modes in fin-lines", IEEE Trans. Microwave Theory Tech., vol. MTT-28, pp. 981-985, Sep. 1980.

55. J.B.Knorr and P.M.Shayda, "Millimeter wave fin-line characteristics", IEEE Trans. Microwave Theory Tech., vol. MTT-28, pp. 737-743, July 1980.

56. A.K.Sharma and W.J.R.Hoefer, "Propagation in coupled unilateral and bilateral finlines", IEEE Trans. Microwave Theory Tech., vol. MTT-31, pp. 498-502, June 1983.

57. S. Tedjini and E.Pic, "New analysis of semiconductor isolators: The modified spectral domain analysis", IEEE Trans. Microwave Theory Tech., vol. MTT-33, pp. 59-64, Jan. 1985.

58. R.E.Collin, Field Theory of Guided Waves chapter 6, Mcgraw Hill 1960.

59. J.E.Sitch and P.B.Johns, "Transmission-line matrix analysis of continuous waveguiding structures using stepped-impedance cavities", Microwave Optics and Acoustics, vol. 1, no. 5, pp. 181-184, Sep. 1977.

60. D.H.Choi and W.J.R.Hoefer, "A Finite Difference Time Domain method and its application", IEEE MTT-S Int. Microwave Symp., (Baltimore) pp.793-796, June 1986.

61. D.H.Choi and W.J.R.Hoefer, "The Finite Difference Time Domain method and its application to eigenvalue problems", To be published in IEEE Trans., Microwave Theory Tech., Dec. 1986.

62. R.D.Richtmyer and K.W.Morton, Difference Methods for Initial Value Problems chapter 4, Interscience Pub. John Wiley & Sons. 2nd Ed. 1967.

63. T.Nakahara and N.Kurauchi, "Transmission modes in the Grooved guide", J. Inst. Electron. Commun. Eng. Japan, vol. 47, no. 7, pp. 43-51, July 1964.

64. A.Oliner and P.Lampariello, "The dominant mode properties of open groove guide : An improved solution", IEEE Trans. Microwave Theory Tech., vol. MTT-33, no. 9, pp. 755-764, Sep. 1985.

65. P.H.Vartanian, W.P.Ayres and A.L.Helgesson, "Propagation in dielectric slab loaded rectangular waveguide", IRE Trans. Microwave Theory Tech., vol. MTT-6, pp. 215-222, April 1958.

66. R.Seckelmann, "Propagation of TE-modes in dielectric loaded waveguides", IEEE Trans. Microwave Theory Tech., vol. MTT-14, pp. 518-527, Nov. 1966.

67. F.E.Gardiol, "Higher-order modes in dielectrically loaded rectangular waveguides", IEEE Trans. Microwave Theory Tech., vol. MTT-16, pp. 919-924, Nov. 1968.

68. Y.Konishi and H.Matsumura, "Short end effect of ridge guide with planar circuit mounted in a waveguide", IEEE Trans. Microwave Theory Tech., vol. MTT-27, pp. 168-170, Feb. 1979.

69. J.B.Knorr, "Equivalent reactance of a shorting septum in a fin-line : Theory and experiment", IEEE Trans. Microwave Theory Tech., vol. MTT-29, pp. 1196-1202, Nov. 1981.

70. N.H.L.Koster and R.H.Jansen, "Some new results on the equivalent circuit parameters of the inductive strip discontinuity in unilateral fin-lines", Arch. Elek. Ubertragung, vol. 35, no. 12, pp. 497-499, 1981.

71. A.R.Mitchell and D.F.Griffiths, The Difference Method in Partial Differential Equations chapter 2, pp. 38-42, John Wiley & Sons. 1980.

72. E.Pic and W.J.R.Hoefer, "Experimental characterization of fin line discontinuities using resonant techniques', IEEE MTT-S Int. Microwave Symp. Digest, pp. 108-110, 1981.